Title	Geometric and electrostatic effects of tectons on formation of hydrogen-bonded organic frameworks
Author(s)	Yang, Zhuxi
Citation	北海道大学. 博士(環境科学) 甲第15138号
Issue Date	2022-09-26
DOI	10.14943/doctoral.k15138
Doc URL	http://hdl.handle.net/2115/87471
Type	theses (doctoral)
File Information	Yang_Zhuxi.pdf

Geometric and electrostatic effects of tectons on formation of hydrogen-bonded organic frameworks

（水素結合性有機フレームワークの形成における

テクトンの幾何学的および静電的な影響）

北海道大学大学院環境科学院

Zhuxi YANG

Acknowledgement

First of all, I would like to appreciate Prof. Nakamura for accepting my doctoral application, giving me the valuable opportunity to continue my studies and research in Hokkaido University. His warm encouragement and help, homelike environment, as well as the free and open academic atmosphere of the Nakamura Lab are the guarantees for the completion of my doctoral course.

At the same time, I will express my great gratitude to Prof. Hisaki for giving me the opportunity to continue my research in Hisaki Lab, graduate school of engineering science, Osaka university, in the last two years of the doctoral course. This thesis was completed under the careful guidance of Prof. Hisaki. In the past three years, each discussion and every meticulous guidance are still vivid in my mind. He is meticulous about his work, passionate about scientific research, and kind and caring for each student.

Without the enthusiastic help of two professors, there would be no publication of papers, approval of the research plan, the acquisition of CSC scholarship.

Secondly, I would like to appreciate the assistant professors Dr. Kiyonori Takahashi, Dr. Ryusei Oketani (Osaka U.), Dr Chen Xue and Dr. Rui-Kang Huang. Every day in the labs, they always tried their best to help me solve the problems I encountered, and encouraged me to explore bravely.

Thirdly, I must thank Dr. Kilingaru I. Shivakumar for his kind help, who acquaint me with new research environment and experimental operations as soon as possible. Also I would like to thank Jia-bing Wu, Dr. Xin Chen, Dr. Si-Min Li, Dr Qin Ji, Chao Wang, Dong-fang Wu who have given me plenty of help in my daily life and experiments.

It was my great honor to have the happy time in Hisaki lab, I would like to express my gratitude to Yoto Suzuki and Taito Hishimoto, for teaching me using different laboratory equipment and research software, and Yuna Yamaguchi, Mao Yamaguchi, Kubo Haruka, for helping me in my life and experiments.

I am grateful to Prof. Norimitsu Tohnai (Osaka U.), Prof. Akinori Saeki (Osaka U.), Ass. Prof. Kazuhide Kamiya (Osaka U.) and Asst. Prof. Soichiro Kawamorita (Osaka U.) for their kind advices and technical supports.

Last but not least, I will express my gratefulness to all of my family members, especially my uncle, my parents and my girl friend Cuiping, for their constant encouragements and supports.

Zhuxi YANG

July 29, 2022

Contents

Chapter 1 1

- 1-1. Crystalline porous materials (CPMs) 2
    - 1-1-1. Metal Organic Frameworks / Porous Coordination Polymers(MOFs / PCPs) 2
    - 1-1-2. Covalent Organic frameworks (COFs) 3
    - 1-1-3. Porous Organic Cages (POCs) 7
    - 1-1-4. Hydrogen-bonded Organic Frameworks (HOFs) 9
- 1-2. The background and defination of Hydrogen bond 12
- 1-3. Categories of hydrogen-bonded organic framework materials 14
    - 1-3-1. Single-component hydrogen-bonded organic framework materials 14
    - 1-3-2. Multi-component hydrogen-bonded organic framework materials 20
- 1-4. Preparation methods for HOF materials 24
    - 1-4-1. Solvothermal synthesis 24
    - 1-4-2. Slow evaporation 25
    - 1-4-3. Slow liquid/vapor diffusion 25
    - 1-4-4. Electrophoretic deposition technology 25
    - 1-4-5. Machanochemistry 27
- 1-5. Gas adsorption and separation 28
- 1-6. Increasing of rigidity and permanent porosity in HOFs 28
- 1.7 Research purpose 29
- Reference 32

Chapter 2 40

- 2-1. Abstract 41
- 2-2. Introduction 42
- 2-3. Results and discussion 44
- 2-4. Conclusion 55
- 2-5. Experiment section 56

Chapter 3 61
  3-1. Abstract 62
  3-2. Introduction 63
  3-3. Result and Discussion 67
  3-4. Conclusion 82
  3-5. Experimental section 82
  Reference 86
Chapter 4 90
  4-1. Abstract 91
  4-2. Introduction 92
  4-3. Results and Discussion 96
  4-4. Conclusion 113
  4-5. Experimental Section 114
  Reference 120
Chapter 5 124
  5-1. Conclusions 125
  5-2. Perspectives 126
  Reference 128
List of publication 129
Appendix 130

Chapter 1

General Introduction

1-1. Crystalline porous materials (CPMs)

Multitudinous crystalline porous materials have been advanced over a period of time,[1] which can be traced back to Prussian blue analogues (PBAs)[2] and inorganic zeolites,[3] in the past several decades, as well as Metal Organic Frameworks / Porous Coordination Polymers (MOFs / PCPs),[4,5] Covalent Organic frameworks (COFs),[6] Porous Organic Cages (POCs),[7] and Hydrogen-bonded Organic Frameworks (HOFs).[8] These CPMs attract considerable attention of researchers due to their wide potential application in many fields, including gas storage and separation, catalysis, energy storage and conversion, sensing, optoelectronics and biomedical applications,[9] which derive from their physical and chemical properties, such as size and shape selectivity, catalytic activity, conductivity, separation ability, etc.[10]

1-1-1. Metal Organic Frameworks / Porous Coordination Polymers(MOFs / PCPs)

PCPs are one of the new functional porous crystalline materials, also known as MOFs or inorganic-organic hybrid material. MOFs have the advantages of structural diversity and designability, in which metal cations or cation clusters (nodes) form one-, two- or three-dimensional coordination network structures through self-assembly with organic ligands or linker molecules.[4,5] Metal ions with different coordination numbers, diverse organic linkers, and different coordination modes of ligands provide an infinite variety of possible combinations for MOFs along with various morphologies.[11]

MOF-5, one of the famous examples in MOFs reported by Yaghi and the co-workers in 1999, contains rigid skeleton and permanent porosity. The three dimensional extended network was constructed by Zn_4O tetrahydron cluster and 1,4-benzenedicarboxylate(BDC) (Figure 1-1). The framework formed by directional organic linkers and metal clusters, and the solvent left after the synthesis process was encapsulated. Subsequent activation gave rise to the permanent porosity instead of the collapse of the framework.[12]

MOFs/PCPs are often analogous to zeolites because they have large specific surface areas, high porosity, and high crystallinity, but their frameworks are more flexible.[13] Compared with traditional inorganic-organic hybrid materials, MOFs havs the characteristics of structural design,[14] adjustable pores,[15] and surface modification,[16,17] so it is potenially and widely applied in gas adsorption and storage,[18] catalytsis,[19] electrically conductive,[20] sensing[21] and other fields.[22,23]

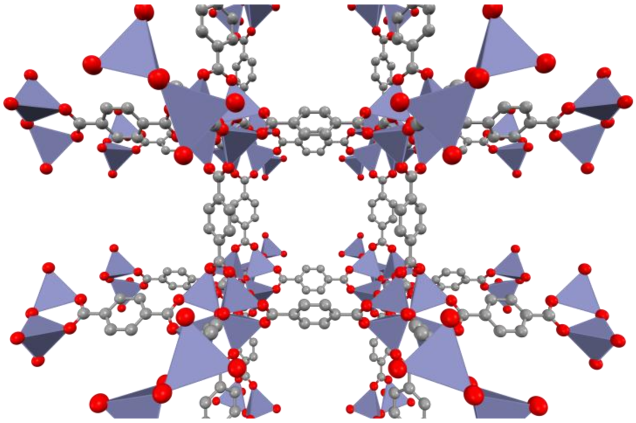

Figure 1-1. Crystal structure of **MOF-5** . [12]

1-1-2. Covalent Organic frameworks (COFs)

Since the initial reported of the COF case, **COF-5**, by Yaghi and co-workers in 2005 (Figure 1-2),[6] covalent organic frameworks (COFs), which comprised the light elements (including C, H, O, B, N atoms) in the scaffold, connected through covalent bonds, and extended in to two or three dimensional networks, have been emerged as another class of porous crystalline materials featured with highly ordered structures, permanent porosity, high stability, achievable surface modification and so on.[24]

Distinguished by dimensionality, COFs can be divided into two- or three-dimensional networks[25] (Typical symmetric monomers for the synthesis of COFs shown in Figure 1-3). The eclipsed layered structure of two-dimensional COFs can provide a unique way to construct ordered π systems, and which could not be achieved

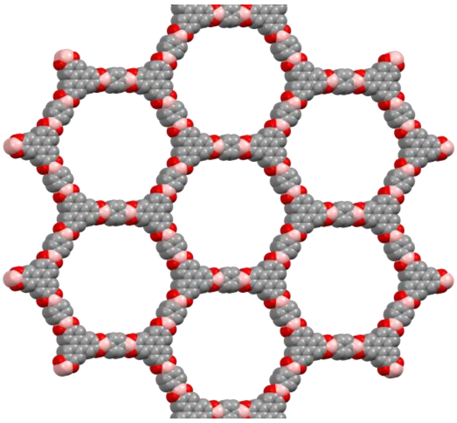

Figure 1-2. Crystal structure of **COF-5**.[6]

by traditional covalent or non-covalent bonds. The π orbitals in its layered structure could directly generate great electronic coupling, thereby effectively promoting the conduction of carriers in its internal π channel.[26] Based on this, it could be utilized as a new type of organic semiconductor materials,[27] not to mention optoelectronic functional materials;[28,29] 3D COFs have spatial networks with more complicated pore structures, high surface area compared with 2D COFs. In addition, modifying the pores inside of COFs or introducing functional guest molecules can also endow COFs with abundant functional properties.[30]

Solvothermal synthesis is the traditional method to obtain COF materials in sealed vessel, affected by many factors including temperature, pressure, reaction time, the volume ratio of solvent and the catalyst.[31] Obviously, if COF materials are to be mass-produced and applied in suitable scenarios, it is necessary to explore other suitable synthesis methods. Through the efforts of researchers, effective methods including microwave, mechanical, ultrasonic synthesis, ionothermal synthesis, and linker replacement strategy have been developed.[32] Diverse synthetic methods provide the possibility for the popularization of functional COF materials.

During the development, crystallinity has always been the common issue, which makes it difficult to obtain an accurate single crystal structures of COFs. At this stage, the structures are mainly determined by simulation, supplemented by the comparison of the PXRD spectrum obtained from the experiment and the simulated ones. However, there are still some COF single crystal structures reported.[33,34,35]

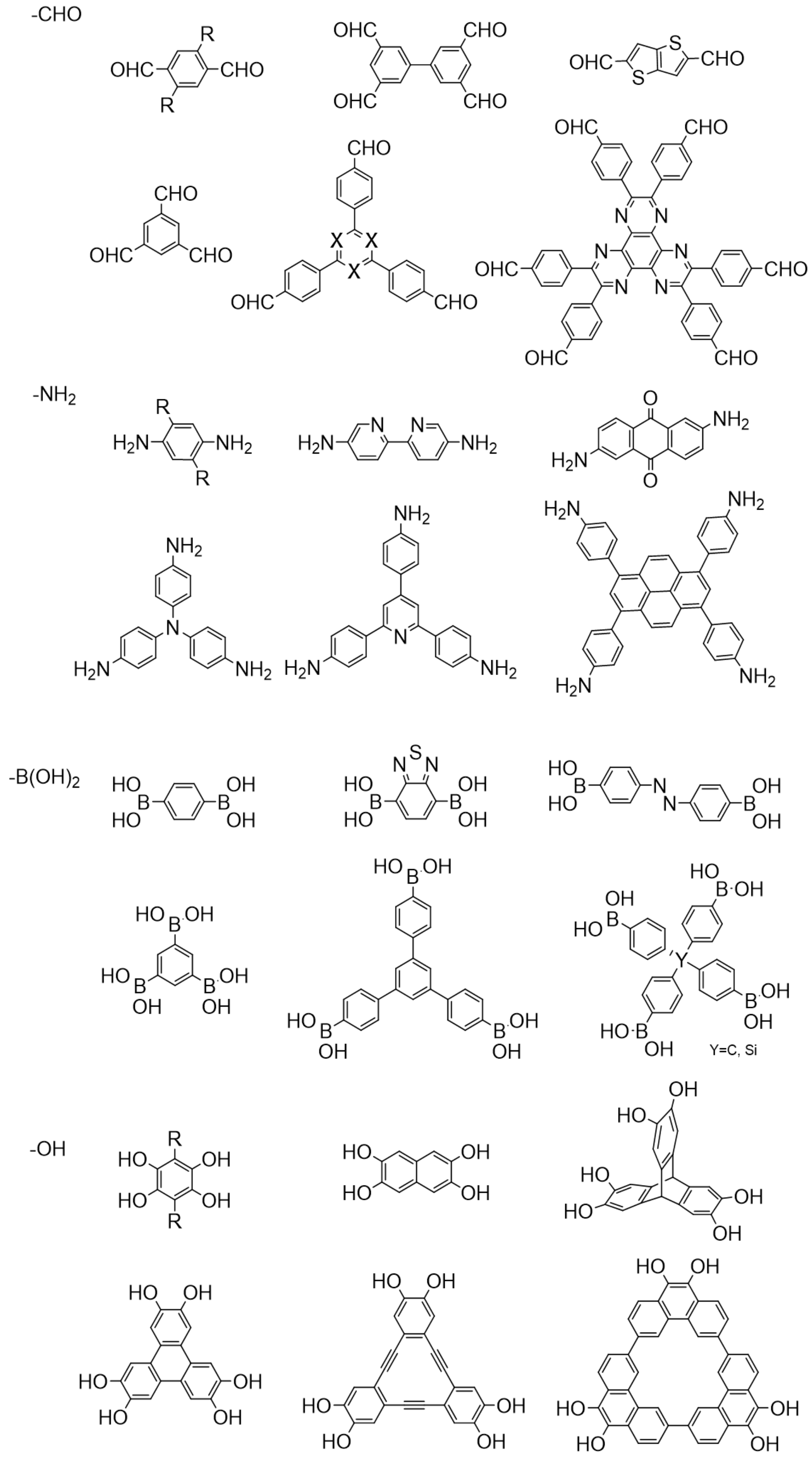

Figure 1-3. Typical monomers of COFs.

1-1-3. Porous Organic Cages (POCs)

Porous organic cages are a class of porous organic molecular materials with cavities, playing an important role in the field of supramolecular chemistry.[36] It consists of discrete building units stacked through weak interactions in the solid state.[37] Compared with MOFs and COFs, they have unique advantages in solubility, which not only facilitates the purification of molecular cages, but facilitates their preparation into corresponding thin-film materials[38] and functional devices.[39,40]

The first case with shape-persistent cage was reported by Fritz's group in 1984, which expressed the coordination performance with Fe^{3+} than **EDTA**.[41] Cooper's group has made excellent contributions in the field of porous material, the same in organic porous cages. In 2009, they reported a series of tetrahedral cages linked by imines, and only Cage **3** (Figure 1-4c) retained the original crystal structure and symmetry after the thermal desolvation. Cage **1** (Figure 1-4a) underwent a crystal-to-crystal transition to monoclinic $P2_1/c$ symmetry with 12% reduction in unit cell after the solvent was removed by slow heating. The acetonitrile in Cage **2** (Figure 1-4b) spontaneously volatilized within 30 min, resulting in the failure to maintain the structure.[42]

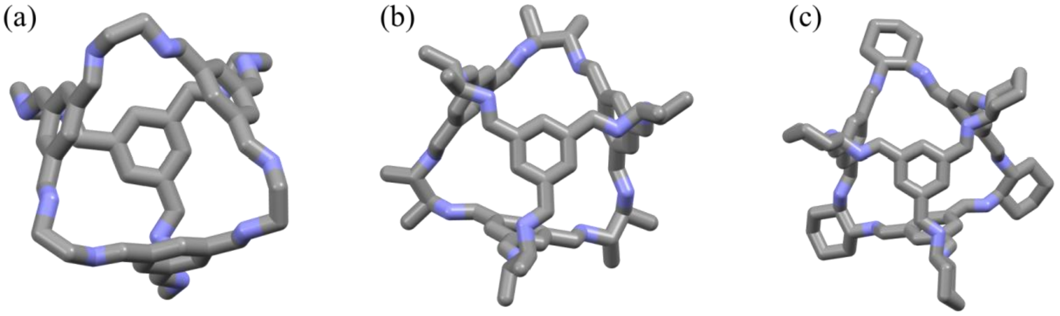

Figure 1-4. Structures for cages 1 (a), 2 (b), and 3 (c).[42] Hydrogen atoms are omitted for clarity.

It is obvious that the partially imine-based cage structures could not be effectively maintaining its original structure after undergoing the loss of solvent molecules. An alternative approach, boronate condensation, was introduced. Mastalerz and colleagues obtained long-lasting, porous [8+12] cages based on this approach in 2014.[43] The organic cage containing the 3.1 nm of inner pore diameter had the largest specific surface area so far, reaching 3758 cm^2 g^{-1}. It is undeniable that boronate group, a classical dynamic covalent bond, is too sensitive to moisture, resulting in an instable cage structure.

In addition to the above two linkages, Doonan et al. also reported a fully carbon-carbon linked cage molecule **C1** (Figure 1-5a). Rapid precipitation of **C1** molecules can generate permanent polymorphic **C1β** and show a high specific surface area of 1153 m^2 g^{-1}, on the contrary, slow crystallization yields **C1α** (Figure 1-5b), which exhibits non-porous property through N$_2$ adsorption.[44]

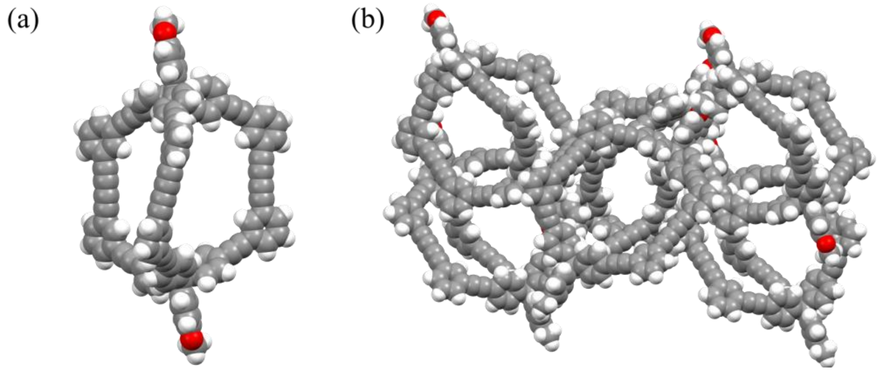

Figure 1-5. Representations of the structures of **C1** (a) and **C1α** (b).[44]

Nowadays, it is clear that researchers can design and synthesize various POCs with different shapes and sizes through coupling reactions,[37] but there are few examples with large cavities (inner diameter > 2 nm).[43] In addition, the networks of the large-cavity organic cages easily collapsed after the inside solvents were removed; it is not easy to crystallize this kind of large cages and conduct structural analysis, because of lacking heavy atoms in the structures.[45]

1-1-4. Hydrogen-bonded Organic Frameworks (HOFs)

Hydrogen-bonded organic frameworks (HOFs), with the alternative name of supramolecular organic frameworks (SOFs), self-assembled by pre-organized intermolucular hydrogen bonds between organic moieties, also is one sub-category of porous organic crystalline materials.[46,47,58] It also can be classified into porous molecular crystals (PMCs),[119,120,121] when the H-bonding was involved to support the porous structures.

MOFs / PCPs are constructed from organic linkers and metal nodes by coordination bonds.[48] The covalent bonds in COFs have an extremely important role in the stability of host framework. However, it is notable that direct crystallization of high dimensional COFs were proved to be a tough work in consideration of free energies in covalent structures.[49] HOFs, with hydrogen bonding and no metal nodes, possess the advantages of (1) solution processability, (2) easy purification, and (3) regeneration (Table 1-1). All these merits arouse much attention of researchers to develop the systematic design strategy and improve the permanent porosity, as well as the application prospect[50] beyond the lab synthesis in recent years.

Due to the above-mentioned advantages, HOFs become potential materials with great application. However, the relatively small bonding energy and poor directionality of hydrogen bonds still provide some resistance to the development. Compared with MOFs and COFs, it is more difficult to obtain HOFs with the pre-designed structures because their final structures are easily affected by the selection of solvent during the crystallization and the ambiguous intermolecular forces during the self-assembly process.

Table 1-1. Comparison of HOFs with MOFs and COFs.[58]

	MOFs	COFs	HOFs
Building unit	Hybrid	Organic	Organic
Connectivity	Coordination bond	Covalent bond	Hydrogen bond
Synthesis	Solvothermal etc.	Solvothermal etc.	Recrystallization etc.
Porosity	Micro/mesoporous	Micro/mesoporous	Mostly microporous
Density	High	Low	Low
Crystallinity	High	Modest	Pretty high
Chemical stability	Sensitive to humidity	Excellent	Good water stability
Recyclability	Troublesome, weak	Troublesome, excellent	Simple, excellent
Designability	Good	Excellent	Moderate

Another key point to be clear is that the activation of HOFs has always been a tricky challenge, given by the unstability of hydrogen bonds. The release of guest molecules would lead to the collapse of the frameworks. Therefore, researchers focus on the exploration of the systematic strategies to obtain HOFs with permanent porosity.

Hydrogen bonding units and organic backbones are two fundamental parts of HOFs, which determines the diversity of architecture and structural stability. The hydrogen bond donors and acceptors in organic building blocks could form H-bond units directly. Some supramolecular synthons composed of multiple hydrogen bonds are more rigid than that contain single pairs of hydrogen bonds. The rigid organic backbones facilitate the formation of robust frameworks, which can avoid the structural instability caused by flexibility of scaffold.

The development of HOFs started from obtaining a two-dimensional hydrogen-bonding network based on benzene-1,3,5-tricarboxylic acid. In 1969, the first case[51] was reported by Duchamp and Marsh, featuring the nonporous crystal caused by interpenetration of undulated honeycomb sheets. The honeycomb sheets linked through hydrogen bonds provided by carboxy groups. In 1987, Herbstein and coworkers introduced long-chain template molecules during the crystallizaion, and successfully obtained a structure containing one-dimensional honeycomb void.[52] Till now, the introduction of templating agents is still an effective method to construct porous HOF materials. In the 1990s, Wuest and colleagues devoted great efforts to the development of HOFs based on the strategy of molecular tectonics.[53,54] In 2011, a DTA-based HOF, also called after **HOF-1,** was verified by Chen's group, the first case of microporous HOFs with permanent porosity. The activated **HOF-1a** exhibited efficient selective adsorption and separation of C_2H_2 / C_2H_4 at ambient temperature,[55] thus setting off the booming development of HOF materials in the field of gas absorption and separation. In 2017, based on the research of Mastalerz and Oppel,[56] Cooper et al. obtained a HOF named **T2-γ** (Figure 1-6b) based on the **T2** molecule (Oppel et al. named it as triptycene trisbenzimidazolon,**TTBI**) (Figure 1-6a) through a combination of prediction and experiment, of which the BET surface area reached to 3230 cm^2 g^{-1}. This material holds the record of largest BET surface area based on HOFs and the lowest density of the molecular solids in the Cambridge database.[57]

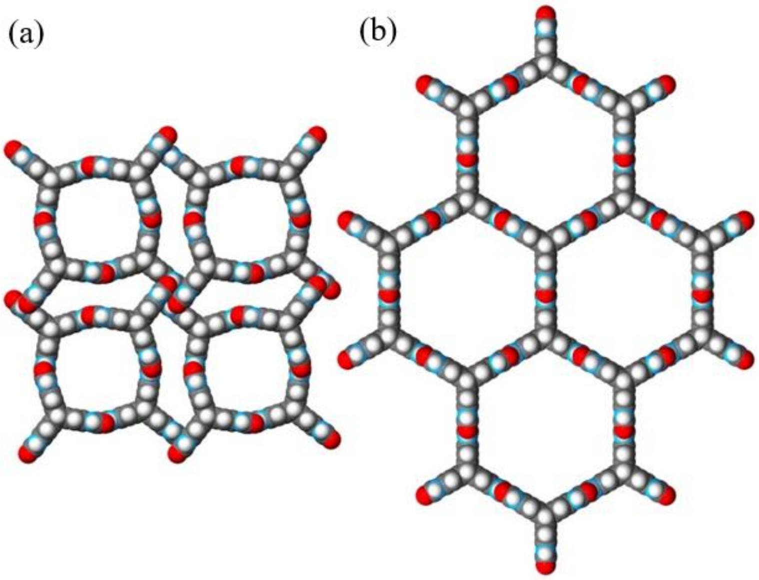

Figure 1-6. Structures of HOF **TTBI** (a) and **T2-γ** (b).[56,57]

1-2. The background and defination of Hydrogen bond

Hydrogen bond is a unique non-covalent bonding phenomenon that widely exists in chemistry[59,60] and biology.[61] The concept of non-covalent interactions related to hydrogen bond could date back to the early 20th century.[62] The definition of hydrogen bonding has been evolving. The term of hydrogen bond was first proposed by Pauling to describe the 'residual entropy' of ice in 1935.[63] Soon after, Pauling clearly put forward the concept of hydrogen bond in his book, pointing out it a kind of electrostatic force of attraction.[64] In the decades that followed, the definition of hydrogen bond has been undated, but was still inaccurate.[65,66] Until 2011, the IUPAC gave an evidence-based, generalized definition of hydrogen bond, which expressed as *' the hydrogen bond is an attractive interaction between a hydrogen atom from a molecule or a molecule fragment X-H in which X is more electronegative than H, and an atom or a group of atoms in the same or different molecule, in which there is evidence of bond formation'*.[67] In 2013, the team from National Center for Nanoscience and Technology of the Chinese Academy of Science made the pioneering process, utilizing noncontact atomic force microscope (NC-AFM) to successfully capture images of hydrogen bonding (Figure 1-7) formed by 8-hydroxyquinoline (8-hq) molecule on a Cu(1 1 1) substrate, accurately determining the bonding sites, orientations and lengths, which provided a favorable visual evidence for hydrogen bonding.[68]

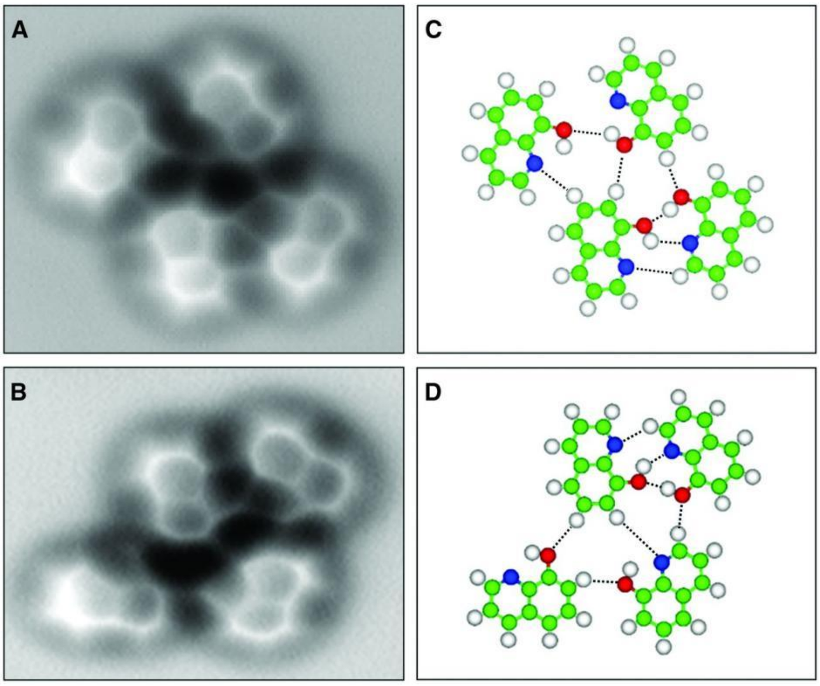

Figure 1-7. AFM measurements of 8-hq assembled clusters on Cu(111). (A and B) Constant-height frequency shift images of typical molecule-assembled clusters and their corresponding structure models (C and D). Imaging parameters: V = 0 V, A = 100 pm, $\Delta z = +10$ pm. Image size: (A) 2.3 by 2.0 nm; (B) 2.5 by 1.8 nm. The dashed lines in (C) and (D) indicate likely H bonds between 8-hq molecules. Green, carbon; blue, nitrogen; red, oxygen; white, hydrogen.[68]

Early views on the hydrogen bond were based on the directional interaction of water molecules ($O^{\delta-}—H^{\delta+}\cdots O^{\delta-}$). After further expansion, it can be represented by $X\text{-}H\cdots Y\text{-}Z$ (or $X^{\delta-}$ - $H^{\delta+}\cdots Y^{\delta-}$, details listed in Table 1-2[69]), where $\cdots$ represents the bond formed, X-H is a hydrogen bond donor, and Y-Z is a hydrogen bond acceptor. Moreover, X, Y can be mainly O, N, F.[70] Even if there are some special cases, the energy of hydrogen bonds are widely distributed in the range of 1-170 kJ mol^{-1}, which is still lower than that of coordination bonds (90-350 kJ mol^{-1}) and covalent bonds (300-600 kJ mol^{-1})[69,71]. Therefore, hydrogen bonding is indeed much less stable than coordination bonds and covalent bonds, giving rise to the less stability of HOF materials.

Table 1-2. H-Bonds details adapted from Steiner and Jeffrey.[69,70]

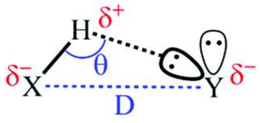	Strong	Moderate	Weak
D/Å	2.2 - 2.5	2.5 - 3.2	> 3.2
H···Y/Å	1.2 - 1.5	1.5 - 2.2	> 2.2
θ/°	170-180	> 130	> 90
X–H vs. H···Y	X–H–H···Y	X–H > H···Y	X–H ≫ H···Y
Bond energy/kJ mol^{-1}	63-167	17-63	< 17

1-3. Categories of hydrogen-bonded organic framework materials

The building blocks of HOFs are organic ligand molecules that contains sticky sites.[72] The backbones in the building blocks are referred to as term “tecton”, which proposed by Wuest et al.[73] On the other hand, hydrogen bonding interaction sites are referred to as term “synthon”, which was defined by Desiraju as “structural units within supermolecules, which can be formed and/or assembled by known or conceivable synthetic operations involving intermolecular interactions.”[74]

In order to obtain rigid and stable HOFs, it is particularly significant to select hydrogen bonds with high bonding energy and directionality. Based on the hydrogen bonding energies, we can find that intermolecular forces containing O-H···O, O-H···N, N-H···N, N-H···O are relatively strong hydrogen bonds. Common synthons that can form these intermolecular forces include carboxylic acid, diaminotrizine (DAT), pyrazole, pyridine, imidazole, urea and so on,[46] which are good candidates for providing hydrogen bonds.

1-3-1. Single-component hydrogen-bonded organic framework materials

Single-component based HOFs are composed of uniform building units through hydrogen bonding interactions, supplemented by π-π interactions or van der Waals forces to form networks. At this stage, most HOF materials appear in the form of single component, which can be classified based on different synthons. In this part, some HOFs based on carboxylic acid and diaminotriazine (DAT) will be included.

1-3-2-1. Carboxylic acid

A carboxylic acid is one of the simplest functional groups used to make molecular self-assembly in hydrogen-bonded organic frameworks.[75,76,77] Several different self-association modes have been in existence: (1) linear dimer (2) linear chain (3) ring(R) (Figure 1-8). Among the modes, the ring synthon is the most characteristic and widespread mode of -COOH based hydrogen-bonded organic framework materials. Taking carboxy dimer $R_2^2(8)$ as an example, '2' and '2' represent the number of H-bond donors and acceptors and '8' means 8 atoms in one ring.[76]

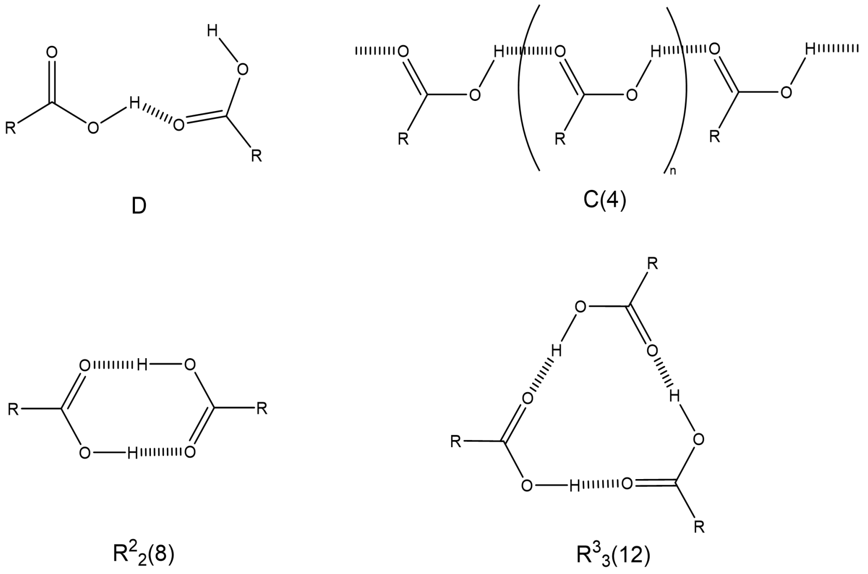

D

C(4)

$R^2_2(8)$

$R^3_3(12)$

Figure 1-8. Some self-association modes of carboxylic groups.[76]

The first appearance of carboxy dimer in HOFs was in the study of the self-assembly process of trimesic acid. The material did not show permanent porosity due to the interpenetration in the structure.[51] In 2019, Cooper et al. consumed passion on new insight of this old molecule through computational prediction that trimesic acid should have a low-density packing stable structure **δ-TMA** and successfully screened **δ-TMA** using high-throughput crystallization experiments. The BET surface area can reach to 920 m^2g^{-1}. In fact, the stability of **δ-TMA** is still ordinary, and it can be easily converted into non-porous **α-TMA**.[79]

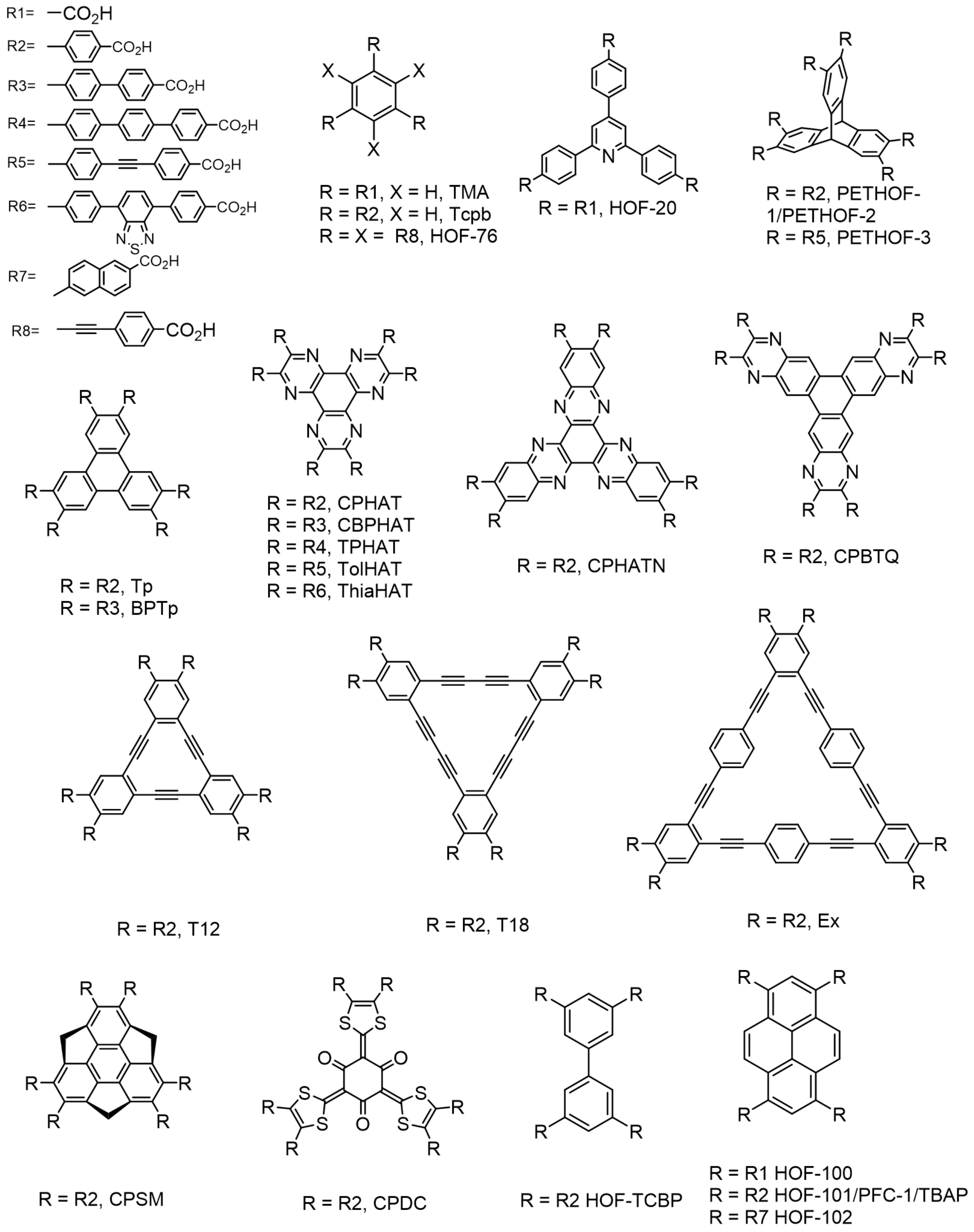

Figure 1-9. Some reported organic building blocks containing carboxylic acids for the construction of HOFs.

Starting from the simplest carboxylic acid based organic building block — trimesic acid,[51,52] researchers have devoted plenty of efforts to design and synthesized a wide variety of building block molecules containing carboxyl groups for construction of the corresponding HOFs (parts of the molecules shown in Figure 1-9). The relatively strong attractive force and good directionality of the carboxylic acid dimer are well reflected in these materials. Notably, most molecules prefer elongated arms such as carboxyphenyl acids. Compared with the only -COOH, the longer arms make sense to improvement of solubility of the molecules and enhancement of the π-conjugation. Most importantly, relatively larger pores could be created accompanying with increase the porosity of HOF.[8,116]

HOF-TCBP was recrystallized by slow volatilization of **H_4TCBP** dissolved in N,N-dimethylformamide (DMF). This HOF material exhibited the advantages of extreme high stability and easy regeneration. It could be found that there is a 1D rhombic channel with the size of 17.81 × 26.34 Å along the *a* axis. The activated material could adsorb 535 cm^3 g^{-1} of N_2, and the BET surface area was calculated around 2066 cm^2 g^{-1}, as well as the 56% of void space. These excellent intrinsic properties made **HOF-TCBP** a good candidate for selective adsorption and separation of light hydrocarbons. Although **H_4TCBP** molecule had a flexible conformation, the five-fold interpenetration in the structure anchored the dihedral angel of center phenyl rings at 36.86°, and that between four outer arm moieties and inner biphenyl rings at 31.29°.[80] The interpenetration contribute to the improvement of the rigidity and stability of the networks, sometimes the decrease of porosity of the materials.[81] O. K. Farha and J. F. Stoddart et al. successfully formed interpenetration isomerism HOFs by using of solvents with different sizes, **PETHOF-1** with a two-fold interpenetrated structure and **PETHOF-2** with a five-fold interpenetrated structure.[118]

Introduction of planar structures with large π conjugated systems is also a feasible method to obtain stable frameworks.[82] Based one pyrene[83] derivatives, some HOF materials with functional properties have been reported. **PFC-1** was first prepared by

Cao and coworkers for synergistic chemo-photodynamic therapy through encapulating doxorubicin(Doxo),[84] which was also known as **TBAP-α** with excellent performance of proton reduction in water.[85] As for **HOF-102**, an analogue with the R7 exchanged arm ashown in Figure 1-9, its fiber composite could be applied in photochemical detoxification of a mustard gas simulant.[86] The same group also found that the electrochemical parameters of **HOF-102** are suitable to support electrocatalysis with catalysts added.[87] Similarly, **HOF-76**, which crystallized from **HCEB** containing π-conjugated system of six alkynyls and phenyl rings, performed excellent stabilities.[117]

Our group have been working on the construction of HOFs base on carboxylic acids combined with π-conjugated cores. The C_3-symmetric π-conjugated cores containing triphenylene (**Tp**),[88] hexadehydrotribenzo[12]annulene (**T12**),[89] dodecadehydrotribenzo[18]annulene (**T18**),[90] expanded cyclic phenylene ethynylene derivatives (**Ex**)[91] and hexaazatriphenylene (**HAT**)[92,93] were selected. Most of these materials have permanent porosity as well as excellent stability. In particular, **CPHATN-1**, a hexaazatrinaphthylene-based hexatopic carcoxylic acid HOF, showed reversible vapor acid-induced color changes because of protonation/deprotonation of nitrogen atoms in the cores.[94]

1-3-1-2. Diaminotriazine (DAT)

DAT is a very powerful functional group for construction of stable porous HOFs, because it comprises multiple sites, which can be used to form multiple hydrogen bonds. The different models can be obtained through hydrogen bonding between two DAT molecules, including head to head, head to waist, and waist to waist (Figure 1-10). The remaining two amino groups in the dimer can be connected with the surrounding DAT to extend into 2D or 3D networks.[95]

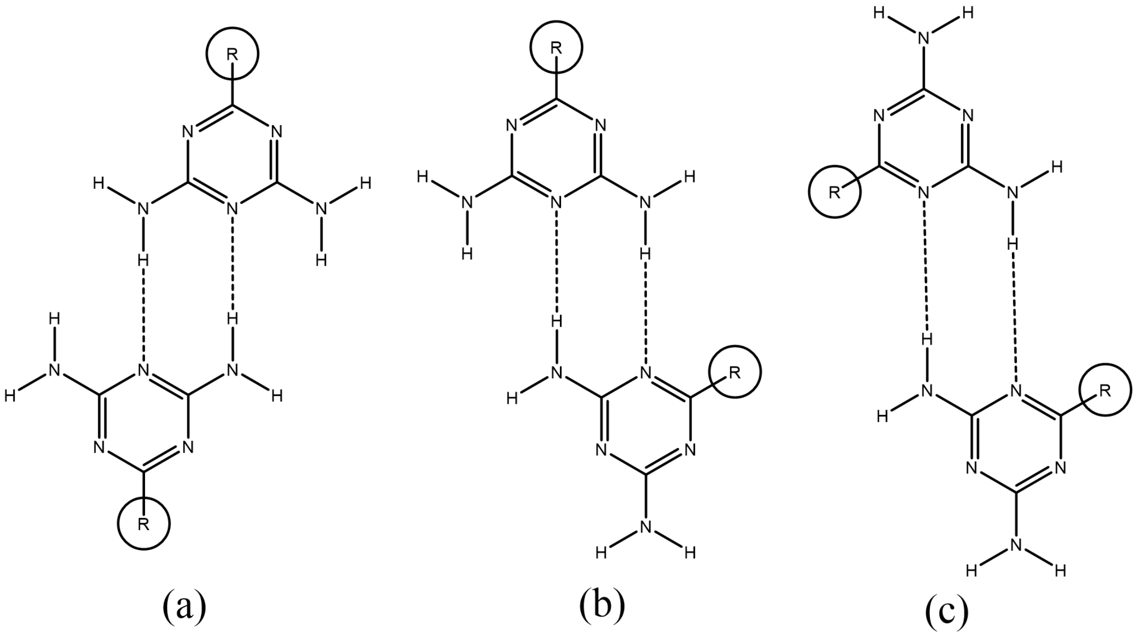

Figure 1-10. Interaction Motifs of DAT Groups: (a) Head-to-Head (Motif I), (b) Head -to-Waist (Motif II), and (c) Waist-to-Waist (Motif III) Patterns.[95]

Wuset and coworkers constructed the first example of DAT-based porous HOF.[53] The first DAT based HOF possessing permanent porosity, also named on **HOF-1**, showed BET surface area of 359 cm^2 g^{-1}, and good thermal stability up to 420 °C, which can be applied in selectively separation of C_2H_2 / C_2H_4 at ambient temperature.[55] Subsequently, Chen and coworkers assembled a series of HOFs relying on DAT.[96-103] Especially in **HOF-6**, the DAT moiety was found to form Motif I and Motif II. Among the structure, Motif I helped to generate two-dimensional layers, and Motif II helped the adjacent layers link and expand into three-dimensional networks.[101]

1-3-2. Multi-component hydrogen-bonded organic framework materials

When HOFs are formed from multi-component building blocks, hydrogen bonds could be formed between different components. In that case, the formation modes of hydrogen bonds are more flexible and diverse. Because of multiple tectons induced, the structural versatility will increase effectively.[8] In addition, strong acidic and basic components can also be utilized to form charge-assisted hydrogen bonds in favour of improvement of the stability in networks.[82]

The binary design strategy was proposed by J. Lv and coworkers, aiming to construct stable networks with porosity.

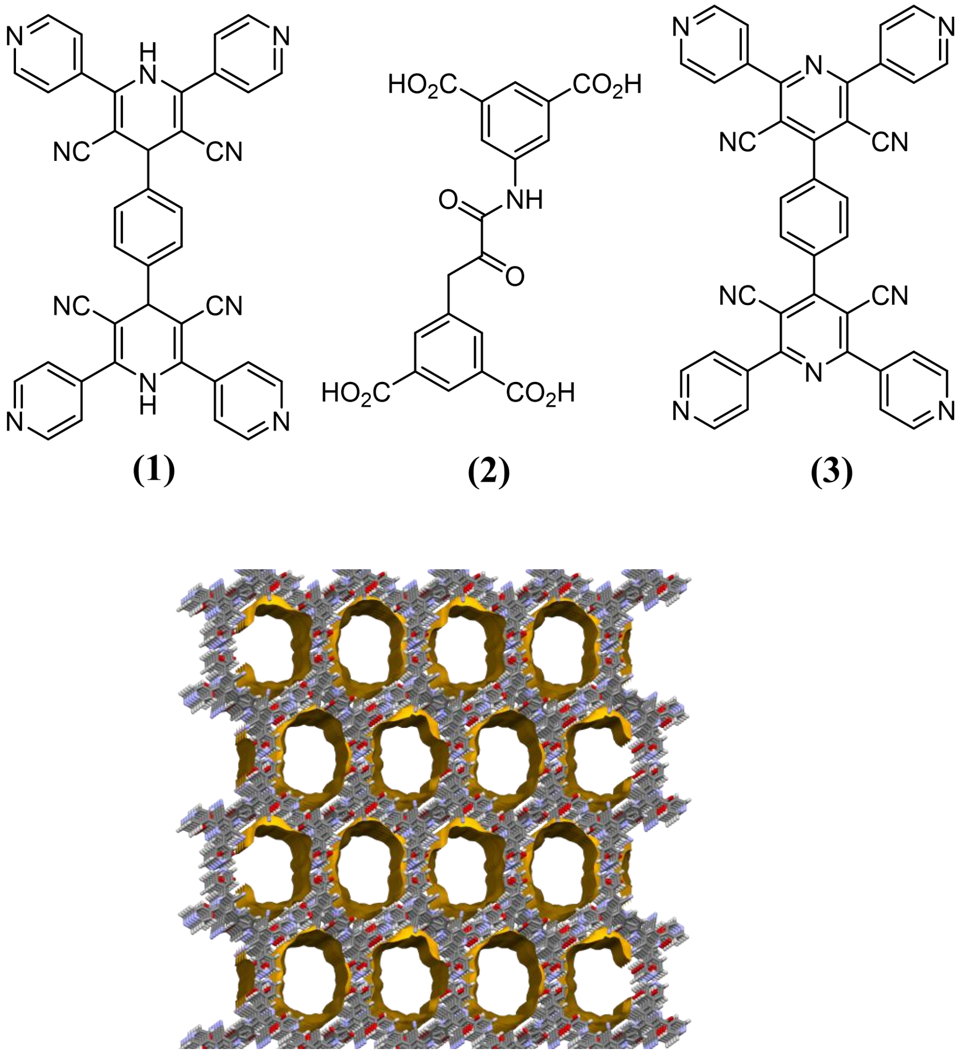

Figure 1-11. Organic modules for constructing **SOF-7** and the 3D structure of **SOF-7** containing 1D channel.[104]

Based on this strategy, **SOF-7** (Figure 1-11), showing excellent stability and permanent porosity, was constructed by modules **1** and **2** in the ratio of 1:1 via solvothermal method. It is worth noting that module **1** appears as in situ oxidation product **3** in the structure.[104]

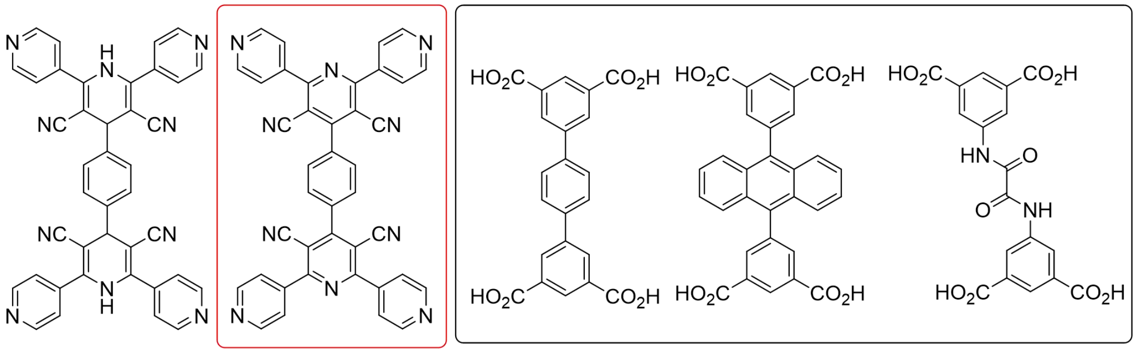

(1) **(2)** **(3)** **(4)** **(5)**

Figure 1-12. Organic modules for constructing **SOF-8**, **-9**, **-10**.[105]

After confirming the feasibility of the binary design strategy, the same research group successively prepared **SOF-8** with 2D stacking layers , **-9** and **-10** with 2D to 3D inclined layers (Figure 1-12). The 3D polycatenated networks were obtained through controlled assembly and the structural regulation was making for better adsorption capacity and selectivity of CO_2.[105]

Porous organic salts constructed from charge-assisted hydrogen bonding is another multi-component HOF material. The key to build such kind of material is to strengthen the ionic bonds formed between acids and bases, resulting in stable POSs.[106] Tohnai et al. constructed a **d-POS** (Figure 1-13) by using disulfonic acid derivative and triphenylmethylamine (TPMA) as a combination of sulfonate anions and ammonium cations. The stable open framework of the obtained **d-POS** enabled the reversible and selective adsorption of gases and organic molecules. The **d-POS** also can exhibit color- and intensity-tunable fluorescence behavior depending on guest molecules.[107]

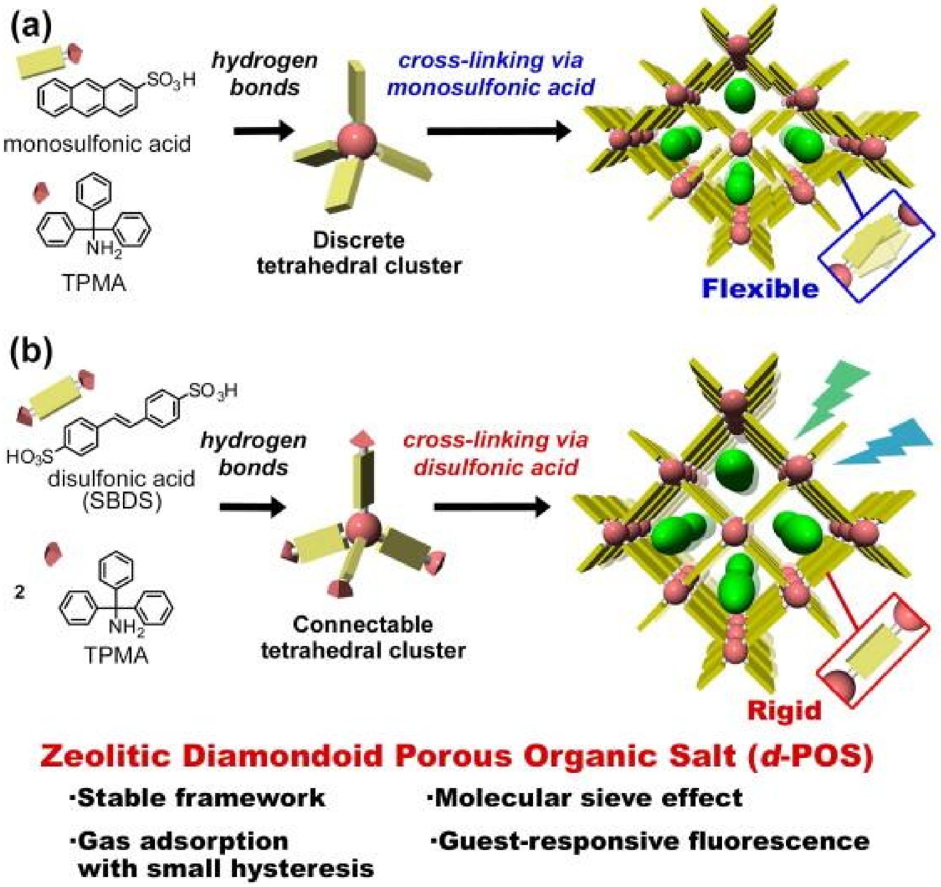

Figure 1-13. Schematic representation of hierarchical construction of diamondoid porous organic salts (**d-POSs**) applying (a) monosulfonic acid and (b) disulfonic acid.[107]

The guanidinium cations and the sulfonate moieties can establish the charge-assisted hydrogen bonds in the form of [(G)N−H···O(S)]. Along this line, **HOF-GS-10** and **-11** (Figure 1-14) were constructed by Ghosh and coworkers. In particular, the proton conductivity of these two HOF materials reached the level of 10^{-2} under the condition of high humidity and room temperature. It broadened the potential application of HOF materials in the filed of full cells.[108]

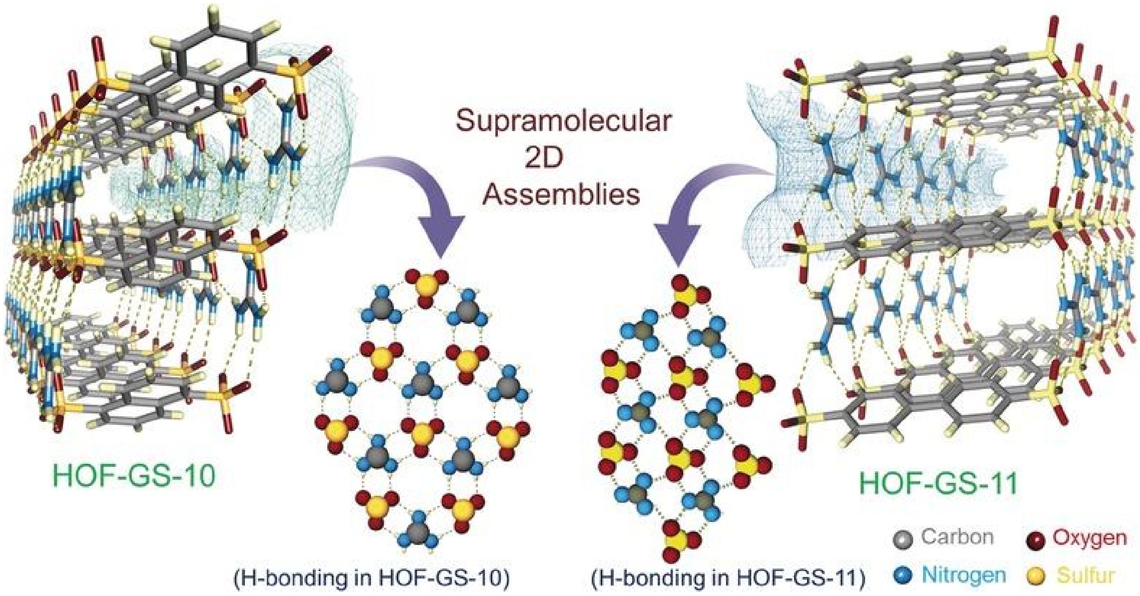

Figure 1-14. Frameworks of **HOF-GS-10** and **HOF-GS-11** and interactions in these two compounds.[108]

1-4. Preparation methods for HOF materials

1-4-1. Solvothermal synthesis

In a closed system with a certain temperature and pressure, an organic solvent is used as a medium. The reactants are dispersed in the liquid phase or supercritical conditions. The product would form during the heating process or precipitated during the cooling process. In 2011, Lv et al. obtained a binary SOF material named **SOF-7** based on this method. By dissolving the two monomer components in DMF at a molar ratio of 1:1 and reacting at 90 °C for 72 h, orange prismatic crystals were obtained.[104] In his subsequent studies, three other binary materials named as **SOF-8**, **-9**, **-10** were also obtained. The different components were mixed and dissolved in DMF, then the reaction mixture was transferred to a 15 mL pressure tube and heated in an oil bath at 90 °C accompanying with autogenous pressure. Orange crystals were obtained in three days.[105]

1-4-2. Slow evaporation

This method utilizes the principle that the solute is precipitated in a supersaturated solvent, which is directly related to the boiling point and volatilization rate of the solvent. Most HOFs materials were obtained through this method. The general operation process is that an appropriate amount of organic component was dissolved in suitable good solvent completely by means of ultrasound or heating, and insoluble impurities were removed with filter membrane. Finally, the mixed solution was transfer to a new vial, and evaporated naturally. To increase the evaporation rate, the vial containing solution could be placed on a heating plate set in a suitable temperature. The method was widely used in this thesis(in **Chapters 2**, **3**, **4**).

1-4-3. Slow liquid/vapor diffusion

The method is based on differences in the solubility of solutes in different solvents. The solute is easily soluble in a good solvent with a higher boiling point, and slightly soluble or insoluble in a poor solvent with a low boiling point. A certain amount of poor solvent is slowly added to the saturated or near-saturated solution in which HOF molecules are dissolved, and it is sealed and kept. It is the slow diffusion of ligand molecules from good solvents into poor solvents, accompanied by the precipitation of crystalline products. It is similar to the liquid-phase diffusion method, but the difference is that the solution containing the ligand molecules is placed in an atmosphere containing a low-boiling poor solvent, and it is sealed for a period of time, so that the poor solvent is volatilized to dissolve the ligand molecules. In the solvent, the ligand diffuses slowly, and the crystalline product is precipitated due to the difference in solubility.

1-4-4. Electrophoretic deposition technology

To fabricate HOF film materials, the electrophoretic deposition (EPD) can be utilized, which has the advantages of low cost, simple equipment, thickness-controlled, and modifiable. HOFs can be deposited on various substrate plates such as Zn plates, Mg alloy plates and FTO glasses(shown in Figure 1-15).[109] In addition, the thickness and morphology of the deposited layer can be adjusted by changing the deposition time and applied voltage. The general steps show follows. Firstly, it is usual to select a suitable substrate plate as the working electrode and the counter electrode. After being cut into two plates with the same size and shape, the substrate plates are washed sequentially with deionized water, acetone and ethanol in an ultrasonic bath for 10-20 min, and dried. Next, HOFs were dispersed in CH_2Cl_2 solution and sonicated for 5 min. Then, the two substrate plates are immersed in the deposition solution. The DC voltage of 15-90V and applied times are adjustable, which are two influence factors of thickness and morphology of films. Finally, a thin film can be obtained at the anode (working electrode).[110,111]

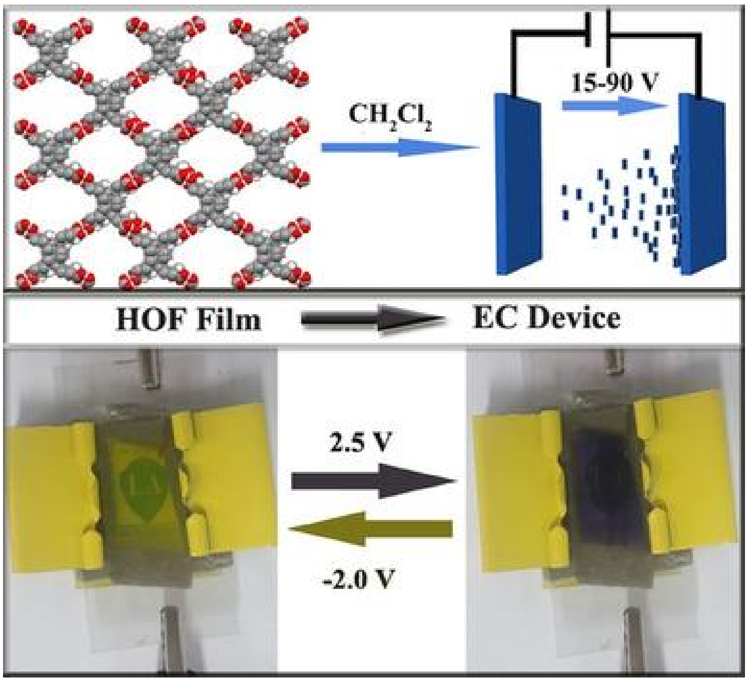

Figure 1-15. Fabrication of HOF films by EPD (C gray, H white, O red).[110]

1-4-5. Machanochemistry

Besides the solvents-based methods, mechanochemical method is an alternative choice. Mechanochemical reaction by grinding has emerged as the powerful solvent-free synthesis tool in a wide range of field, enabling certain synthetic strategies, reactions, and target compounds that were previously unattainable. This method eliminates the consumption of large quantities of reaction solvents and offers the possibility to reduce the generation of waste.[112] Liu and Cao et al. prepared a series of nano-sized HOFs and derivatives loaded with Pd nanoparticles by ball milling (Figure 1-16), and confirmed the feasibility of mass production of HOF materials by ball milling. Taking HOF **PFC-1** as an example to describe the general preparation process. An appropriate amount of **H_4TBAPy** powder was taken into a 25 ml stainless steel container equipped with two stainless steel balls. After adding 100 μl ethanol, the container was placed on the machine. The mixture was transformed to pale yellow powder through grounding at a frequency of 15 Hz for 20 min.[113]

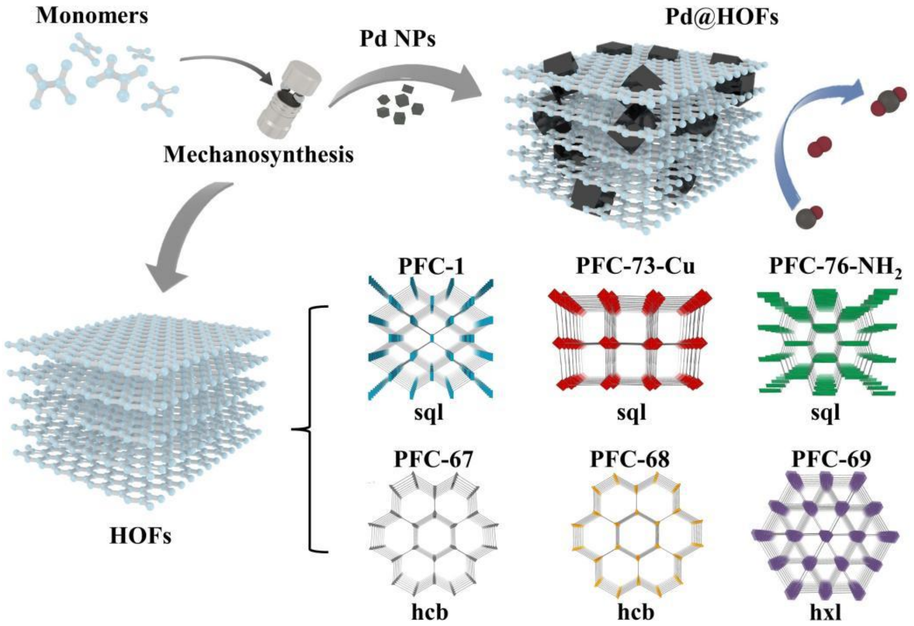

Figure 1-16. Diagram for mechanical synthesis of HOFs and Pd@HOFs .[113]

1-5. Gas adsorption and separation

The selective gas adsorption and separation is the process of realizing the separation and purification of mixed gas according to the difference in the adsorption capacity of different components. HOFs are suitable candidate as adsorbents because of their tunable pore shape and size, as well as the pore surfaces capable of being modified. Rational design of HOFs with specific pore size and shape or introduction of active sites for adsorption is the effective method to achieve the excellent capacity of gas adsorption and separation.

Excessive CO_2 emission leads to global climate problems, so the emission reduction has attracted extensive attention of scientific researchers around the world. The development of CO_2 adsorbents with high adsorption capacity and good selectivity is of great significance for alleviating the greenhouse effect.[114] In general, the frameworks have a stronger interaction force with CO_2 than that with N_2, which shows better performance in selective adsoption of CO_2 / N_2. Taking our own research as an example, **BTIA-1a** hardly absorbed N_2, however, showed a good capacity of CO_2 adsorption, reaching 172 cm^3 (STP) g^{-1} at 195 K.[115]

1-6. Increasing of rigidity and permanent porosity in HOFs

The only hydrogen bonds in HOF materials may be week enough for construction stable structure with permanent porosity. Some HOFs exhibit relatively poor stability, and are prone to structural transformation and even collapse during the activation. Meanwhile, when microcrystals are formed during the transformation process, it is difficult to explore the transformation mechanism because their structures cannot be accurately obtained through common instruments and techniques. In order to improve the stability of HOFs, researchers have explored several effective methods, including (1) Utilizing larger π-conjugated systems; (2) Introduction of multiple hydrogen bonds; (3) Interpenetration existing in the structures; (4) Electrostatic interaction.

1.7 Research purpose

As a class of porous crystalline materials, HOFs have the merits of adjustable pore size and shape, permanent porosity, relatively high surface areas and functionalization. Due to the reversibility of hydrogen bonding, this kind of materials also have the unique advantages of solution processability and essy regeneration. These merits make it a reliable platform for multiple application.

Nonetheless, HOFs with high stability are rarely reported because of the weak bonding energy of hydrogen-bonding, which limits the development and application. Previously few methods for construction of rigid HOFs with permanent porosity have been reported. The π-π interaction combined with hydrogen bonds are proved to be an useful mean to form HOFs with permanent porosity. However, its intensity and orientation are too weak to be effectively controlled. In addition to the π-π interaction, another building interaction different from that working for the formation of the primary 2D network.

In connection with this, I propose that: two kinds of interactions, such as directional hydrogen bond between carboxy groups and slip-stacking of benzo[c][1,2,5]thiadiazole (BT) groups with unidirectional alignment, can provide a well-defined stable 2D porous HOFs. The author's hypothesis is shown in Figure 1-17.

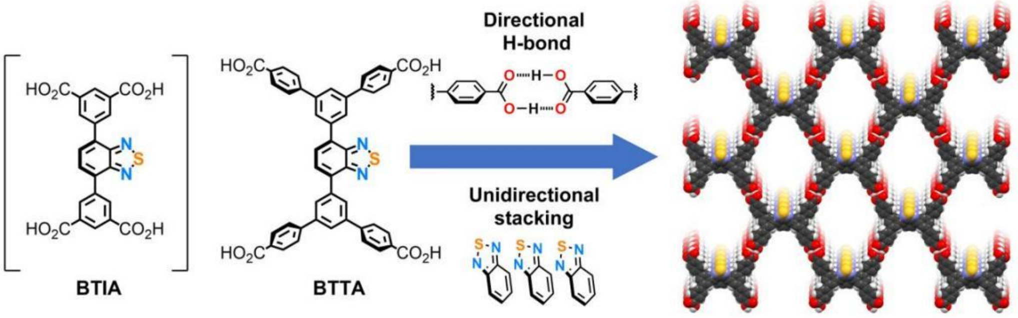

Figure 1-17. The hypothesis for construction of 2D well-defined stable porous BT-based HOFs.

On the other hand, to make HOFs better application platforms, the functionalization methods also remains to be systematically explored. In this stage, there have been three approaches for functionalization of HOFs, including: (1) Pre-incorporation of active sites into building blocks; (2) Postsynthetic functionalization; (3) Temporary masking of functional groups.

In the previous work, Pre-incorporation of active sites into building blocks has been verified to be one of good choices of functionalization. The N atoms were introduced into the building unit in advance, which did not participate in the formation of hydrogen bonds, but maintaining open sites after HOF materials obtained. Besides, it is well known that post-modification is an efficient method functionalization, which can endow materials with diverse properties. However, complex post-modification operations and tedious characterization processes are required, adding difficulty to achieve the target.

In the case of temporary masking, it is a useful approach because of easy process and potential for generalized application. However, the design strategy is still ambiguous. I expect geometrically mismatched H-bonded networks could provide free carboxy groups in the pore of HOFs, which can be served as active sites in the follow-up study. The author’s hypothesis is shown in Figure 1-18.

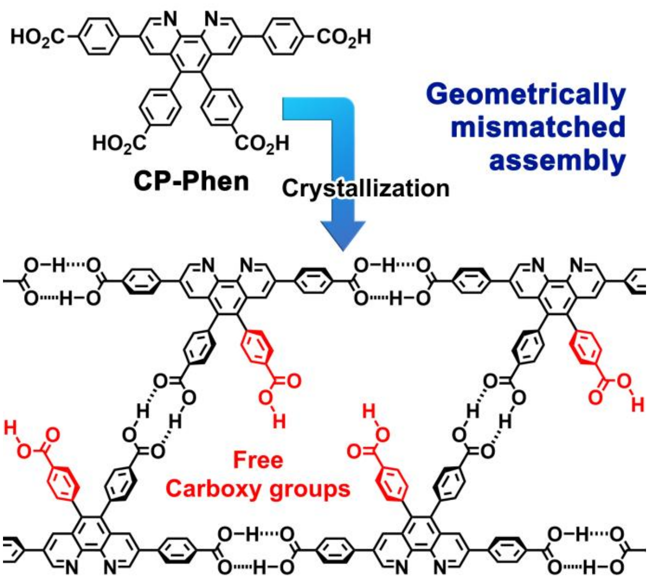

Figure 1-18. The hypothesis for construction of geometrically mismatched assembled Phen-based HOF.

Reference

1. J. Zhou, B. Wang, *Chem. Soc. Rev.* **2017**, *46*, 6927-6945.
2. Y. Xu, S. Zheng, H. Tang, X. Guo, H. Xue, H. Pang, Energy Storage Mater. 2017, 9, 11-30.
3. Z. Wang, J. Yu, R. Xu, *Chem. Soc. Rev.* **2012**, *41*, 1729-1741.
4. S. Kitagawa, R. Kitaura, S. Noro, *Angew. Chem. Int. Ed.* **2004**, *43*, 2334-2375.
5. O. M. Yaghi, G. Li, H. Li, *Nature* **1995**, *378*, 703-706.
6. A. P. Cote, A. I. Benin, N. W. Ockwig, M. O'Keeffe, A. J. Matzger, O. M. Yaghi, *Science* **2005**, *310*, 1166-1170.
7. T. Tozawa, J. T. A. Jones, S. I. Swamy, S. Jiang, D. J. Adams, S. Shakespeare, J. Parker, A. Trewin, J. Bacsa, A. M. Z. Slawin, A. Steiner, A. I. Cooper. *Nat. Mater.* **2009**, *8*, 973-978.
8. I. Hisaki, X. Chen, K. Takahashi, T. Nakamura, *Angew. Chem. Int. Ed* **2019**, *131*, 11278-11288.
9. J. Xu, Y. Xu, X. -H. Bu, *Small* **2021**, *17*, 2102331.
10. Z. Huang, T. Willhammar, X. Zou, *Chem. Sci.* **2021**, *12*, 1206-1219.
11. N. Garg, A. Deep, A. L. Sharma, *Coord. Chem. Rev.* **2021**, *445*, 214073.
12. H. Li, M. Eddaoudi, M. O'Keeffe, O. M. Yaghi, *Nature* **1999**, *402*, 276-279.
13. S. I. Noro, T. Nakamura, *NPG Aisa Mater.* **2017**, 9, e433.
14. X M. Eddaoudi, H. Li, O. M. Yaghi, *J. Am. Chem. Soc.* **2000**, *122*, 1391–1397.
15. Z. Ji, H. Wang, S. Canossa, S. Wuttke, O. M. Yaghi, *Adv. Funct. Mater.* **2020**, *30*, 2000238.
16. C. V. McGuire, R. S. Forgan. *Chem. Commun.* **2015**, *51*, 5199-5217.
17. R. S. Forgan, *Dalton Trans.* **2019**, *48*, 9037-9042.
18. H. Li, L. Li, R. -B. Lin, W. Zhou, Z. Zhang, S. Xia, B. Chen, *EnergyChem* **2019**, *1*, 100006.
19. D. Yang, B. C. Gates, *ACS Catal.* **2019**, *9*, 1779–1798.

20. L. S. Xie, G. Skorupskii, M. Dincă, *Chem. Rev.* **2020**, *120*, 8536–8580.
21. H. -Y. Li, S. -N. Zhao, S. -Q, Zang, J. Li, *Chem. Soc. Rev.* **2020**, *49*, 6364-6401.
22. D. W. Lim, H. Kitagawa, *Chem. Rev.* **2020**, *120*, 8416-8467.
23. A. E. Baumann, D. A. Burns, B. Liu, V. S. Thoi, *Commun. Chem.* **2019**, *2*, 86.
24. O. M. Yaghi, *J. Am. Chem. Soc.* **2016**, *138*, 15507-15509.
25. K. Geng, T. He, R. Liu, S. Dalapati, K. T. Tan, Z. Li, S. Tao, Y. Gong, Q. Jiang, D. Jiang, *Chem. Rev.* **2020**, *120*, 8814-8933.
26. S. Patwardhan, A. A. Kocherzhenko, F. C. Grozema, L. D. A. Siebbeles. *J. Phys. Chem. C* **2011**, *115*, 11768-11772.
27. S. Wang, X. Xu, Y. Yue, K. Yu, Q. Shui, N. Huang, H. Chen, *Small Struct.* **2020**, *1*, 20000.
28. V. K. Yadav, S. H. Mir, V. Mishra, T. G. Gopakumar, J. K. Singh, *Phys. Chem. Chem. Phys.* **2020**, *22*, 21360-21368.
29. N. Keller, T. Bein, *Chem. Soc. Rev.* **2021**, *50*, 1813-1845.
30. X. Guan, F. Chen, Q. Fang, S. Qiu, *Chem. Soc. Rev.* **2020**, *49*, 1357-1384.
31. Y. Li, W. Chen, G. Xing, D. Jiang, L. Chen, *Chem. Soc. Rev.* **2020**, *49*, 2852-2868.
32. H. R. Abuzeid, A. F. M. EL-Mahdy, S. -W. Kuo, *Giant* **2021**, *6*, 10544.
33. T. Ma, E. A. Kapustin, S. X. Yin, L. Liang, Z. Zhou, J. Niu, L. -H. Wang, J. Sun, J. Li, X. Wang, W. D. Wang, W. Wang, J. Sun, O. M. Yaghi, *Science* **2018**, *361*, 44-51.
34. Y. -B. Zhang, J. Su, H. Furukawa, Y. Yun, F. Gándara, A. Duong, X. Zou, O. M. Yaghi. *J. Am. Chem. Soc.* **2013**, *135*, 16336-16339.
35. F. J. Uribe-Romo, J. R. Hunt, H. Furukawa, C. Klöck, M. O'Keeffe, O. M. Yaghi. *J. Am. Chem. Soc.* **2009**, *131*, 4570–4571.
36. H. Wang, Y. Jin, N. Sun, W. Zhang, J. Jiang, *Chem. Soc. Rev.* **2021**, *50*, 8874-8886.
37. J. D. Evans, C. J. Sumby, C. J. Doona. *Chem. Lett.* **2015**, *44*, 582‑588.
38. A. He, Z. Jiang, Y. Wu, H. Hussain, J. Rawle, M. E. Briggs, M. A.Little, A. G. Livingston, A. I. Cooper, *Nat. Mater.* **2022**, *21*, 463-470.

39. M. Liu, L. Chen, S. Lewis, S. Y. Chong, M. A. Little, T. Hasell, I. M. Aldous, C. M. Brown, M. W. Smith, C. A. Morrison, L. J. Hardwick, A. I. Cooper, *Nat. Commun*. **2016**, *7*, 12750.
40. A. Petronico, T. P. Moneypenny II, B. G. Nicolau, J. S. Moore, R. G. Nuzzo, A. A. Gewirth, *J. Am. Chem. Soc.* **2018**, *140*, 7504-7509.
41. D. -C. W. Kiggen, F. Vögtle, *Angew. Chem. Int. Engl.* **1984**, *23*, 714-715.
42. T. Tozawa, J. T. A. Jones, S. I. Swamy, S. Jiang, D. J. Adams, S. Shakespeare, R. Clowes, D. Bradshaw, T. Hasell, S. Y. Chong, C. Tang, S. Thompson, J. Parker, A. Trewin, J. Bacsa, A. M. S. Slawin, A. Steiner, A. I. Cooper, *Nat. Mater.* **2009**, *8*, 973-978.
43. G. Zhang, O. Presly, F. White, I. M. Oppel, M. Mastalerz, *Angew. Chem. Int. Ed.* **2014**, *53*, 1516-1520.
44. A. Avellaneda, P. Valente, A. Burgun, J. D. Evans, A. W. Markwell-Heys, D. Rankine, D. J. Nielsen, M. R. Hill, C. J. Sumby, C. J. Doonan, *Angew. Chem. Int. Ed.* **2013**, *52*, 3746-374.
45. K. Su, W. Wang, S. Du, C. Ji, M. Zhou, D. Yuan, *J. Am. Chem. Soc.* **2020**, *142*, 18060-18072.
46. I. Hisaki, X. Chen, K. Takahashi, T. Nakamura, *Angew. Chem. Int. Ed.* **2019**, *58*, 11160-11170.
47. J. Tian, H. Wang, D. -W. Zhang, Y. Liu, Z. -T. Li, *Natl. Sci. Rev.* **2017**, *4*, 426-436.
48. H. -C. J. Zhou, S. Kitagawa, *Chem. Soc. Rev.* **2014**, *43*, 5415-5418.
49. S. Kandambeth, K. Dey, R. Banerjee, *J. Am. Chem. Soc.* **2019**, *141*, 1807−1822.
50. B. Wang, R. -B. Lin, Z. Zhang, S. Xiang, B. Chen, *J. Am. Chem. Soc.* **2020**, *142*, 14399-14416.
51. D. J. Duchamp, R. E. Marsh, *Acta Crystallogr. Sect. B* **1969**, *25*, 5-19.
52. F. H. Herbstein, M. Kapon, G. M. Reisner, *J. Inclusion Phenom.* **1987**, *5*, 211-214.
53. P. Brunet, M. Simard, J. D. Wuest, *J. Am. Chem. Soc.* **1997**, *119*, 2737-2738.
54. J. D. Wuest. *Chem. Commun.* **2005**, 5830-5837.

55. Y. He, S. Xiang, B. Chen, *J. Am. Chem. Soc.* **2011**, *133*, 14570-14573.
56. M. Mastalerz, I. M. Oppel, *Angew. Chem. Int. Ed.* **2012**, *51*, 5252-5255.
57. A. Pulido, L. Chen, T. Kaczorowski, D. Holden, M. A. Little, S. Y. Chong, B. J. Slater, D. P. McMahon, B. Bonillo, C. J. Stackhouse, A. Stephenson, C. M. Kane, R. Clowes, T. Hasell, A. I. Cooper, G. M. Day, *Nature* **2017**, *543*, 657-664.
58. J. Yang, J. Wang, B. Hou, X. Huang, T. Wang, Y. Bao, H. Hao, *Chem. Eng. J.* **2020**, *399*, 125873.
59. C. B. Aakeröy, K. R. Seddon, *Chem. Soc. Rev.* **1993**, *22*, 397-407.
60. G. R. Desiraju, *Cryst. Growth Des.* **2011**, *11*, 4, 896-898.
61. R. W. Newberry, R. T. Raines, *Nat. Chem. Biol.* **2016**, *12*, 1084-1088.
62. W. M. Latimer, W. H. Rodebushi, *J. Am. Chem. Soc*. **1920**, *42*, 1419-1433.
63. L. Pauling, *J. Am. Chem. Soc*. **1935**, *57*, 2680-2684.
64. L. Pauling, *The nature of the chemical bond*. Cornell University Press, Ithaca, New York, **1939**.
65. G. C. Pimentel, A. L. McClellan, *The hydrogen bond*. Freeman, W. H. San Francisco, **1960**.
66. T. Steiner, W. Saenger, *J. Am. Chem. Soc*. **1993**, *115*, 4540-4547.
67. E. Arunan, G. R. Desiraju, R. A. Klein, J. Sadlej, S. Scheiner, I. Alkorta, D. C. Clary, R. H. Crabtree, J. J. Dannenberg, P. Hobza, H. G. Kjaergaard, A. C. Legon, B. Mennucci, D. J. Nesbitt, Definition of the Hydrogen Bond (IUPAC Recommendations 2011). *Pure Appl. Chem*. **2011**, *83*, 1637-1641.
68. J. Zhang, P. -C. Chen, B. K. Yuan, W. Ji, Z. -H. Cheng, X. H. Qiu, *Science*, **2013**, *342*, 611-614.
69. R.-B. Lin, Y. He, P. Li, H. Wang, W. Zhou, B. Chen, *Chem. Soc. Rev.* **2019**, *48*, 1362-1389
70. T. Steiner, *Angew. Chem. Int. Ed*. **2002**, *41*, 48−76.
71. J. Jiang, Y. Zhao, O. M. Yaghi, *J. Am. Chem. Soc.* **2016**, *138*, 3255-3265.
72. Y. -F. Han, Y. -X. Yuan, H. -B. Wang, *Molecules* **2017**, *22*, 266.

73. M. Simard, D. Su, J. D. Wuest, *J. Am. Chem. Soc*. **1991**, *113*, 4696-4698.

74. G. R. Desiraju, *Angew. Chem. Int. Ed.* **1995**, *34*, 2311−2327.

75. I. Hisaki, *J. Incl. Phenom. Macrocycl. Chem.* **2020**, *96*, 215-231.

76. M. R. D. Nunzio, Y. Suzuki, I. Hisaki, A. Douhal, *Int. J. Mol. Sci.* **2022**, *23*, 1929.

77. P. Li. M. R. Ryder, J. F. Stoddart, *Acc. Mater. Res.* **2020**, 1, 77−87.

78. O. Ivasenko, D. Perepichka, *Chem. Soc. Rev.* **2011**,*40*, 191−206.

79. P. Cui, D. P. McMahon, P. R. Spackman, B. M. Alston, M. A. Little, G. M. Day, A. I. Cooper, *Chem. Sci.* **2019**,*10*, 9988−9997.

80. F. Hu, C. Liu, M. Wu, J. Pang, F. Jiang, D. Yuan, M. Hong, *Angew. Chem. Int. Ed.* **2017**, *56*, 2101-2104.

81. J. D. Wuest. *Nat. Commun.* **2020**, *11*, 4652.

82. L. F. Chen, B. Zhang, L. L. Chen, H. Liu, Y. Hu, S. Qiao, *Mater. Adv.* **2022**, *3*, 3680-3708.

83. Y. Zhao, D. Xue, H. Qi, C. Zhang, *RSC Adv.* **2017**, *7*, 22882-22891.

84. Q. Yin, P. Zhao, R. -J. Sa, G. -C. Chen, J. Lv, T. -F. Liu, R. Cao, *Angew. Chem. Int. Ed.* **2018**, *57*, 7691-769.

85. C. M. Aitchison, C. M. Kane, D. P. McMahon, P. R. Spackman, A. Pulido, X. Wang, L. Wilbraham, L. Chen, R. Clowes, M. A. Zwijnenburg, R. S. Sprick, M. A. Little, G. M. Day, A. I. Cooper, *J. Mater. Chem. A* **2020**, *8*, 7158-7170.

86. K. Ma, P. Li, J. H. Xin, Y. Chen, Z. Chen, S. Goswami, X. Liu, S. Kato, H. Chen, X. Zhang, J. Bai, M. C. Wasson, R. R. Maldonado, R. Q. Snurr, O. M. Farha, Cell Rep. Phys. Sci. **2020**, *1*, 100024.

87. S. Goswami, K. Ma, J. Duan, K. O. Kirlikovali, J. Bai, J. T. Hupp, P. Li, O. K. Farha, *Langmuir* **2022**, *38*, 1533-1539.

88. I. Hisaki, N. Ikenaka, N. Tohnai, M. Miyata, *Chem. Commun.* **2016**, *52*, 300-303.

89. I. Hisaki, S. Nakagawa, Y. Suzuki, N. Tohnai, *Chem. Lett.* **2018**, *47*, 1143-1146.

90. I. Hisaki, S. Nakagawa, H. Sato, N. Tohnai, *Chem. Commun.* **2016**, *52*, 9781-9784.

91. I. Hisaki, S. Nakagawa, N. Ikenaka, Y. Imamura, M. Katouda, M. Tashiro, H. Tsuchida, T. Ogoshi, H. Sato, N. Tohnai, M. Miyata, *J. Am. Chem. Soc.* **2016**, *138*, 6617-6628.

92. I. Hisaki, N. Ikenaka, E. Gomez, B. Cohen, N. Tohnai, A. Douhal, *Chem. Eur. J.* **2017**, *23*, 11611-11619.

93. Y. Suzuki, M. Gutiérrez, S. Tanaka, E. Gomez, N. Tohnai, N. Yasuda, N. Matubayashi, A. Douhal, I. Hisaki, *Chem. Sci.* **2021**, *12*, 9607-9618.

94. I. Hisaki, Y. Suzuki, E. Gomez, Q. Ji, N. Tohnai, T. Nakamura, A. Douhal, *J. Am. Chem. Soc.* **2019**, *141*, 2111-2121.

95. S. C. Pal, D. Mukherjee, R. Sahoo, S. Mondal, M. C. Das, *ACS Energy Lett.* **2021**, *6*, 4431-4453.

96. P. Li, Y. He, J. Guang, L. Weng, J. C. -G. Zhao, S. Xiang, B. Chen, *J. Am. Chem. Soc.* **2014**, *136*, 547-549.

97. P. Li, Y. He, Y. Zhao, L. Weng, H. Wang, R. Krishna, H. Wu, W. Zhou, M. O'Keeffe, Y. Han, B. Chen, *Angew. Chem. Int. Ed.* **2015**, *54*, 574-577.

98. P. Li, Y. He, H. D. Arman, R. Krishna, H. Wang, L. Weng, B. Chen, *Chem. Commun.* **2014**, *50*, 13081-13084.

99. H. Wang, B. Li, H. Wu, T. -L. Hu, Z. Yao, W. Zhou, S. Xiang, B. Chen, *J. Am. Chem. Soc.* **2015**, *137*, 9963-9970.

100. H. Wang, Z. Bao, H. Wu, R. -B. Lin, W. Zhou, T. -L. Hu, B. Li, J. C. -G. Zhao, B. Chen, *Chem. Commun.* **2017**, *53*, 11150-11153.

101. W. Yang, F. Yang, T. -L. Hu, S. C. King, H. Wang, H. Wu, W. Zhou, J. -R. Jiang, H. D. Arman, B. Chen, *Cryst. Growth Des.* **2016**, *16*, 5831-5835.

102. W. Yang, B. Li, H. Wang, O. Alduhaish, K. Alfooty, M. A. Zayed, P. Li, H. D. Arman, B. Chen, *Cryst. Growth Des.* **2015**, *15*, 2000-2004.

103. H. Wang, H. Wu, J. Kan, G. Chang, Z. Yao, B. Li, W. Zhou, S. Xiang, J. C. -G. Zhao, B. Chen, *J. Mater. Chem. A* **2017**, *5*, 8292-8296.

104. J. Lv, C. P. Krap, M. Suyetin, N. H. Alsmail, Y. Yan, S. -H. Yang, W. Lewis, E.

Bichoutskaia, C. C. Tang, A. J. Blake, R. Cao, M. Schröder, *J. Am. Chem. Soc*. **2014**, *136*, 12828-12831.

105. J. Lv, C. P. Krap, F. Trousselet, Y. Yan, N. H. Alsmail, B. Karadeniz, N. M. Jacques, W. Lewis, A. J. Blake, F. X. Coudert, R. Cao, M. Schröder, *Cryst. Growth Des*. **2018**, *18*, 2555-2562.
106. G. Xing, T. Yan, S. Das, T. Ben, S. Qiu, *Angew. Chem. Int. Ed*. **2018**, *57*, 5345-5349.
107. A. Yamamoto, T. Hirukawa, I. Hisaki, M. Miyata, N. Tohnai, *Tetrahedron Lett*. **2013**, *54*, 12698-1273.
108. A. Karmakar, R. Illathvalappil, B. Anothumakkool, A. Sen, P. Samanta, A. Desai, S. Kurungot, S. K. Ghosh, *Angew. Chem. Int. Ed*. **2016**, *55*, 10667-10671.
109. A. -A. Zhang, Y. -L Li, Z. -B. Fang, L. Xie, R. Cao, Y. Liu, T. -F. Liu, *ACS Appl. Mater. Interfaces* **2022**, *14*, 21050-21058.
110. J. -F. Feng, T. -F. Liu, R. Cao, *Angew. Chem. Int. Ed.* **2020**, *59*, 22392-22396.
111. J. -F. Feng, X. -Y. Yan, Z. -Y. Ji, T. -F. Liu, R. Cao, *ACS Appl. Mater. Interfaces* **2020**, *12*, 29854-29860.
112. T. Friščić, C. Mottillo, H. M. Titi, *Angew. Chem. Int. Ed.* **2020**, *59*, 1018−1029.
113. W. -K. Qin, D. -H. Si, Q. Yin, X.-Y. Gao, Q. -Q. Huang,Y. -N. Feng, L. Xie, S. Zhang,. X.-S. Huang, T.-F. Liu, R. Cao, *Angew. Chem.***2022**, e202202089.
114. M. Oschatz, M. Antonietti, *Energy Environ. Sci.* **2018**, *11*, 57-70.
115. Z. Yang, A. Moriyama, R. Oketani, T. Nakamura, I. Hisaki, *Chem. Lett.* **2021**, *50*, 1909-1912.
116. C. A. Zentner, H. W. H. Lai, J. T. Greenfield, R. A. Wiscons, M. Zeller, C. F. Campana, O. Talu, S. A. FitzGerald, J. L. C. Rowsell, *Chem. Commun.* **2015**, *51*, 11642-11645.
117. X. Zhang, L. Li, J. -X. Wang, H. -M. Wen, R. Krishna, H. Wu, W. Zhou, Z. -N. Chen, B. Li, G. Qian, B. Chen, *J. Am. Chem. Soc.* **2020**, *142*, 633‑640.
118. P. H. Li, P. Li, M. R. Ryder, Z. Liu, C. L. Stern, O. K. Farha, J. F. Stoddart, A*ngew.*

Chem. **2019**, *131*, 1678-1683.

119. A. Comotti, R. Simonutti, S. Stramare, P. Sozzani, *Nanotechnology* **1999**, *10*, 70-76.

120. P. Sozzani, A. Comotti, R. Simonutti, T. Meersmann, J. W. Logan, A. Pines, *Angew. Chem. Int. Ed.* **2000**, *39*, 2695-2699.

121. P. Sozzani, S. Bracco, A. Comotti, L. Ferretti, R. Simonutti, *Angew. Chem. Int. Ed.* **2005**, *44*, 1816-1820.

Chapter 2

Two-dimensional Porous Framework Assembled through Hydrogen-bonds and Dipole-dipole Interactions

2-1. Abstract

I demonstrate that a dipole-dipole interaction of benzo[c]-[1,2,5]thiadiazole moieties, directional H-bond formation of carboxy groups, and a rigid molecular skeleton enable a structurally-predictable two-dimensional hydrogen-bonded organic framework **BTIA-1** from tetratopic carboxylic acid. Activated form **BTIA-1a** by traditional method was revealed to have BET surface area of 237 $m^2\ g^{-1}$ and show selective adsorption of CO_2. Meanwhile, the solvent exchange process was conducted, resulting BET surface area of 720 $m^2\ g^{-1}$.

2-2. Introduction

Porous molecular crystals with definite size, shape, morphology, and function of the pore are challenging to construct by design, because various intermolecular interactions simultaneously occur during the self-assembly processes. In the case of porous molecular crystals formed through hydrogen bonding, which are particularly called hydrogen-bonded organic frameworks (HOFs),[1] low dimensional H-bonded network motifs such as two dimensional (2D) hexagonal networks[2] are capable of being constructed by design because of highly-directional, and therefore, predictable H-bonding.[3] The entire structure of HOFs, on the other hand, is not easy to construct due to ambiguous interactions between the low-dimensional motifs, such as π-π and C-H···π interactions.[2] Regarding this, Cooper, Day, and coworkers successfully obtained a desired HOF with the largest surface area and the lowest density based on guidance of structure-property maps established by crystal structure prediction (CSP) methodology.[4] Yet, it is still difficult to predict crystal structures of HOFs composed of flexible molecules with versatile conformations.[5]

On the other hand, designed HOFs may be achieved by hierarchical utilization of the different types of appropriate non-covalent interactions such as hydrogen bonds and other interactions. Indeed, our group previously demonstrated that combination of directional H-bonds between carboxy groups and shape-fitted docking of twisted hexaazatriphenylene derivatives is capable of providing predictable isostructural HOFs.[6]

In this study, I planned to construct a HOF by utilizing moderately large dipole moment of the benzo[c][1,2,5]thiadiazole (BT) group, in addition to H-bonds. BT is one of the important key groups for functional organic materials.[7,8] Combination of BT with electron donor moieties allows effective charge separation to be applied for OLET, OFET, sensors, and other devices.[9] The BT also has a dipole moment of 4.8 Debye, allowing porous framework incorporating BT groups to absorb CO_2 gas selectively through dipole-quadrupole interactions between the BT groups and CO_2.[10]

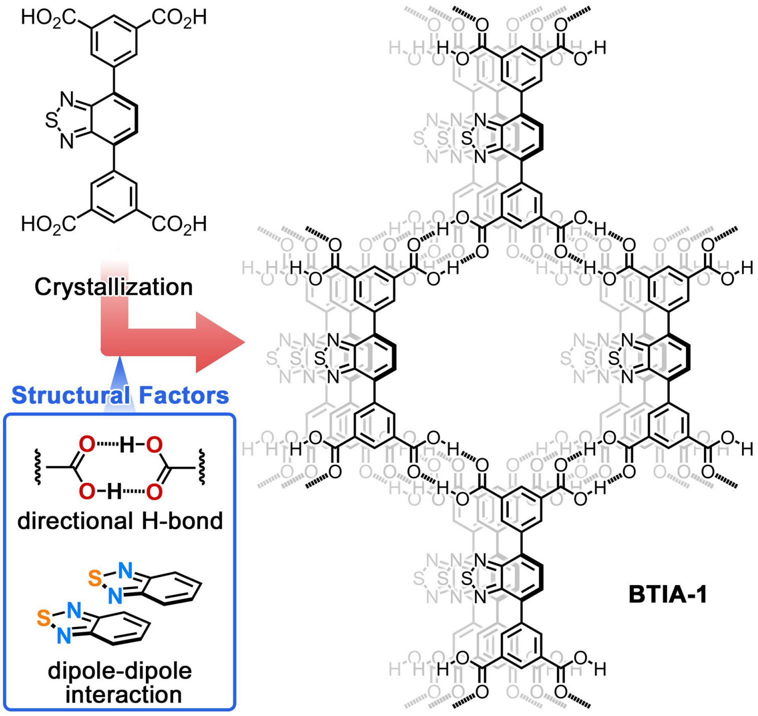

Figure 2-1. Construction of a predictable layered HOF (**BTIA-1**) through directional H-bonds of carboxy groups and dipole-dipole interactions of benzothiadiazole groups.

In this chapter, I demonstrate that BT-incorporated tetratopic carboxylic acid, namely 5,5'-(benzo[*c*][1,2,5]thiadiazole-4,7-diyl)diisophthalic acid **BTIA**, provides a predictable HOF (**BTIA-1**) with layered honeycomb networks (**Figure 2-1**). Although **BTIA-1** has not given single crystals suitable for single crystal X-ray diffraction analysis, the powder X-ray diffraction (PXRD) pattern is in good agreement with that of the crystal structure generated by crystal structure prediction (CSP) methodology based on a classic force field. The activated HOF **BTIA-1a** through common heating method is thermally stable up to 270 °C, has the Brunauer-Emmett-Teller (BET) surface area of 237 $m^2 g^{-1}$, and shows selective CO_2 adsorption. On the other hand, **BTIA-1a**, obtained by solvent exchange process, showed BET surface area of 720 $m^2 g^{-1}$. It is noteworthy that directional electrostatic interactions (i.e. self-complementary H-bonded dimers of carboxy groups, and dipole-dipole interactions between the benzothiadiazole moieties) made it easy to predict a structure of the framework even by a classic force field calculation. I believe that the results can contribute to designing, constructing, and characterizing molecular porous materials.

2-3. Results and discussion

Synthesis and crystallization

Cmpound **BTIA** was synthesized by Suzuki-Miyaura crosscoupling reaction of 4,7-dibromobenzo[c][1,2,5]dithiazole and dimethyl 5-(4,4,5,5-tetramethyl-1,3,2-dioxaborolan-2-yl)- isophthalate, followed by hydrolysis in the presence of NaOH (Scheme 2-1), according to literature,[10a] and crystallized from slow evaporation of a mixed solution of DMF and methyl benzoate at 60 °C, which is the optimized condition to obtain a crystalline precipitate (Figure 2-2). The precipitate was revealed to include methyl benzoate with a 1:4 host-guest ratio based on TG and ^{1}H NMR analyses.

Scheme 2-1. synthesis (a) and crystallization (b) of **BTIA**

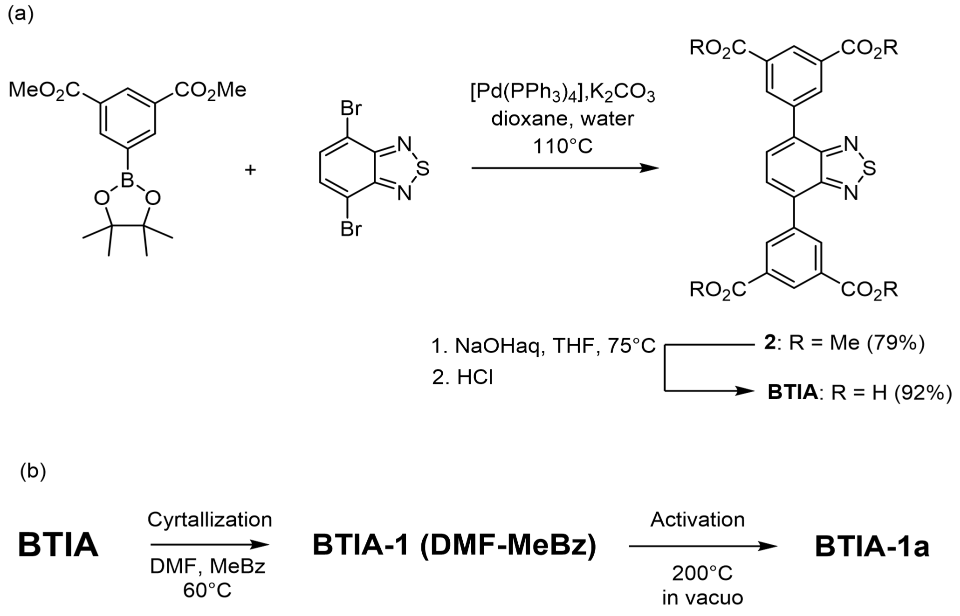

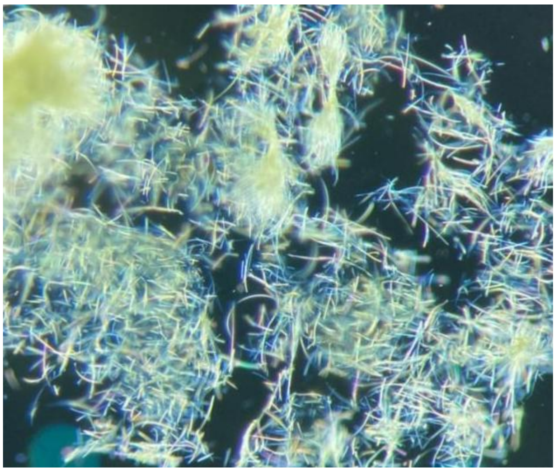

Figure 2-2. Morphology of the fibrous crystalline precipitate of **BTIA-1**.

Crystal structure confirmation of BTIA-1

To my dismay, the resultant fibrous crystals are too thin for single crystal X-ray diffraction analysis. This morphology is probably caused by anisotropic crystal growth in a direction of π-stacking of **BTIA** due to dipole-dipole interactions between the BT moieties. To sleuth a crystal structure of the precipitate, I conducted crystal structure prediction of **BTIA**. The molecular structure of **BTIA** was optimized by the GGA/PBE function with the DNP-3.5 basis set. Charge distribution on each of atoms was also calculated for the optimized structure. By using the optimized conformation, crystal structures belonging to space groups P-1, $P2_1$/c, $P2_1$, $P2_12_12_1$, $C2$/c, and $P1$ were generated by Monte Carlo calculation, clustered, and optimized by the force field (Dreiding) to give 7938 crystal structures. The resultant crystal structures were plotted on an energy-density map as shown in Figure 2-3a. The expected structure and the related similar structures are located in region-A with E = ca. –10 kcal mol^{-1} and d = ca. 1.0 g cm^{-3} , which is possible to form experimentally. The region-A contains 14 structures with space groups P-1, $P2_1$/c, $P2_1$, and $C2$/c, and $P1$, all of which have a layered structure of H-bonded honeycomb 2D sheets (Figure 2-4). Their representative PXRD patterns are shown in Figure 2-3b, in which CSP-$P1$(34) [34th-stable predicted structure among those belonging to space group *P*1] shows the most agreed PXRD pattern with an experimentally observed one with diffraction peaks at 6.7°, 11.5°, 11.7°, 13.2°, 13.4°, 17.5°, and 17.6°. CSP-*P*1(34) has cell parameters of a = 3.813 Å, b = 15.205 Å, c = 15.206 Å, α = 62.20°, β = 91.95°, γ = 88.04°, V = 778.05 Å^3. In CSP-*P*1(34), carboxy groups form complementary H-bonded dimer to give 2D network (Figure 2-3c) and the BT moieties are unidirectionally slip-stacked through dipole-dipole interactions (Figure 2-3d), resulting porous layered frameworks (Figure 2-3e). Other structures in region-A have different orientations of the BT moieties (Figures 2-4, Table 1). The region-B contains less porous crystal structures with different types of H-bonding (Figure 2-5). The PXRD patterns of the structures in Region-B do not match the experimental one.

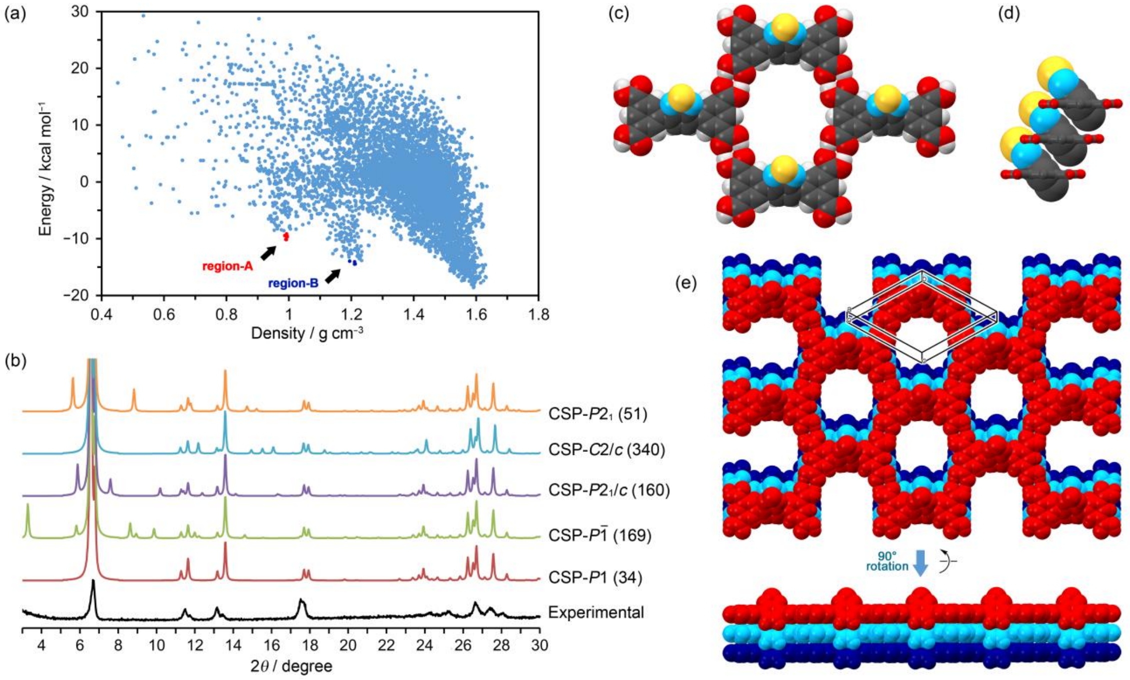

Figure 2-3. Crystal structure prediction of compound **BTIA**. (a) Energy-density plot of the generated crystal structures. (b) PXRD patterns of the representative structures of the region A as well as that observed. (c) H-bonded motif of the most probable structure [CSP-*P*1(34)] corresponding to **BTIA-1**. (d) Unidirectionally slip-stacked

benzothiadiazole moieties in CSP-*P*1(34). (e) Stacking manner of the 2D layers in CSP-*P*1(34).

Table 1. Cell parameters of predicted crystals structures in region-A.

	*P*1(34)	*P*-1(169)	$P2_1/c$(160)	*P*1(35)	P2_1/c(161)
a [Å]	3.8125	778.05	16.4065	15.1877	17.9071
b [Å]	15.0253	36.3176	52.0809	15.7981	26.0419
c [Å]	15.2055	3.8124	15.7076	3.8141	7.6261
α [°]	62.2030	47.7463	90	105.7430	90
β [°]	91.9477	74.0667	166.5920	92.1979	90
γ [°]	88.0414	77.8717	90	116.0913	90
V [Å^3]	778.05	1556.08	3112.24	777.782	3112.22
D [gcm^{-3}]	0.991	0.991	0.991	0.991	0.991
E [kcal mol^{-1}]	-10.144	-10.131	-10.129	-10.128	-10.114

	$P2_1$(51)	*P*1(36)	*P*-1(171)	$P2_1/c$(186)	$C2/c$(340)
a [Å]	16.4054	17.2313	44.3717	15.7402	28.4588
b [Å]	26.0418	15.1775	15.7086	26.0535	28.4588
c [Å]	3.8129	3.8142	3.8093	17.0230	17.9065
α [°]	90	87.7821	86.2730	90	90
β [°]	107.1981	62.1686	67.1347	26.3829	152.1386
γ [°]	90	113.2755	133.0820	90	90
V [Å^3]	1556.14	779.158	1556.69	3102.09	6205.32
D [gcm^{-3}]	0.991	0.989	0.990	0.994	0.994
E [kcal mol^{-1}]	-10.114	-10.084	-10.047	-9.668	-9.545

	P-1(178)	*C2/c*(342)	*C2/c*(348)	*C2/c*(365)
a [Å]	7.5745	15.8184	28.1066	17.9788
b [Å]	19.2922	26.0688	26.0909	25.8972
c [Å]	15.5658	15.1154	15.0251	45.5901
α [°]	60.7087	90	90	90
β [°]	77.8118	86.8387	145.3929	162.9674
γ [°]	52.0665	90	90	90
V [Å^3]	1551.32	6223.6	6257.8	6217.66
D [gcm^{-3}]	0.994	0.991	0.985	0.992
E [kcal mol^{-1}]	-9.545	-9.516	-9.425	-9.122

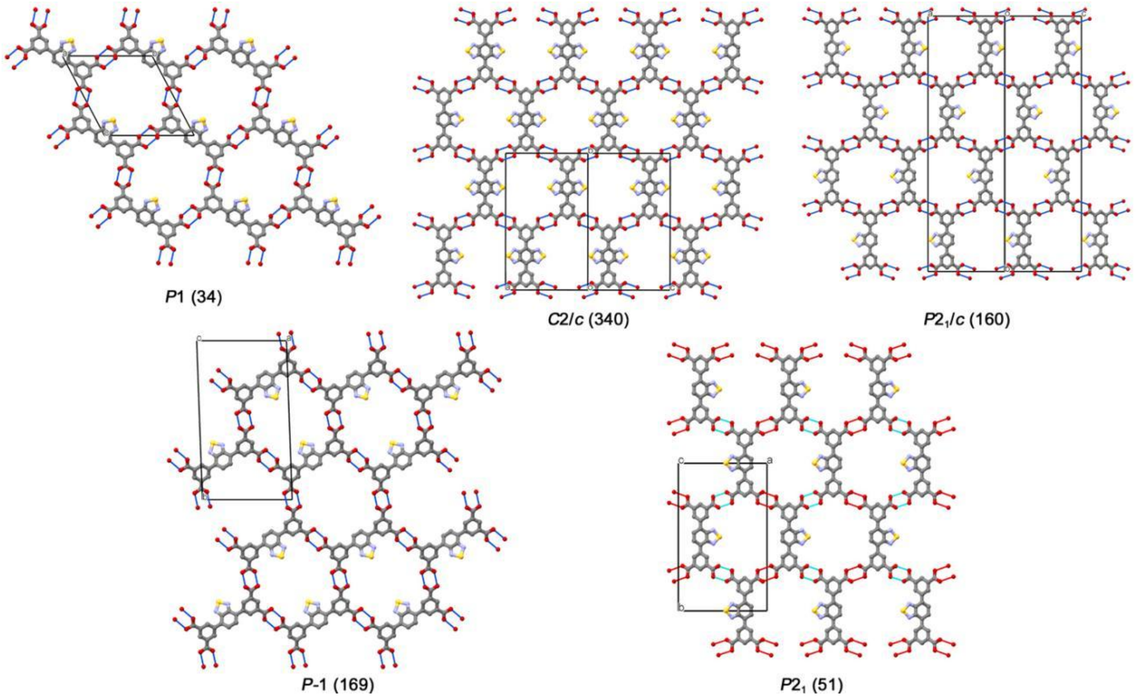

*P*1 (34)

*C*2/*c* (340)

P2_1/*c* (160)

P-1 (169)

P2_1 (51)

Figure 2-4. Molecular packing diagrams of predicted crystal structures in region-A.

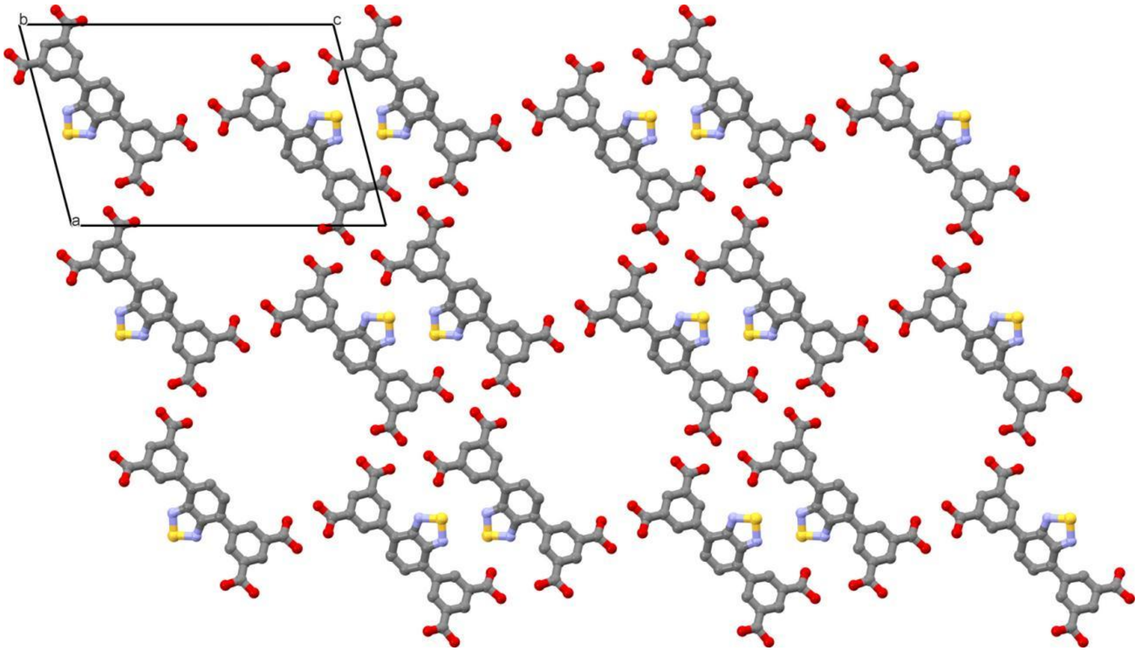

Figure 2-5. Typical molecular packing diagram of predicted crystals in region-B.

Thermal behaviors

The TG curve of as-formed crystalline bulk reaches plateau at 250 °C due to the complete removal of DMF and methyl benzoate (Figure 2-6), which was also confirmed by ^{1}H NMR spectrum of the heated sample dissolved in DMSO-d_6 (Figure S2-3 in appendix). Weight loss observed at higher temperature than 370 °C is due to thermal decomposition of the compound. As-formed crystalline bulk of **BTIA-1** was then subject to variable temperature- (VT-) PXRD measurement (Figure 2-7). During increasing temperature up to ~270 °C, positions of the diffraction peaks such as 6.7°, 11.5°, 13.2°, and 17.5° are constant, although their intensity gradually increased due to removal of the included solvent molecules. Further heating results in change of the pattern and decrease of the peak intensity. For example, new peaks at 10.7° and 16.3° start to appear at ca. 300 °C, indicating structural changes of the framework.

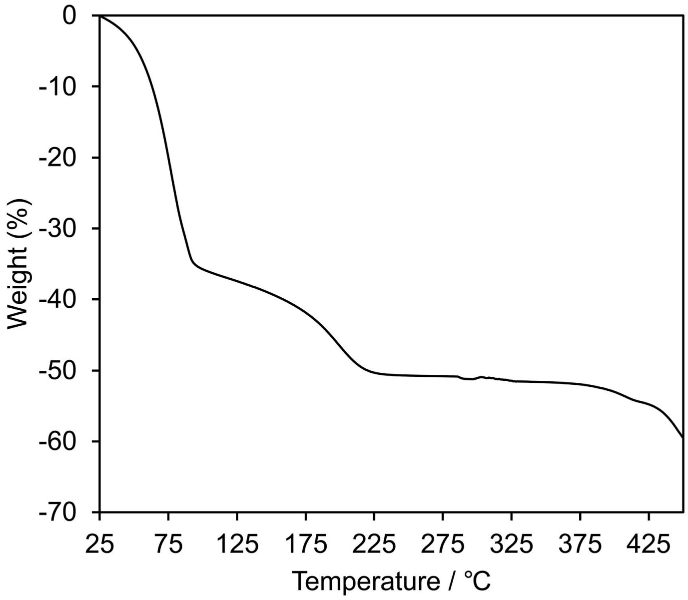

Figure 2-6. TG analysis of HOF **BTIA-1**.

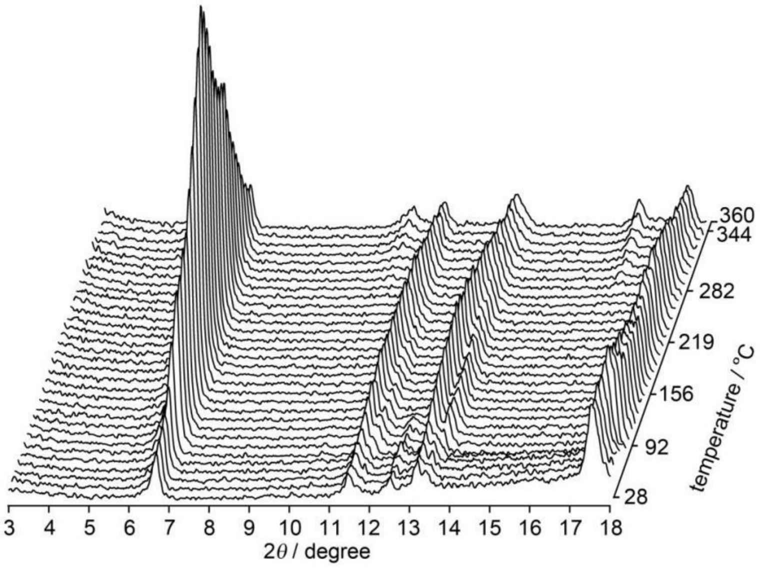

Figure 2-7. VT-PXRD pattern changes of **BTIA-1** upon heating.

Evaluation of permanent porosity

The activation of the framework was performed by heating at 200 °C under a vacuum condition (Figure 2-12, Figure S2-4 in Appendix). The resultant activated material was subject to gas sorption experiment to evaluate porosity (Figure 2-8). The HOF showed almost no adsorption of N_2 at 77 K in the low-pressure region. On the other hand, the HOF showed type-I CO_2 adsorption isotherms with uptake of 62.6 cm^3 (STP) g^{-1} at $Pe / P_0 = 1.0$ at 195 K. The BET surface area was calculated to be 237 m^2 g^{-1} based on the CO_2 sorption (Figure 2-9). The observed CO_2 selective absorption probably caused by attractive electrostatic interactions between quadrupolar CO_2 molecules and the channel wall composed of dipolar benzothiadiazole moieties. On the other hand, I also conducted a solvent exchange process followed by moderate activation at 80 °C (Figure 2-13). Similarly, **BTIA-1a** showed no N_2 uptake at 77 K, while gave a type I sorption isotherm for CO_2 at 195 K. The amount of the CO_2 gas, i.e. 172 cm^3 (STP) g^{-1} (Figure 2-9), is much increased than that previously value collected by normal activation condition. The present system shows BET surface area of 720 m^2 g^{-1} (Figure 2-11).

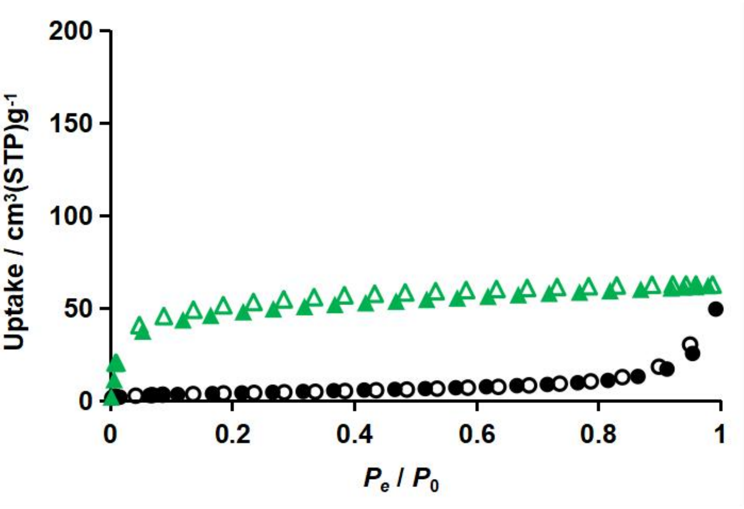

Figure 2-8. Gas sorption isotherms of the activated HOF **BTIA-1a** via a common method. Conditions; 77 K for N_2 (black), 195 K for CO_2 (green). Solid symbol: absorption. Open symbol: desorption.

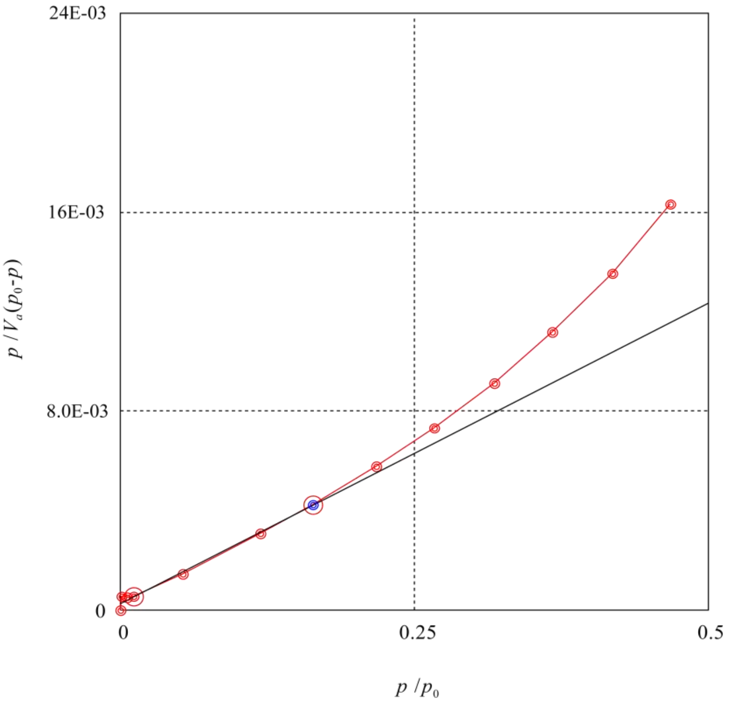

Slope	2.4235E-02	
Intercept	2.3839E-04	
Correlation coefficient	0.9996	
BET range limit (p/p0=0.1640)	6th point	
$Va(p_0\text{-}p)_{max}$	3910.8	
V_m	40.860	[cm^3 (STP) g^{-1}]
SA(BET)	2.3713E+02	[m^2 g^{-1}]
C	102.66	
Total volum (p/p0=0.990)	0.1718	[cm^3 g^{-1}]

Figure 2-9. BET analysis based on CO_2 adsorption data of **BTIA-1a** (heating process).

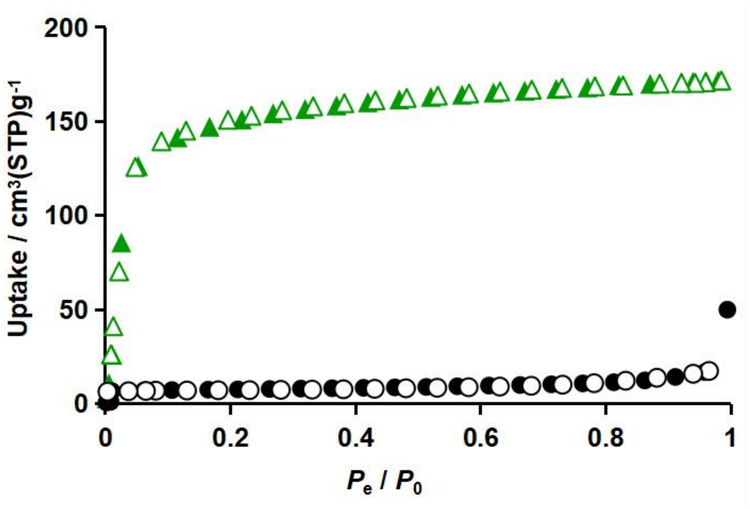

Figure 2-10. Gas sorption isotherms of the activated HOF **BTIA-1a** via a solvent exchange process. Conditions; 77 K for N_2 (black), 195 K for CO_2 (green). Solid symbol: absorption. Open symbol: desorption.

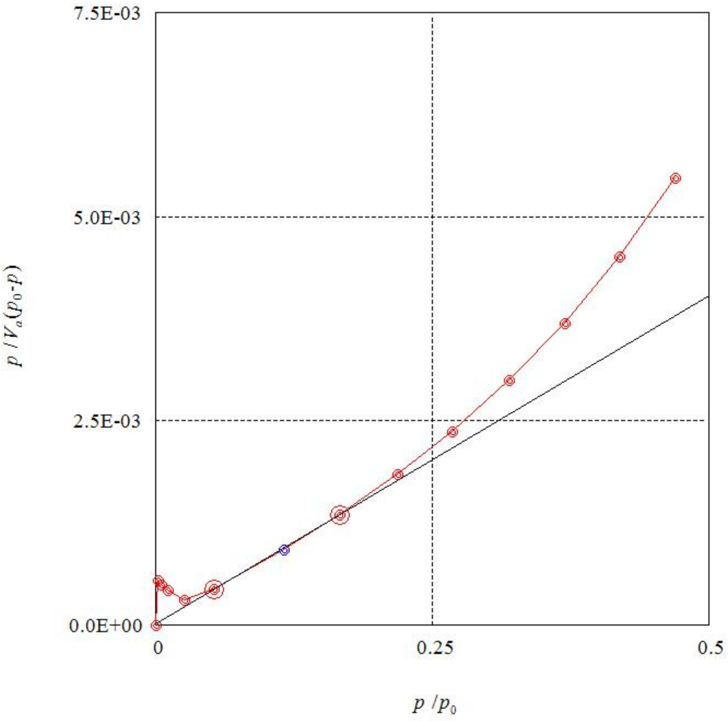

Slope	8.0439E-03	
Intercept	8.9481E-06	
Correlation coefficient	0.9995	
BET range limit (p/p0=0.1669)	6th point	p/p0=0.1153
$V_a(p_0\text{-}p)_{max}$	1.2693E+04	
V_m	124.18	[cm^3 (STP) g^{-1}]
SA(BET)	7.2065E+02	[m^2 g^{-1}]
C	899.95	
Total volum (p/p0=0.990)	0.4732	[cm^3 g^{-1}]

Figure 2-11. BET analysis based on CO_2 adsorption data of **BTIA-1a** (solvent exchange process).

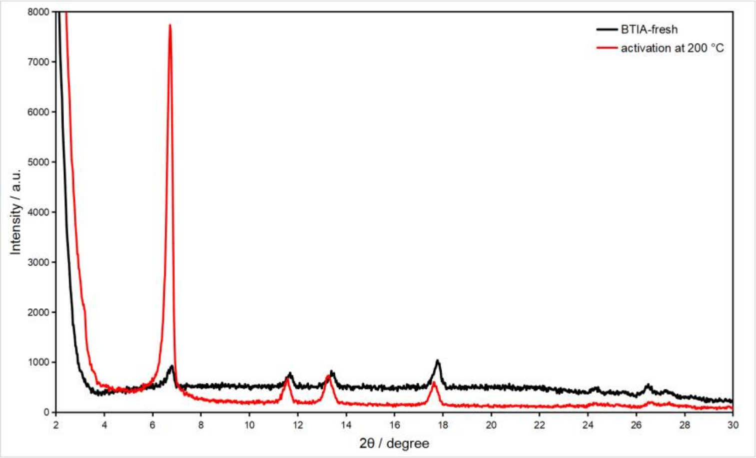

Figure 2-12. PXRD patterns of **BTIA-1a** activated at 200 °C.

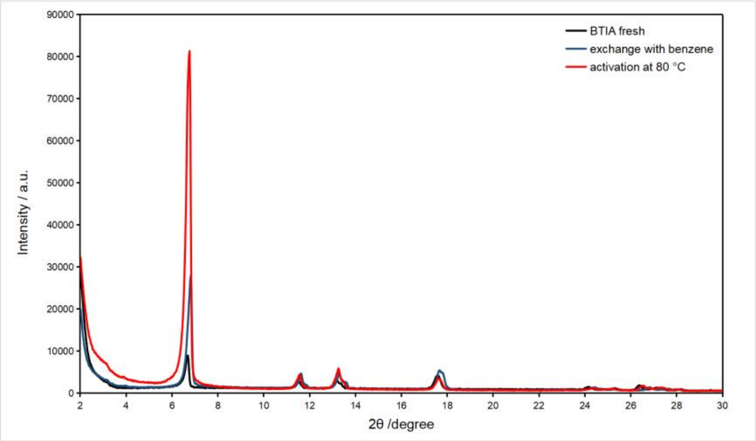

Figure 2-13. PXRD patterns of **BTIA-1a** activated through solvent exchange process.

2-4. Conclusion

In this chapter, I demonstrated that a dipole-dipole interaction between the benzo[c][1,2,5]thiadiazole (BT) moieties, in addition to directional H-bond formation and a rigid molecular skeleton, play a role to form structurally-predictable 2D HOF. Tetratopic carboxylic acid **BTIA** forms 2D HOF **BTIA-1**, and its activated form **BTIA-1a** via a solvent process with BET surface area of 720 m^2 g^{-1} showed selective adsorption of CO_2 and retained the original structure at least up to 270 °C. It is noteworthy that the calculation methodology applied for CSP is very classic force field based, which is, in many cases, difficult for predicting the framework. In this case, however, rigid small molecular structure with less conformations, highly directional supramolecular synthon (i.e. self-complementary dimer of carboxy groups), and dipole-dipole interactions between the BT moieties made it easy to predict a structure of the framework. We hope the present strategy can contribute to constructing predictable porous molecular crystals.

2-5. Experiment section

General

All reagents and solvents were used as received from commercial suppliers. ^{1}H NMR spectra were measured on a Bruker AV400M (400 MHz) spectrometer. Residual protons of deuterated solvents were used as internal standards for the measurements: δ = 7.26 ppm ($CDCl_3$), δ = 2.50 ppm (DMSO-d_6) for ^{1}H NMR. Thermo gravimetric (TG) analyses were performed on Rigaku TG8120 under an N_2 purge (100 mL/min) at a heating rate of 5 K min^{-1} . Powder X-ray diffraction (PXRD) data were collected on a Rigaku Ultima-IV (40 kV, 44 mA) using Cu-Kα radiation at room temperature and with a scan rate of 2.0° min^{-1} . Variable temperature PXRD (VT-PXRD) data were collected on same apparatus as PXRD with a temperature control unit. The temperature of the sample was increased from room temperature to 360 °C with a rate of 1.0° min^{-1}. PXRD scan of each measurement was collected with a difference in the temperature of ca. 5.1 °C. Gas sorption experiment was undertaken on the activated bulk sample BTIA-1, which was performed on BELSORP-max (BEL, Japan). The adsorption isotherms of N_2 and CO_2 were corrected at 77 K and 195 K, respectively. Brunauer–Emmett–Teller (BET) specific surface area: $S_{A(BET)}$ was calculated based on CO_2 absorption isotherms.

Synthesis of ester derivative 2 and target compound BTIA

Tetracarboxylic acid **BTIA** was synthesized as followed according to the literature.[10a]

Ester derivative 2

A mixture of 4,7-dibromobenzo[c][1,2,5]dithiazole (8.75 g, 29.8 mmol), dimethyl 5-(4,4,5,5-tetramethyl-1,3,2-dioxaborolan-2-yl)isophthalate (21.0 g, 65.6 mmol), K_2CO_3 (12.4 g, 89.7 mmol), and $Pd(PPh_3)_4$ (1.75 g, 1.51 mmol) in deoxygenated 1,4-dioxane (700 mL) and water (30 mL) was stirred at 110 °C for 36 h. The solvent was removed in vacuo and the resultant solid was washed with acetone, water, and CH_2Cl_2 to give 2 (12.2 g, 79%) as a yellow solid. ^{1}H NMR (400 MHz, $CDCl_3$) δ (ppm): 8.87 (d, 2H, J = 1.2 Hz), 8.79 (t, 1H, J = 1.2 Hz), 7.93 (s, 1H), 4.01 (s, 6H). (Figure S2-1 in appendix)

Tetracarboxylic acid BTIA

A mixture of **2** (5.14 g, 9.87 mmol) in THF (400 mL) and 6 M NaOHaq (200 mL) was stirred at 75 °C for 72 h. After removing THF in vacuo, the resultant water suspension was neutralized by HClaq. The precipitate was washed with water and methanol, separated by centrifuge, and dried in vacuo to give **1** (4.23 g, 92%) as a yellow solid. ^{1}H NMR (400 MHz, DMSO-d_6) δ (ppm): 8.80 (d, 4H, J = 1.6 Hz), 8.57 (t, 2H, J = 1.6 Hz), 8.14 (s, 2H). (Figure S2-2 in appendix)

Crystal structure prediction

A molecular model of **BTIA** was optimized by the DFT calculation at the GGA-PBE level by the DMol^3 program. A polymorph calculation was conducted on the optimized model with a Preiding force field by using the Polymorph program equipped in Material Studio ver 6.1.[11] Space groups of P-1, $P2_1/c$, $P2_1$, $P2_12_12_1$, $C2/c$, and $P1$ were applied for the calculation. Totally 7938 structures were obtained as a result of sequential Monte Carlo calculation, clustering, and optimization by the force field (Dreiding). Comparison of the PXRD patterns between the generated structures and experimentally obtained HOF **BTIA-1** led to one candidate structure CSP-$P1$(34) with structural parameters of a = 3.813 Å, b = 15.205 Å, c = 15.206 Å, α = 62.20°, β = 91.95°, γ = 88.04°, V = 778.05 Å^3.

Reference

1. a) Y. -F. Han, Y. -X. Yuan, H. -B. Wang, *Molecules,* **2017***, 22*, 266; b) J. Luo, J. -W. Wang, J. -H. Zhang, S. Lai, D. -C. Zhong, *CrystEngComm* **2018**, *20*, 5884–5898; c) R. -B. Lin, Y. He, P. Li, H. Wang, W. Zhou, B. Chen, *Chem. Soc. Rev.* **2019**, *48*, 1362–1389; d) I. Hisaki, X. Chen, K. Takahashi, T. Nakamura, *Angew. Chem. Int. Ed.* **2019**, *58*, 11160–11170; e) P. H. Li, M. R. Ryder, J. F. Stoddart, *Acc. Mater. Res*. **2020**, *1*, 77–87.
2. a) K. Kobayashi, T. Shirasaka, E. Horn, N. Furukawa, *Tetrahedron Lett.* **2000**, *41*, 89–93; b) I. Hisaki, S. Nakagawa, N. Ikenaka, Y. Imamura, M. Katouda, M. Tashiro, H. Tsuchida, T. Ogoshi, H. Sato, N. Tohnai, M. Miyata, *J. Am. Chem. Soc*. **2016**, *138*, 6617–6628; c) I. Hisaki, Y. Suzuki, E. Gomez, Q. Ji, N. Tohnai, T. Nakamura, A. Douhal, *J. Am. Chem. Soc.* **2019**, *141*, 2111–2121.
3. G. R. Desiraju, *Angew. Chem., Int. Ed. Engl.* **1995**, *34*, 2311–2327.
4. a) A. Pulido, L. Chen, T. Kaczorowski, D. Holden, M. A. Little, S. Y. Chong, B. J. Slater, D. P. McMahon, B. Bonillo, C. J. Stackhouse, A. Stephenson, C. M. Kane, R. Clowes, T. Hasell, A. I. Cooper, G. M. Day, *Nature* **2017**, *543*, 657–664; b) G. M. Day, A. I. Cooper, *Adv. Mater.* **2018**, *30*, 1704944.
5. P. Cui, E. S. Grape, P. R. Spackman, Y. Wu, R. Clowes, G. M. Day, A. K. Inge, M. A. Little, A. I. Cooper, *J. Am. Chem. Soc.* **2020**, *142*, 12743–12750.
6. a) I. Hisaki, N. Ikenaka, E. Gomez, B. Cohen, N. Tohnai, A. Douhal, *Chem. Eur. J.* **2017**, *23*, 11611–11619; b) I. Hisaki, Y. Suzuki, E. Gomez, B. Cohen, N. Tohnai, A. Douhal, *Angew. Chem. Int. Ed.* **2018**, *57*, 12832–12837; c) Y. Suzuki, M. Gutiérrez, S. Tanaka, E. Gomez, N. Tohnai, N. Yasuda, N. Matubayasi, A. Douhal, I. Hisaki, *Chem. Sci.* **2021**, *12*, 9607–9618.
7. a) B. A. D. Neto, A. A. M. Lapis, E. N. da Silva Júnior, J. Dupont, *Eur. J. Org. Chem.* **2013**, 228–255; b) B. A. D. Neto, P. H. P. R. Carvalho, J. R. Correa, *Acc. Chem. Res*. **2015**, *48*, 1560–1569.

8. a) I. Hisaki, N. Q. E. Affendy, N. Tohnai, *CrystEngComm* **2017**, *19*, 4892–4898; b) T. Takeda, M. Ozawa, T. Akutagawa, *Angew. Chem., Int. Ed.* **2019**, *58*, 10453–10460.
9. a) M. Melucci, L. Favaretto, A. Zanelli, M. Cavallini, A. Bongini, P. Maccagnani, P. Ostoja, G. Derue, R. Lazzaroni, G. Barbarella, *Adv. Funct. Mater.* **2010**, *20*, 445–452; b) S. Ren, R. Dawson, D. J. Adams, A. I. Cooper, *Polym. Chem.* **2013**, *4*, 5585–5590; c) D. Zhao, D. Yue, K. Jiang, Y. Cui, Q. Zhang, Y. Yang, G. Qian, *J. Mater. Chem. C* **2017**, *5*, 1607–1613; d) K. Ma, Y. Zhao, X. Han, J. Ding, X. Meng, H. Hou, *Cryst. Growth Des.* **2018**, *18*, 7419–7425; e) A. Mallick, A. M. El-Zohry, O. Shekhah, J. Yin, J. Jia, H. Aggarwal, A.-H. Emwas, O. F. Mohammed, M. Eddaoudi, *J. Am. Chem. Soc.* **2019**, *141*, 7245–7249; f) M. Echeverri, C. Ruiz, S. Gámez-Valenzuela, M. Alonso-Navarro, E. Gutierrez-Puebla, J. L. Serrano, M. C. R. Delgado, B. Gómez-Lor, *ACS Appl. Mater. Interfaces* **2020**, *12*, 10929–10937.
10. a) C. Song, Y. He, B. Li, Y. Ling, H. Wang, Y. Feng, R. Krishna, B. Chen, *Chem. Commun.* **2014**, *50*, 12105–12108; b) C. Song, Y. Ling, L. Jin, M. Zhang, D.-L. Chen, Y. He, *Dalton Trans.* **2016**, *45*, 190–197.
11. Material Studio ver 6.1. Accelrys Software Inc.: San Diego, CA, 2011.

Chapter 3

Slip-Stacking of Benzothiadiazole Can Provide a Robust Structural Motif for Porous Hydrogen-bonded Organic Frameworks

3-1. Abstract

Many of organic porous materials have a layered stacking structure of two-dimensionally networked porous sheets, while a well-controlled stacking of the sheets is still challenging to be achieved. Regarding this, I applied orthogonally working two intermolecular interactions; that is a directional hydrogen bond between carboxy groups and slip-stacking of benzo[c][1,2,5]thiadiazole (BT) groups with unidirectional alignment, to construct a well-defined porous two-dimensional (2D) hydrogen-bonded organic framework (HOF). In this chapter, I obtain a porous 2D HOF composed of benzo[c][1,2,5]thiadiazole (BT) derivative **BTTA**. The HOF has thermal stability up to 275 °C, permanent porosity with Brunner-Emmett-Teller (BET) surface area of 1145 m^2 g^{-1}, and photoconductivity. The BT-based HOF can be a promising platform for multifunctional porous material.

3-2. Introduction

Carboxy groups form a self-complementary dimer through a directional hydrogen-bond in many cases of naturally-occurred and artificial supramolecular assemblies.[1] This kind of predictable intermolecular interaction manners is called supramolecular synthon,[2] and has been used for construction of exotic supramolecular architectures from preorganized building block molecules (i.e. tectons).[2,3] Recently, the dimer has been used intensively to construct porous framework named hydrogen-bonded organic frameworks (HOFs),[4] in addition to other hydrogen bonding groups such as diaminotriazine,[5] urea,[6] imidazole,[7a] pyrazole,[7b] sulfonate,[8] carboxylate,[9] and so on. Compared with others, the carboxylic acid dimer allows us to design the networked structure more easily.[4e,10]

One of the common building block families of HOFs is a tetracarboxylic acid, as represented by biphenyl and pyrene derivatives, **H_4TCBP**[11] and **H_4TBAPy**,[12] respectively, possessing two sets of dicarboxy-m-terphenyl (DmT) moieties (Chart 3-1). When the two DmT moieties in a molecule are twisted such as **H_4TCBP**, the molecule forms a three-dimensional (3D) network assembly, which is further interpenetrated to give a weave HOF. On the other hand, when the two DmT moieties in a molecule are on the same plane as in the case of **H_4TBAPy**, the molecule gives a two-dimensional (2D) network assembly, which further stacks to give a layered HOF. Particularly, in the later case, its structural hierarchy, namely, 2D porous sheets and stacking of the sheets along the perpendicular direction to give layered HOFs, could be a simple and facile design principle to construct porous HOFs using various functional π-conjugated molecules. However, 2D layered HOFs frequently show unexpected structural transformation after solvent removal from the pores during activation, in contrast to weave HOFs. For example, Day, Inge, Little, Copper, and coworkers, recently reported that anthracene derivative **ABTPA** possessing DmT groups at 9- and 10-positions gave a 2D HOF that transformed by activation from solvent-filled HOF **ABTPA-1** with the face-to-face arrangement of the anthracene moiety to the empty HOF **ABTPA-2** with the face-to-edge arrangement, which was confirmed by 3D electron diffraction technique.[13] our group also reported that a series of layered HOFs based on hexa- and tetracarboxylic acids experienced sliding of layers[14] or rearrangements of intermolecular hydrogen bonds[15] during activation to yield empty HOFs with molecular arrangements different from the original frameworks. In some cases, the structure after transformation can be characterized by single crystal X-ray analysis, Rietveld refinement based on PXRD patterns, electron diffraction analysis, and crystal structure prediction.[13,14b,15a] However, in most cases, the molecular arrangements remain unclear, which disturbs revealing structure-property relationship of porous HOFs and prevents 2D HOFs being

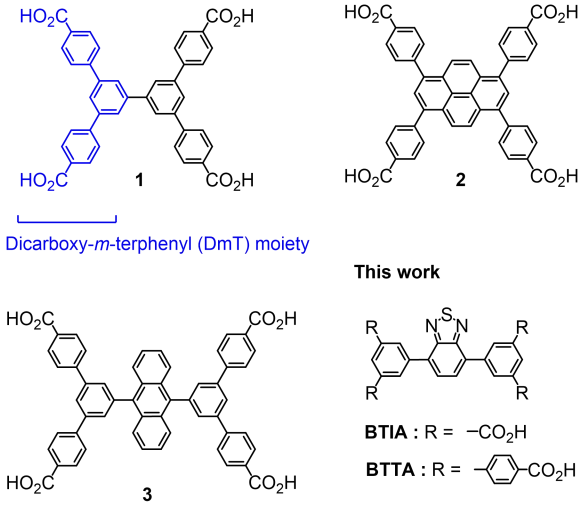

Chart 3-1. Tetracarboxylic acids with dicarboxy-m-terphenyl (DmT) moieties as a building block to construct HOFs.

promising candidate of designable porous materials. For overcoming the above mentioned problems, it is useful to apply a secondary building interaction different from that working for formation of a primary 2D network. For example, Miljanić and coworkers applied a π/π stacking interaction with charge transfer nature between electron-rich pyrazoles and electron-poor tetrafluorobenzene rings to construct stable

2D honeycomb HOFs with Brunner-Emmett-Teller (BET) surface area of 1159 m^2 g^{-1}.[7]

In connection with this, I have proposed that unidirectionally aligned slip-stacking of benzo[c][1,2,5]thiadiazole (BT) can be applied as an additional supramolecular synthon to construct a stable 2D HOF.[16] Electron withdrawing nature of BT makes it a useful building block of organic electronic devices.[17] Meanwhile, large dipole moment (4.8 Debye) of BT also plays an important role from supramolecular point of view. Namely, introduction of BT moieties in frameworks can enhance intermolecular interactions through dipole-dipole or dipole-quadruple interactions.[18] Indeed, I previously revealed that a tetracarboxylic acid possessing a BT moiety, 5,5'-(benzo[c][1,2,5]thiadiazole-4,7-diyl)diisophthalic acid (**BTIA**) gave layered HOF **BTIA-1**, in which BT moieties are slip-stacked unidirectionally to regulate lamination manner of 2D honeycomb sheets.[16] Based on this finding, I subsequently planned to construct an isostructural HOF with larger pores based of an expanded BT derivative, **BTTA** (Figure 3-1).

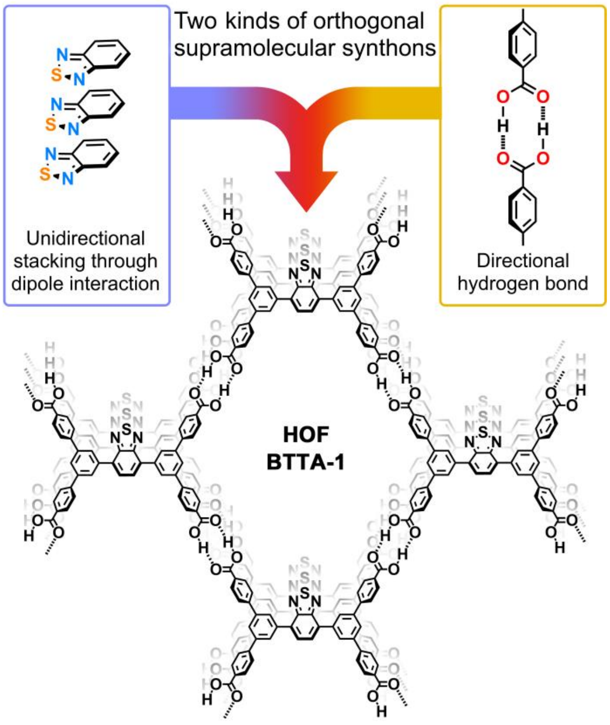

Figure 3-1. Construction of well-defined 2D HOF **BTTA-1** through orthogonal supramolecular synthons: unidirectional stacking of benzothiadiazole (BT) and directional hydrogen bounds of carboxy groups.

In this chapter, I describe a crystal structure of HOF **BTTA-1**, thermal stability up to ca. 275 °C, and permanent porosity with BET surface area of 1145 m^2 g^{-1}. **BTTA** forms a 2D porous sheet through hydrogen bonds between the carboxy groups and the sheets are laminated through unidirectional slip-stacking of the BT moieties to give a layered HOF with the same crystal structure with **BTIA-1**. This indicates that combination of two kinds of orthogonal supramolecular synthons can be a powerful strategy to construct robust HOFs. Moreover, time-resolved microwave conductivity (TRCM) measurement disclosed that these HOFs showed photoconductivity. These results indicate that 1D unidirectional stacking motif of the BT moieties can work not only as a useful supramolecular synthon to provide isostructural HOFs but as a conductive pathway of charge carrier. Therefore, BT-based HOFs can be a promising platform for multifunctional porous materials.

3-3. Result and Discussion

Synthesis and Crytallization

Suzuki-Miyaura cross-coupling reaction of pinacol boronate derivative **1**[19] and 4,7-dibromobenzo[c][1,2,5]thiadiazole (**2**) gave diphenylbenzothiadiazole derivative **3**. Hydrolysis of **3** in the presence of KOH gave tetracarboxylic acid 5',5''''-(benzo[c][1,2,5]thiadiazole-4,7-diyl)bis(([1,1':3',1''-terphenyl]-4,4''-dicarboxylic acid)) **BTTA**, which was characterized by ^{1}H and ^{13}C NMR spectroscopy and high-resolution mass spectrometry. The synthesized **BTTA** was recrystallized by slow evaporation of a mixed solution of N,N-dimethylformamide (DMF) and 1,2,4-trichlorobenzene (TCB) at 70 °C to give solvent-included HOF **BTTA-1(TCB)** as needle- or column-shaped crystals with typical dimension of 30 μm × 20 μm × 15 μm (Figure 3-2).

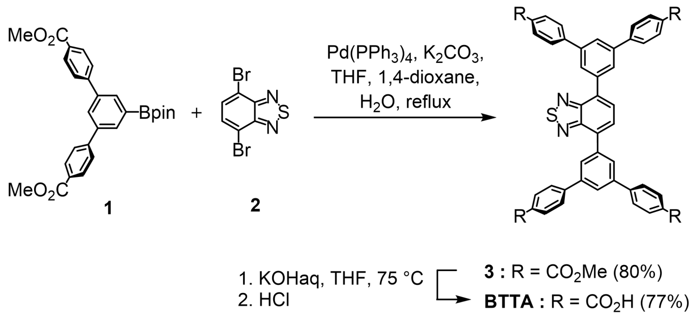

Scheme 3-1. synthesis of **3** and **BTTA**.

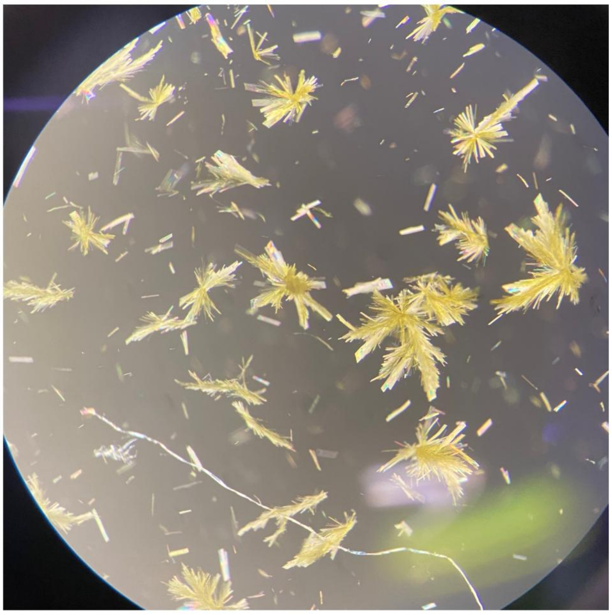

Figure 3-2. Crystalline morphology of **BTTA-1(TCB)**.

Crystal structure of HOF BTTA-1(TCB)

A crystal structure of **BTTA-1(TCB)** was determined by single crystalline X-ray diffraction (SCXRD) analysis as shown in Figure 3-3. **BTTA-1(TCB)** crystallized into non-centrosymmetric space group *C*m (Table 3-1). The **BTTA** molecule has a mirror plane perpendicular to the central BT moiety. A dihedral angle between the BT part and benzene ring A [ω(BT-A)] is 41.6° and those between benzene rings A and B [ω(A-B)], and A and C [ω(A-C)], are 29.5° and 29.2°, respectively (Figure 3-3a). Compared with the theoretically optimized conformation of **BTTA**, the observed value of ω(BT-A) is smaller by 3.2° while that of ω(A-B) and ω(A-C) is larger by ca. 9°, due to packing force in the crystalline state (Figure 3-4). Carboxy groups in **BTTA** form self-complementary hydrogen-bonded dimers between the peripheral carboxy groups with O···O distances of 2.61 Å and 2.62 Å to give a 2D networked sheet structure possessing rhombic pores with a size of 20 Å × 24 Å (Figure 3-3b). The sheets are slip-stacked along the c axis with interlayer distances of 3.47 Å to give a porous

Table 3-1. Crystal data of morphology of **BTTA-1(TCB)**

	BTTA-1(TCB)
System	monoclinic
Space group	*Cm* (No. 8)
Formula	C_{46} H_{28} N_2 O_8 S
Fw	768.76
a / Å	29.8700(6)
b / Å	34.7553(7)
c / Å	3.71190(10)
α / °	90
β / °	97.792(2)
γ / °	90
V / Å^3	3817.89(15)
Z	2
D / g cm3	0.669
Crystal size / mm	0.3 0.3 0.15
Crystal color	yellow
*R*1 (I > 2.0σ(I))	0.0714
*wR*2 (all)	0.1839
Unique reflection No.	23388
Obs. reflection No.	8247
GOF	0.947
λ / Å	0.81054(synchrotron)
T / K	100
CCDC no.	2165689

framework possessing 1D channels that have smooth surface of the inside wall and an aperture with a dimension of 18.6 Å × 21.8 Å. Molecules of TCB used in recrystallization are accommodated in the channel, while they were not capable of solving crystallographically due to severe disorder. Interestingly, the BT moieties are unidirectionally slip-stacked (Figure 3-3d). Intermolecular distance between the BT moiety is 3.45 Å and the stacked benzothiadiazole moiety is slipped by 1.36 Å along the direction parallel to the dipole moment. It is noteworthy that the present noncentrosymmetric molecular arrangement of **BTTA-1(TCB)** is closely similar with that of **BTIA-1** that is estimated by the crystal structure prediction technique.[16] In more details, although space group of the predicted structure of **BTIA-1(TCB)**, i.e. *P*1, is different from that of **BTTA-1(TCB)**, i.e. *Cm*, this discrepancy originates from software limitation. Even the molecular conformation of **BTIA** applied for the calculation has *Cs* symmetry, this was not recognized in the calculation, and therefore the resultant crystal belongs to space group *P*1. Consequently, these two crystals have basically the same molecular arrangements. These results indicate the importance of the directional interaction between the BT moieties.

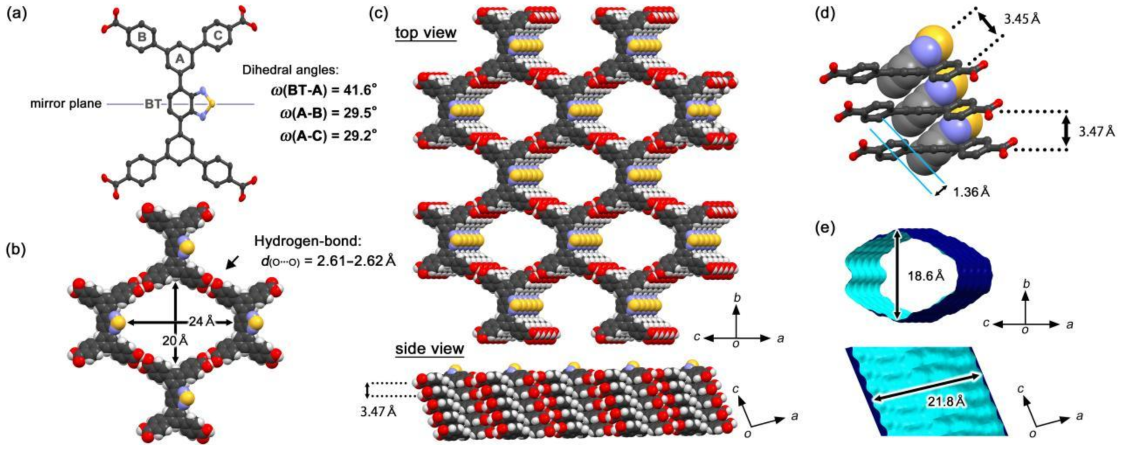

Figure 3-3. Crystal structures of HOF **BTTA-1(TCB)**. (a) Molecular structure of **BTTA** with anisotropic displacement ellipsoids with 50% probability. (b) Rhombic motif of

hydrogen-bonded network. (c) Packing diagram. (d) Relative orientation of the stacking molecules, in which benzothiadiazole moieties are drawn by the Space-fill model. (e) Visualized surface of 1D pore. The channels accommodate solvent molecules of 1,2,4-trichlorobenzene (TCB), which are not shown due to severe disorder.

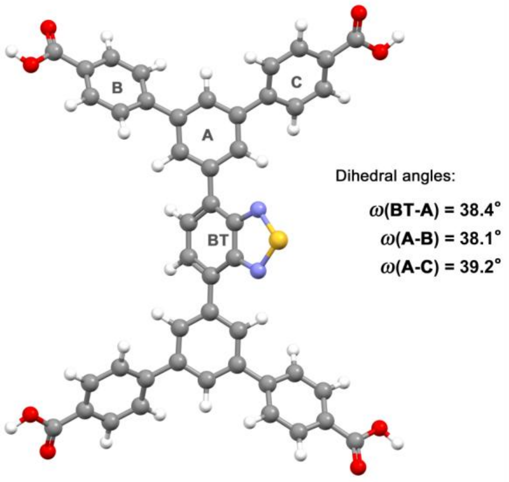

Figure 3-4. Molecular Conformation of **BTTA** optimized at B3LYP/6-31G* level of theory.

To obtain deeper insight for the assembly manner of BT moieties, I explored crystal structures of acyclic 4,7-diphenylbenzo[c][1,2,5]thiadiazole derivatives in CSD (Figure 3-5, Table 3-2). Among 34 structures obtained from the search, 6 crystal structures have unidirectional 1D stacking, as in the case of the present HOF **BTTA-1**. On the other hand, 9 structures have antiparallel dimeric or 1D-stacked arrangements. Additionally, other arrangements such as unidirectional herring-bone arrangement are also observed. To my disappointment, 14 structures have no contact between BT moieties because of bulkiness of the other part of the molecule, which preventing the BT moieties from contacting each other. These results indicate that interactions between BT moieties are not crucial for molecular packing. However, the unidirectional stacking is still a useful structural motif to control stacking manner of 2D HOF, combined with directional hydrogen bonds and structurally less hindered symmetric molecular skeleton.

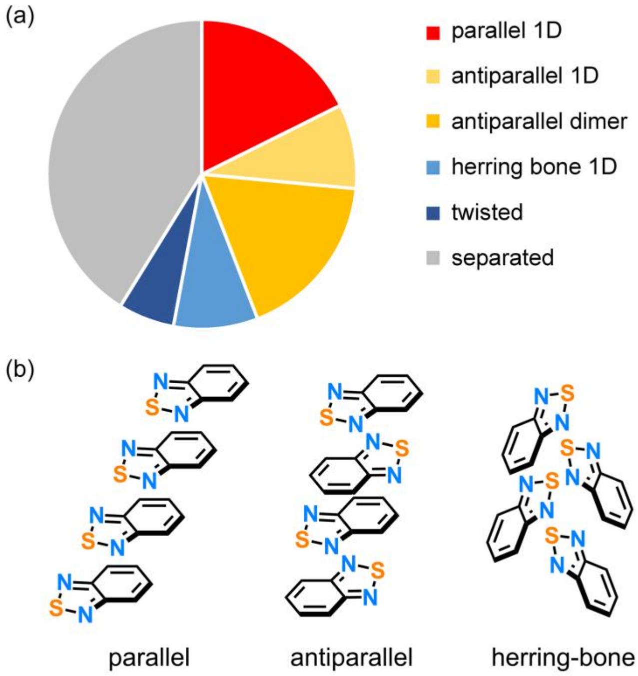

Figure 3-5. (a) Classification of BT part's arrangements observed in 34 kinds of crystal structures of acyclic 4,7-diphenylbenzo[c][1,2,5]thiadiazole derivatives extracted from CSD. (b) Representative arrangements of BT parts with parallel, antiparallel, and herring-bone manners.

CSD Database Search

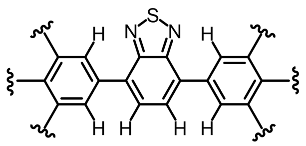

- No metal contained
- No cyclic structure

Table 3-2. Classification of crystals composed of acyclic BT derivatives extracted from the CSD

Refcode	Stacking manner	Arrangement in plane[a]
BIJFAC	Unidirectionally stacked 1D	Head-to-head
BIJFAC03	Twisted stacked 1D	Head-to-head
BIJFEG	Antiparallel stacked dimer	Head-to-head
BIJFEG02	Antiparallel stacked dimer	Head-to-head
EFALAB	Antiparallel stacked 1D	separated
ENUCAU	separated	separated
EQOPOS	Antiparallel stacked 1D	separated
GAGZIB	separated	separated
GALPAN	Unidirectionally stacked 1D	Head-to-head
GALRAP	Unidirectionally stacked 1D	Head-to-head
HUPDOO	Antiparallel stacked dimer	separated
IKEBUY	Unidirectionally stacked 1D	separated
IKEKAN	Antiparallel stacked dimer	Head-to-head
JEHLOA	separated	Head-to-head
JOBVEE	separated	separated
JURTEY	separated	separated
MOYYOR	separated	separated
NIRXIY	separated	separated
NIRZUM	separated	separated
NOXKES	separated	Head-to-tail
ONUJIT	Antiparallel stacked dimer	Head-to-head
OXABIB	Unidirectionally heringbone 1D	Head-to-tail
QITQIW	Twisted stacked 1D	Head-to-head
QITQOC	Unidirectionally stacked 1D	Head-to-head
RUBNEK	separated	Head-to-head
RUBNIO	separated	separated
RUBNOU	Antiparallel slipped 1D	separated
VINXEY	Antiparallel stacked dimer	separated
VINXIC	Unidirectionally heringbone dimer	Head-to-tail
VISFOV	Unidirectionally stacked 1D	separated
YEFHAT	Unidirectionally heringbone 1D	Head-to-tail
YEVWEE	separated	separated
YOPVOQ	separated	separated
YUQNUW	separated	separated

[a] Arrangement of BT in plane.

head-to-tail head-to-head

Thermal analysis

To estimate stoichiometry of the included solvent molecules, as-formed crystalline bulk of **BTTA-1(TCB)** was subjected to thermal gravimetric (TG) analysis as shown in Figure 3-6. The TG curve reaches plateau at ca. 180 °C with weight loss of 58%, which indicates that the framework contains TCB molecules with a host/guest molar ratio of 1/6. ^{1}H NMR spectrum of the as-formed crystals dissolved in DMSO-d_6 also supports this stoichiometry (Figure S3-5 in Appendix). Additional weight loss observed at higher than 300 °C probably corresponds to gradual thermal decomposition of the compound itself.

As-formed crystalline bulk of **BTTA-1(TCB)** was then subjected to variable temperature (VT) PXRD measurement (Figure 3-7) to reveal changes in the structure and crystallinity upon heating and removing solvent molecules. PXRD patterns at around room temperature shows almost no peaks probably due to scattering of diffracted X-ray by chlorine atoms in disordered TCB molecules in the channel. Indeed, when a single crystal was picked from the crystalline bulk and subjected to SCXRD with strong X-ray source or longer exposure time, the diffraction peaks appropriate for the analysis were observed. During increasing temperature up to 174 °C, the diffraction peaks appeared and their intensity gradually increased due to removal of the severely disordered solvent molecules.[14] The observed pattern are in good agreement with that simulated from SXRD data. For example, diffraction peaks such as 3.88°, 5.00°, 5.92°, 7.80°, 8.10°, 11.68°, and 12.88° correspond to (1 1 0), (0 2 0), (2 0 0), (2 2 0), (1 3 0), (2 4 0), and (1 5 0) plane, respectively. This pattern remained up to ca. 275 °C and rapidly decayed at higher temperature.

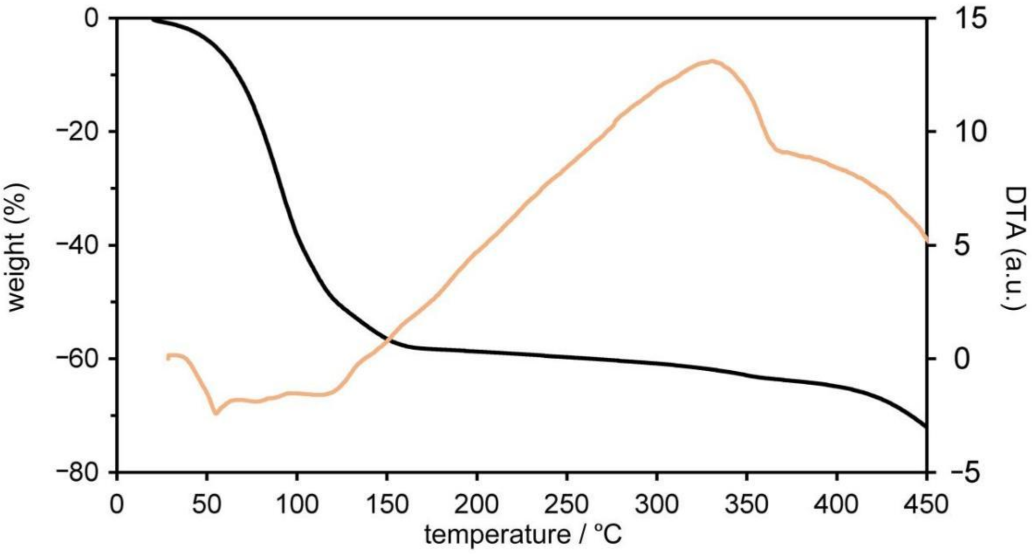

Figure 3-6. TG (black) and differential thermal (orange) curves of crystalline bulk of **BTTA-1(TCB)**.

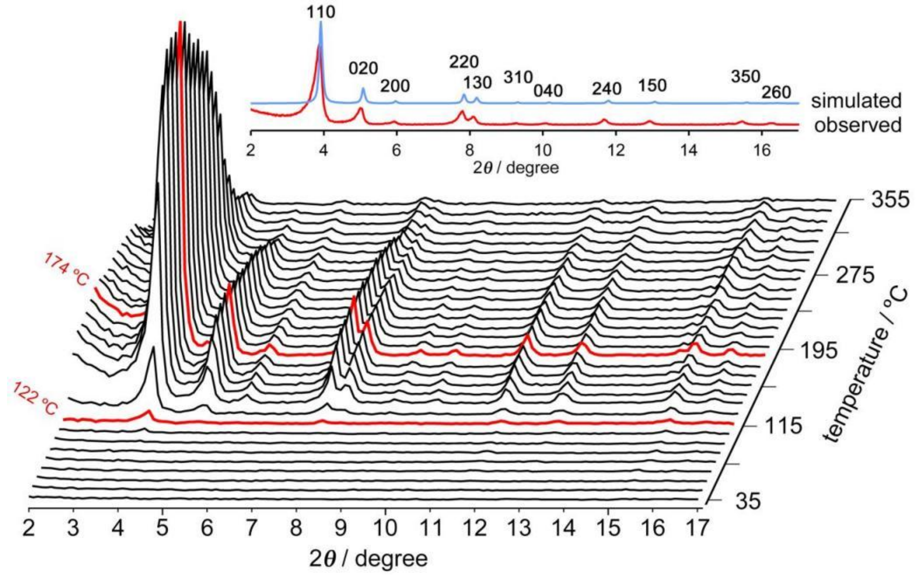

Figure 3-7. VT-PXRD pattern changes of **BTTA-1(TCB)** upon heating from room temperature to 360 °C. Inset: Comparison of the patterns simulated from SCXRD data and observed at 174 °C. The obvious pattern started to appear at 122 °C and its intensity was maximized at 174 °C.

Evaluation of permanent porosity

Although activation of solvent included framework **BTTA-1(TCB)** at 120 °C under a vacuum condition resulted in partial collapse of the porous structure, solvent exchange from TCB to benzene followed by mild heating at 80 °C under a vacuum condition successfully gave activated HOF **BTTA-1a**. A PXRD pattern of **BTTA-1a** was good agreement with the simulated pattern of **BTTA-1(TCB)**, indicating that the framework retained after activation (Figure 3-8). I confirmed that the framework was retained after heating at 275 °C for 24 h and that the compound did not decompose at this temperature from ^{1}H NMR (Figure S3-6 and Figure S3-7 in Appendix). Single crystallinity of **BTTA-1a**, on the other hand, was lost during activation, which was confirmed by observation with optical microscope.

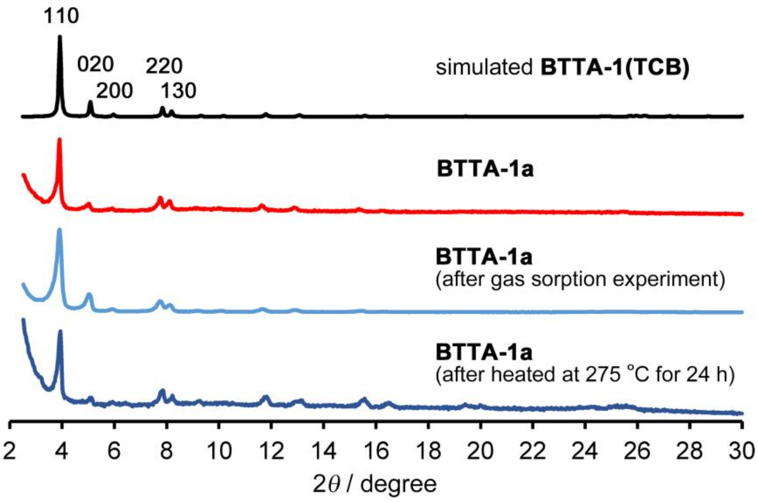

Figure 3-8. Stability of the framework of **BTTA-1a**. PXRD pattern of **BTTA-1a**, which shows good agreement with the simulate pattern of **BTTA-1(TCB)**, retains after gas sorption experiments or heating for 24 h at 275 °C.

Activated HOF **BTTA-1a** prepared by the solvent exchange were subjected to gas sorption experiments. A N_2 sorption isotherm recorded at 77 K shows rapid rise at low pressure and continuous increase up to relative pressure of $P_e/P_0 = 1.0$. The profile may be categorized in type-I isotherm, indicating existence of both micro- and macro-pores (Figure 3-9). More strictly, the isotherm shows ambiguous stepped curve at $P_e/P_0 = 0.02$, which is often observed HOFs with large aperture of the pore.[7,20] This presumably originates from coexistence of adsorption sites with different affinities for the gas molecules (i.e., the benzothiadiazole and carboxyphenyl moieties). BET surface area was calculated to be 1145 $m^2\ g^{-1}$ based on the N_2 sorption experiment (Figure 3-10), indicating **BTTA-1a** has a moderate porosity compared with reported HOFs composed the related tetratopic molecules (Table 3-3). Nonlocal density functional theory (NLDFT) calculation indicates that **BTTA-1a** has the pore width of 11 Å (Figure 3-11). CO_2 sorption experiments were also conducted, showing an adsorption isotherm with gradual slope at lower pressure than P_e/P_0 = ca. 0.2, which is also often observed for HOFs with large aperture of the pore.[7,20] The framework was retained after the gas sorption experiments.

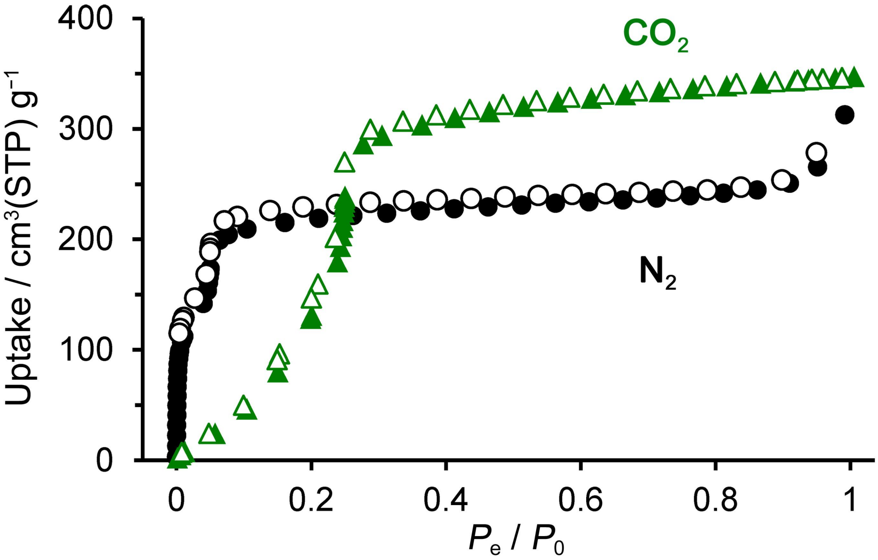

Figure 3-9. Gas sorption isotherms of the activated HOF **BTTA-1a** for nitrogen (black

circle) at 77 K and carbon dioxide (green triangle) at 195 K. Solid and open symbols correspond to adsorption and desorption processes, respectively.

Table 3-3. N_2 uptake and BET surface areas of the related HOFs that reported before.

HOFs	N_2 uptake / cm^3g^{-1}	SA_{BET} / m^2g^{-1} (activation method)	Ref.
HOF-14a	881	2573	28
HOF-TCBP	535	2066	11a
PFC-1	606.7 415	2122 1014	12a 29
HOF-15a	474 204	1964 (sc-CO_2) 791 (solvent degassed)	11b
HOF-20a	372	1323	30
ABTPA-2	ca. 392	1183	13
ZJU-HOF-10	293 (sc-CO_2) 78 (volumn activation)	1169 (sc-CO_2) 295 (volumn activation)	31
BTTA-1a	312	1145	This work
HOF-100	235	900	32
HOF-FAFU-1	ca. 270	840	33
HOF-30a	118	361	34
BTIA-1a	-----	237[a] (conventional) 720[a] (solvent exchange)	16

[a] Calculated on the basis of CO_2 sorption isotherms.

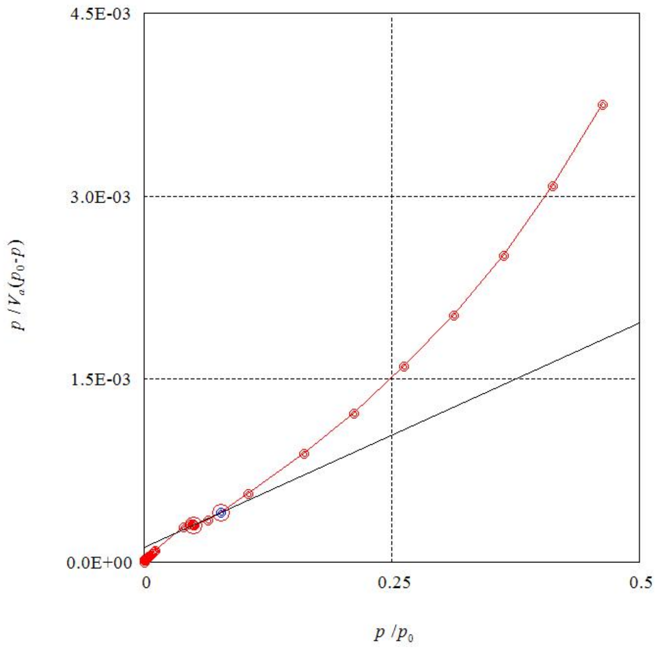

Slope	3.6816E-03	
Intercept	1.1960E-04	
Correlation coefficient	0.9860	
BET range limit (p/p0=0.1669)	25th point	(p/p0=7.7088E-02)
Va(p_0-p)$_{max}$	1.9073E+04	
V$_m$	263.08	[cm^3 (STP) g^{-1}]
SA(BET)	1.1450E+03	[m^2 g^{-1}]
C	31.783	
Total volum (p/p0=0.990)	0.4799	[cm^3 g^{-1}]

Figure 3-10. BET analysis based on N_2 adsorption data of **BTTA-1a**

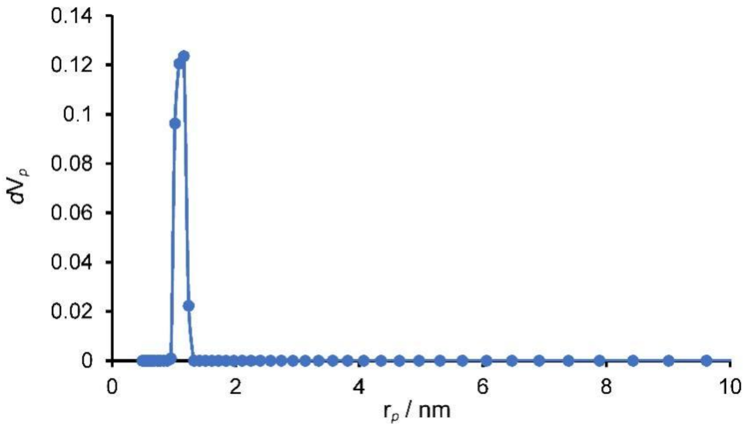

Figure 3-11. Pore distribution of **BTTA-1a.**

Optoelectronic properties

UV-vis absorption and fluorescence spectra of **BTTA** and **BTIA** and their ester derivatives (**3** and **4**, respectively) were measured in solution states (Figure 3-12, Figure 3-13). Ester **3** also has absorption bands at 280 and 381 nm and emission band at 475 nm with shoulder at ca. 500 nm, which is slightly red-shifted compared with **4**, which has absorption bands at 235, 278, and 372 nm and emission band at 468 nm with shoulder at ca. 450 nm. Fluorescence quantum yields of **3** and **4** in dichloromethane solutions are 0.60 and 0.70, respectively. Similarly, as shown in Figure 3-12, **BTTA** has absorption bands at 280 and 386 nm and emission band at 488 nm with shoulder at ca. 520 nm, meanwhile **BTIA** has absorption bands at 275 and 386 nm and emission band at 482 nm. Fluorescence quantum yields of **BTTA** and **BTIA** in DMSO solutions are 0.20 and 0.28, respectively. In solid states, HOFs **BTTA-1(TCB)** and **BTIA-1(TCB)** show no significant fluorescence due to strong quenching in aggregation states.

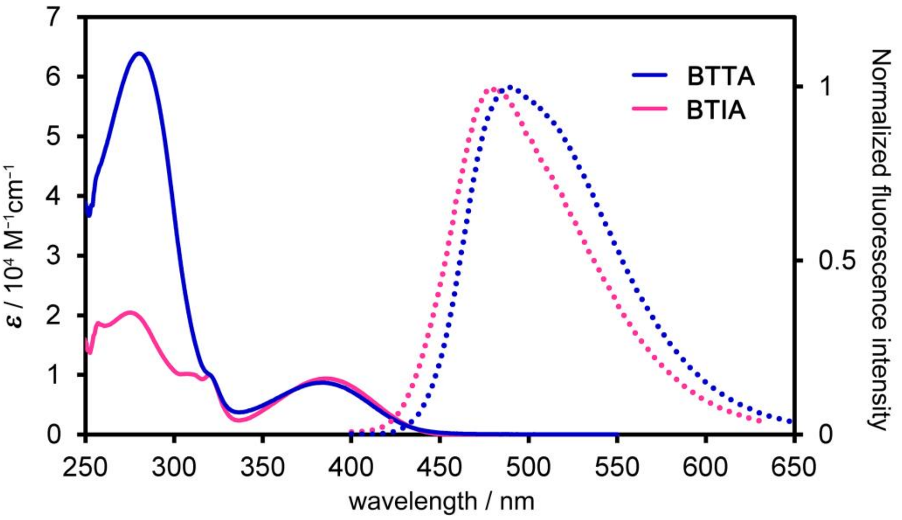

Figure 3-12. UV-vis and fluorescence spectra of **BTTA** and **BTIA** in DMSO solution.

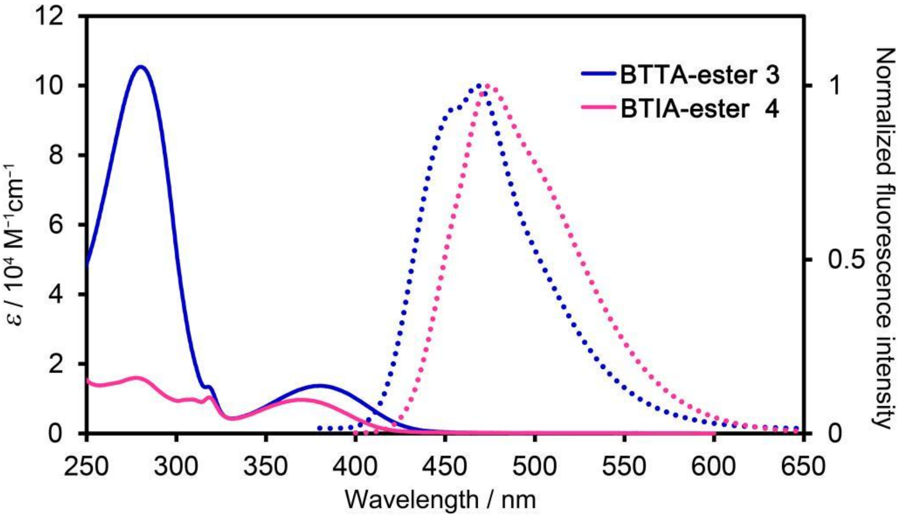

Figure 3-13. UV-vis and fluorescence spectra of ester derivatives **3** and **4**.

Photoconductivity

Unidirectional 1D-stacked structure of BT moieties prompted me to investigate charge carrier transportation ability of HOFs **BTIA-1** and **BTTA-1**. To evaluate photo-conductivity of the HOFs, crystalline powder of as-formed HOFs, **BTIA-1(TCB)** and **BTTA-1(TCB)**, and their activated forms **BTIA-1a** and **BTTA-1a**, respectively, were subjected to flashphotolysis time-resolved microwave conductivity (FP-TRMC) measurements[21] with excitation at 355 nm (Figure 3-14). All samples showed a prompt rise within the time resolution upon photo-excitation, followed by a slow decay. Despite structural differences of spacer moieties, **BTIA-1** and **BTTA-1** show the quite similar signal profiles, indicating that the 1D stacked structure of BT works as a carrier transports path in the HOFs. The maximum values of $\varphi\Sigma\mu$ ($\varphi\Sigma\mu_{\text{max}}$) are 2.5×10^{-9} and 2.7×10^{-9} m^2 V^{-1} s^{-1} , for **BTIA-1(TCB)** and **BTTA-1(TCB)**, respectively, where φ and $\Sigma\mu$ denote the yield of photogenerated charge carriers (quantum efficiency) and the sum of mobilities for negative and positive carriers, respectively. The activated HOFs, **BTIA-1a** and **BTTA-1a** show smaller signals than the solvent included HOFs: Their $\varphi\Sigma\mu$ max values are 1.3×10^{-9} and 1.4×10^{-9} m^2 V^{-1} s^{-1}, respectively. These results imply that TCB molecules accommodated in channel pores in the framework also works as a pathway of charge carrier.

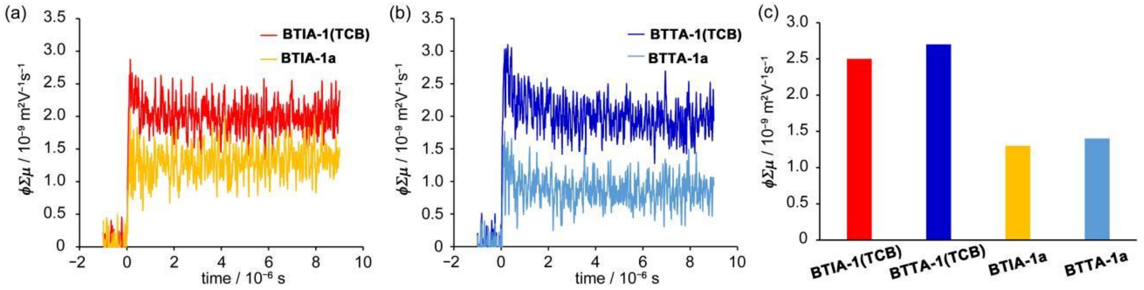

Figure 3-14. Photocurrent transients of HOFs (a) **BTIA-1** and (b) **BTTA-1** with and without activation measured by TRMC technique. (c) The $\varphi\Sigma\mu_{\max}$ values of the HOFs.

3-4. Conclusion

In this chapter, I constructed a new hydrogen-bonded organic framework (HOF) based on benzo[c][1,2,5]thiadiazole- (BT-) based tetracarboxylic acid **BTTA**. The HOF has a layered stacking structure of hydrogen-bonded 2D honeycomb sheets. It is remarkable that orthogonally-working two kinds of interactions, that is directional hydrogen bond between carboxy groups and slip-stacking of BT groups with unidirectional alignment, play important roles to give the well-defined porous layered HOF. The HOF shows thermal stability up to 275 °C, permanent porosity with BET surface area of 1145 m^2 g^{-1} , and photoconductivity. The present BT-based HOF can be a promising platform for multifunctional porous material.

3-5. Experimental section

General

All reagents and solvents were used as received from commercial suppliers. ^{1}H NMR spectra were measured by a Bruker AV400M spectrometer. Residual protons and carbons of deuterated solvents were used as internal standards for the measurements: δ = 7.26 ppm ($CDCl_3$) and 2.50 ppm (DMSO-*d*6) for ^{1}H NMR and δ = 77.0 ppm ($CDCl_3$)

and 29.76 ppm (DMSO-*d*6) for ^{13}C NMR. Thermogravimetric (TG) analysis was performed on Rigaku TG8120 under an N_2 purge (300 mL min^{-1}) at a heating rate of 10 K min^{-1}. Fluorescence and excitation spectra were measured on JASCO FP-8500 spectrofluorometer. Absolute fluorescence quantum yield in a solution state was determined with integrating sphere. HR-MS analysis was performed on a JEOL JMS-700 spectrometer. Theoretical calculation was performed on Gaussian 09.[22] Molecular structures were optimized by DFT method at B3LYP/6-31G* level. Powder X-ray diffraction (PXRD) data were collected on a Rigaku Ultima-IV (40 kV, 44 mA) using graphite-monochromatized Cu-Kα radiation at room temperature. A scan rate is 2.0° min^{-1}. N_2 and CO_2 sorption experiments were conducted at 77 K and 195 K, respectively, on a Micromeritics 3Flex and BELSORP-max. TRMC experiments were performed for the powder sample on a quartz substrate. The microwave frequency and its power were ~9 GHz and ~3 mW, respectively. The third harmonic generation of a Nd:YAG laser (355 nm, Continuum Inc., Surelite II, 5−8 ns pulse duration, 10 Hz) was used for the excitation (incident photon density $I_0 = 9.1 \times 10^{15}$ photons cm^{-2} $pulse^{-1}$). The photoconductivity ($\Delta\sigma = A^{-1}\ \Delta P_r P_r^{-1}$ where A is the sensitivity factor, P_r is the reflected microwave power, and ΔP_r is the change in P_r upon exposure to light) was converted into the product of the quantum yield (φ) and sum of the charge carrier mobilities $\Sigma\mu$ ($= \mu_+ + \mu_-$) using the relationship $\varphi\Sigma\mu = \Delta\sigma(eI_0F_{\mathrm{light}})^{-1}$, where e and F_{Light} are the electron charge and correction (or filling) factor, respectively. The experiments were performed at room temperature in the air.

Single crystal X-ray measurement and analysis

Diffraction data of **BTTA-1(TCB)** was collected at Spring-8 (BL40XU) with synchrotron radiation (λ = 0.81054 Å). Diffraction Data collection, cell refinement, and data reduction were carried out with CrysAlis PRO.[23] SHELXT was used for the structure solution of the crystals.[24] These calculations were performed with the observed reflections [$I > 2\sigma(I)$] with the program OLEX-2 crystallographic software.[25] Structural refinement was performed by SHELXL.[26] All non-hydrogen atoms except for highly disordered solvent molecules accommodated in voids were refined with anisotropic displacement parameters, and hydrogen atoms were placed in idealized positions and refined as rigid atoms with the relative isotropic displacement parameters. SQUEEZE function equipped in the PLATON program was used to treat severely disordered solvent molecules in voids.[27] Variable temperature PXRD measurement was performed on a Rigaku Ultima-IV using graphite-monochromatized Cu-Kα radiation with a temperature control unit under ambient atmosphere. Temperature of the sample was increased from room temperature to 360 °C with a rate of 1.0 °C min^{-1}. During temperature increasing, XRD patterns ranged from 2.0° to 17° was repeatedly recorded with a scan rate of 3° min^{-1} . Therefore, each PXRD scan has a temperature width of ca. 5 °C.

Synthesis of ester 3

Dimethyl 5'-(4,4,5,5-tetramethyl-1,3,2-dioxaborolan-2-yl)-[1,1':3',1''- terphenyl]-4,4''-dicarboxylate (**1**), was synthesized according to literature.[19] The pinacol boronate **1** (0.655 g, 1.39 mmol), 4,7-dibromobenzo[c][1,2,5]thiadiazole (**2**) (0.188 g, 0.640 mmol), K_2CO_3 (0.264 g, 1.91 mmol), and $Pd(PPh_3)_4$ (38.0 mg, 0.0329 mmol) was added to a 100 mL three-necked flask. The deoxygenated solvents dioxane (15 mL), THF (15 mL) and H_2O (5 mL) was added to the flask and the suspension was stirred at 110 °C for 24 h under the protection of N_2 atmosphere. After cooling to the room temperature, the solvent was removed in a rotary evaporator, and the solid was washed by CH_2Cl_2 and H_2O, then dried in vacuo to give **3** (0.417 g, 80%) as a yellow solid. M.p. 289 °C; ^{1}H NMR (400 MHz, $CDCl_3$) δ 8.27 (d, *J* = 1.6 Hz, 4H), 8.18 (d, *J* = 8.4 Hz, 8H), 7.97 (s, 2H), 7.96 (t, *J* = 1.6 Hz, 2H), 7.83 (d, *J* = 8.4 Hz, 8H), 3.97 (s, 12H) (Figure S3-1 in appendix). ^{13}C NMR (100 MHz, $CDCl_3$) δ 167.1, 154.3, 145.3, 141.5, 138.8, 133.4, 130.5, 129.7, 128.5, 128.2, 127.5, 126.5, 52.4 ppm. HR-MS (FD): calcd. For $C_{50}H_{36}N_2O_8S$ [M]+ 824.2192; found: 824.2194. (Figure S3-2 in appendix)

Synthesis of BTTA

To a solution of ester **3** (0.200 g, 0.24 mmol) dissolved in THF (30 mL) was added 3 M KOHaq (30 mL). After reflux at 75 °C for 115 h, the THF was distilled off under reduced pressure and 6M HClaq was added till further precipitate was not formed anymore. The precipitate was treated by centrifugation, washed with water, and dried in vacuo to give the BTTA (0.144 g, 0.187 mmol) in 77% as a yellow solid. Mp > 300 °C; ^{1}H NMR (400 MHz, DMSO-d_6) δ 8.41 (s, 4H), 8.30 (s, 2H), 8.16 (s, 2H), 8.10 (d, J = 8.0 Hz, 8H), 8.05 (d, J = 8.0 Hz, 8H) (Figure S3-4 in appendix). ^{13}C NMR (100 MHz, DMSO-d_6) δ 167.2, 153.4, 143.9, 140.3, 138.4, 132.2, 130.2, 130.0, 128.9, 127.7, 127.3, 125.7 ppm (Figure S3-4); HR-MS (FD): calcd. For $C_{46}H_{28}N_2O_8S$ [M]+ 768.1566; found: 768.1567.

Reference

1. S. Patai, Acidity and Hydrogen Bonding of Carboxyl Groups, 1st ed.; The Chemistry of Carboxylic Acids and Esters. John Wiley & Sons Press, 1969, pp 211−293. DOI: 10.1002/9780470771099.
2. G. R. Desiraju, *Angew. Chem., Int. Ed. Engl.* **1995**, *34*, 2311−2327.
3. O. Ivasenko, D. F. Perepichka, *Chem. Soc. Rev.* **2011**, *40*, 191−206.
4. a) J. Luo, J.-W. Wang, J.-H. Zhang, ; S. Lai, D. -C. Zhong, *CrystEngComm* **2018**, *20*, 5884−5898; b) R.-B. Lin, Y.-B. He, P. Li, H. -L. Wang, W. Zhou, B. Chen, *Chem. Soc. Rev.* **2019**, *48*, 1362−1389; c) I. Hisaki, X. Chen, K. Takahashi, T. Nakamura, *Angew. Chem. Int. Ed.* **2019**, *58*, 11160−11170; d) B. Wang, R. -B. Lin, Z.-J. Zhang, S.-C. Xiang, B. Chen, *J. Am. Chem. Soc.* **2020**, *142*, 14399−14416; e) P.-H. Li, M. R. Ryder, J. F. Stoddart, *Acc. Mater. Res.* **2020**, *1*, 77−87.
5. a) P. Li, Y. -B. He, H. D. Arman, R. Krishna, H. -L. Wang, L. -H. Weng, B. Chen, *Chem. Commun.* **2014**, *50*, 13081−13084; b) P. Li, Y.-B. He, J. Guang, L.-H. Weng, J. C.-G. Zhao, S.-C. Xiang, B. Chen, *J. Am. Chem. Soc.* **2014**, *136*, 547−549.
6. a) M. Mastalerz, I. M. Oppel, *Angew. Chem. Int. Ed.* **2012**, *51*, 5252−5255; b) A. Pulido. L. -J. Chen, T. Kaczorowski, D. Holden, M. A. Little, S. Y. Chong, B. J. Slater, D. P. Mcmahon, B. Bonillo, C. J. Stackhouse, A. Stephenson, C. M. Kane, R. Clowes, T. Hasell, A. I. Cooper, G. M. Day, *Nature* **2017**, *543*, 657−664.
7. a) W. -Q. Yan, X. -P. Yu, T. Yan, D.-F. Wu, E.-L. Ning, Y. Qi, Y.-F. Han, Q. -W. Li, *Chem. Commun.* **2017**, *53*, 3677−3680; b) T.-H. Chen, I. Popov, W. Kaveevivitchi, Y.-C. Chuang, Y. S. Chen, O. Daugulis, A. J. Jacobson, O. Š. Miljanić, *Nat. Commun.* **2014**, *5*, 5131−5138.
8. (a) A. Karmakar, R. Illathvalappil, B. Anothumakkool, A. Sen, P. Samanta, ; A. V. Desai, S. Kurungot, S. Ghosh, *Angew. Chem. Int. Ed.* **2016**, *55*, 10667−10671 (b) A. Yamamoto, S. Uehara, T. Hamada, M. Miyata, I. Hisaki, N. Tohnai, *Cryst. Growth Des.* **2012**, *12*, 4600−4606.
9. P. Wied, F. Carraro, J. M. Bolivar, C. J. Doonan, P. Falcaro, ; B. Nidetzky. *Angew.*

Chem.Int. Ed. **2022**, *61*, e202117345.

10. I. Hisaki, *J. Incl. Phenom. Macro. Chem.* **2020**, *96*, 215−231.
11. a) F. -L. Hu, C. -P. Liu, M. -Y. Wu, J. -D. Pang, F. -L. Jiang, D. -Q. Yuan, M. -C. Hong, *Angew. Chem. Int. Ed.* **2017**, *56*, 2101−2104; b) W. Yang, J. -X. Wang, B.-Q. Yu, B. Li, H. -L. Wang, J.-Z. Jiang, *Cryst. Growth Des.* **2022**, *22*, 1817−1823.
12. a) Q. Yin, P. Zhao, R.-J. Sa, G. -C. Chen, J. Lü, T. -F. Liu, R. Cao, *Angew. Chem. Int. Ed.* **2018**, *57*, 7691−7696; b) S. Goswami, K. -K. Ma, J. -X. Duan, K. O. Kirlikovali, J. -Q. Bai, J. T. Hupp, P. Li, O. M. Farha, *Langmuir* **2022**, *38*, 1533−1539; c) K.-K. Ma, P. Li, J. H. Xin, Y.-W. Chen, Z. -J. Chen, S. Goswami, X. -F. Liu, S. Kato, H. -Y. Chen, X. Zhang, J. -Q. Bai, M. Wasson, R. R. Maldonado, R. Q. Snurr, O. K. Farha, *Cell Rep. Phys. Sci.* **2020**, *1*, 100024−100034.
13. P. Cui, E. S. Grape, P. R. Spackman, Y. Wu, R. Clowes, G. M. Day, A. K. Inge, M. A. Little, A. I. Cooper, *J. Am. Chem. Soc.* **2020**, *142*, 12743−12750.
14. a) I. Hisaki, S. Nakagawa, N. Tohnai, M. Miyata, *Angew. Chem. Int. Ed.* **2015**, *54*, 3008−3012; b) I. Hisaki, S. Nakagawa, N. Ikenaka, Y. Imamura, M. Katouda, M. Tashiro, H. Tsuchida, T. Ogoshi, H. Sato, N. Tohnai, M. Miyata, *J. Am. Chem. Soc.* **2016**, *138*, 6617−6628.
15. a) H. Kubo, R. Oketani, I. Hisaki, *Chem. Commun.* **2021**, *57*, 8568−8571; b) Q. Ji, K. Takahashi, S. I. Noro, Y. Ishigaki, K. Kokado, T. Nakamura, I. Hisaki, *Cryst. Growth Des.* **2021**, *21*, 4656−4664.
16. Z. X.Yang, A. Moriyama, R. Oketani, T. Nakamura, I. Hisaki, *Chem. Lett.* **2021**, *50*, 1909−1912.
17. a) B. A. D. Neto, A. A. M. Lapis, E. N. D. Silva, J. Dupont, *Eur. J. Org. Chem.* **2013**, 228−225; b) B. A. D. Neto, P. H. P. R. Carvalho, J. R. Correa, *Acc. Chem. Res.* **2015**, *48*, 1560–1569; c) M. Melucci, L. Favaretto, A. Zanelli, M. Cavallini, A. Bongini, P. Maccagnani, P. Ostoja, G. Derue, R. Lazzaroni, G. Barbarella, *Adv. Funct. Mater.* **2010**, *20*, 445–452; d) S. J. Ren, R. Dawson, D. J. Adams, A. I. Cooper, *Polym. Chem.* **2013**, *4*, 5585–5590; e) D. Zhao, D. Yue, K. Jiang, Y. J. Cui, Q. Zhang,

Y. Yang, G. D. Qian, *J. Mater. Chem. C* **2017**, *5*, 1607–1613; f) K. Ma, Y. -N. Zhao, J. Ding, X. -R. Meng, H. -W. Hou, *Cryst. Growth Des.* **2018**, *18*, 7419–7425; g) A. Mallick, A. M. EI-Zohry, O. Shekhah, J. Yin, J. -T. Jia, H. Aggarwal, A. Emwas, O. F. Mohammed, M. Eddaoudi, *J. Am. Chem. Soc.* **2019**, *141*, 7245–7249; h) M. Echeverri, C. Ruiz, S. Gamez-Valenzuela, M. Alonso-Navarro, E. Gutierrez-Puebla, J. L. Serrano, M. C. R. Delgado, B. Gomez-Lor, *ACS Appl. Mater. Interfaces* **2020**, *12*, 10929–10937.

18. a) C. -L. Song, Y. -B. He, B. Li, Y. -J. Ling, H. -L.Wang, Y. -L. Feng, R. Krishna, B. Chen, *Chem. Commun.* **2014**, *50*, 12105– 12108; b) C. -L. Song, Y. -J Ling, L.-T. Jin, M. -X. Zhang, D. -L. Chen, Y. -B. He, *Dalton Trans.* **2016**, *45*, 190−197.
19. a) J. -T. Jia, L. Wang, F. X. Sun, X. -F. Jing, Z. Bian, L. -X. Gao, R. Krishna, G. -S. Zhu, *Chem. Eur. J.* **2014**, *20*, 9073–9080; b) A. Mallick, A. M. EI-Zohry, O. Shekhah, J. Yin, J. -T. Jia, H. Aggarwal, A. Emwas, O. F. Mohammed, M. Eddaoudi, *J. Am. Chem. Soc.* **2019**, *141*, 7245–7249.
20. Y. Suzuki, M. Gutierrez, S. Tanaka, E. Gomez, N. Tohnai, N. Yasuda, N. Matubayasi, A. Douhai, I. Hisaki, *Chem. Sci.* **2021**, *12*, 9607–9618.
21. a) A. Saeki, Y. Koizumi, T. Aida, S. Seki, *Acc. Chem. Res.* **2012**, *45*, 1193–1202; b) A. Saeki, *Polym. J.* **2020**, *52*, 1307–1321.
22. Gaussian 09, revision D.01; Frisch, M. J.; Trucks, G. W.; Schlegel, H.B. et al. Gaussian, Inc., Wallingford CT, 2009.
23. Rigaku Oxford Diffraction (2015), Software CrysAlisPro 1.171.38.41o. Rigaku Corporation, Tokyo, Japan.
24. G. M. Sheldrick, *Acta Crystallogr. Sect. A* **2015**, *71*, 3–8.
25. O. V. Dolomanov, L. J. Bourhis, R. J. Gildea, J. A. K. Howard, H. Puschmann, OLEX2: A Complete Structure Solution, Refinement and Analysis Program. *J. Appl. Cryst.* **2009**, *42*, 339– 341.
26. G. M. Sheldrick, *Acta Crystallogr. Sect. C Struct. Chem.* **2015**, *71*, 3–8.
27. a) A. L. Spek, *Acta Crystallogr. Sect. D* **2009**, *65*, 148–155; b) P. V. D. Sluis, A. L.

Spek, *Acta Crystallogr. Sect. A* **1990**, *46*, 194−201.

28. B. Wang, X. -L. Lv, J. Lv, L. Ma, R. -B. Lin, H. Cui, J. Zhang, Z. -J. Zhang, S. -C. Xiang, B. -L. Chen, *Chem. Commun.* **2020**, *56*, 66−69.
29. Q.Yin, Y. -L. Li, L. Li, J. Lv, T. -F. Liu, R. Cao, *ACS Appl. Mater. Interfaces* **2019**, *11*, 17823−17827.
30. B. Wang, R. He, L. -H. Xie, Z. -J. Lin, X. Zhang, J. Wang, H. -L. Huang, Z. -J. Zhang, K. S. Schanze, J. Zhang, S. -C. Xiang, B. -L. Chen, *J. Am. Chem. Soc*. **2020**, *142*, 12478−12485.
31. J. -X. Wang, X. -W. Gu, Y. -X. Lin, B. Li, G. -D. Qian, *ACS Materials Lett.* **2021**, *3*, 497−503.
32. K. -K. Ma, P. Li, J. H. Xin, Y. -W. Chen, Z. -J. Chen, S. Goswami, X. -F. Liu, S. Kato, H. -Y. Chen, X. Zhang, J. -Q. Bai, M. C. Wasson, R. R. Maldonado, R. Q. Snurr, O. K. Farha, *Cell Rep. Phys. Sci*. **2020**, *1*, 100024−100034.
33. Z. -J. Lin, J. -Y. Qin, X. -P. Zhang, K. -C. Wu, G. -J. Cao, B. -L. Chen, *ACS Appl. Mater. Interfaces* **2022**, *14*, 21098−21105.
34. B. -Q. Yu, S. -B. Geng, H. -L. Wang, W. Zhou, Z. -J. Zhang, B. -L. Chen, J. -Z. Jiang, *Angew. Chem. Int. Ed.* **2021**, *60*, 25942−25948.

Chapter 4

Geometrically mismatched H-bonded framework composed of tetratopic carboxylic acid

4-1. Abstract

Porous organic frameworks possessing interactive free sites in the pore have attracted much attention due to their potential to show the site-originated specific functionalities. Herein, I demonstrate that such a framework could be constructed using a concept of geometrically mismatched frameworks composed of phenanthroline-based tetratopic carboxylic acid **CP-Phen**. Simple recrystallization of **CP-Phen** yielded a solvent included porous framework **CP-Phen-1**, in which three of four carboxy groups form hydrogen-bonded dimer to form a ladder-shaped framework, while the remained one does not participate in framework formation due to geometrical mismatch, instead of trapping solvent molecules through weak hydrogen-bonding. This result implies that the proposed strategy is effective to provide free interactive sites in porous frameworks. Although **CP-Phen-1** undergoes two-step structural transformation presumably accompanied by hydrogen-bond rearrangements upon loss of solvent molecules, the activated framework shows good thermal stability up to 360 °C and selective CO_2 adsorption.

4-2. Introduction

The rational design and synthesis of novel crystalline porous materials for specific application is one of the important topics in crystal engineering.[1] Researchers have devoted much effort to constructing application-oriented metal-organic frameworks (MOFs) based on the pre- or post-synthetic modification of metal nodes and organic ligands.[2] The multiple applicability of MOFs is highly dependent on the properties of pristine frameworks and incorporated functional groups or sites,[3] such as uncoordinated nitrogen,[4] halogen,[5] sulfonic acid,[6] and carboxy groups.[7] Particularly, free carboxy groups in MOFs are nonnegligible because of the Brønsted acidity, polatity and binding capacity with organic molecules and metal ions.[3] Free carboxy groups can be obtained in the final structure by adjusting the pH during the synthesis, making the modified MOFs with the promising application. For examples, Tian and coworkers reported three-dimensional porous coordination polymers (PCPs) possessing grafted carboxy groups on their pore surface. The densely incorporated free carboxy groups can provide the PCPs flexibility, and also, possibility for high proton conduction.[8] Christopher and coworkers demonstrated free carboxy and hydroxy groups in MFM-303(Al) played critical roles for immobilizing NH_3 molecules which was identified by in situ synchrotron X-ray diffraction and inelastic neutron scattering.[9]

A porous molecular crystal self-assembled by pre-organized intermolecular hydrogen bonds (H-bonds) between organic moieties, which is often called hydrogen-bonded organic framework (HOF) or supramolecular organic framework (SOF), is also one sub-category of porous organic crystalline materials.[10] To construct HOFs, carboxylic acid,[11] diaminotriazine,[12] heterocycles,[13] and urea[14] have been applied as functional moieties providing both H-bond donors and acceptors. In most studies, H-bond donors and acceptors in organic moieties are matched in pairs, and form H-bonding units in dimers, trimers or chains to maintain stability of the framework structures. Although many novel HOF materials with unprecedented structures and fascinating topologies have been reported, it is rare that some H-bond donors/acceptors remain free in the frameworks. In other words, it remains to be explored that how to synthematically obtain HOFs with free hydrogen-bonding groups or active sites, which is a prerequisite for functionalization of HOFs.

To date, the functionalization of HOFs has been conducted by the following three approaches. (1) Pre-incorporation into building blocks: our group reported hexaazatriphenylene-based HOF **CPHATN-1**, which showed acid vapor-responsive color change duo to the protonation/deprotonation of N atoms embedded in its π-conjugated core.[15] (2) Postsynthetic functionalization: H. Wang and coworkers fabricated a heterogeneous Pd-catalyst by postsynthetic metalation of **HOF-19**, making for excellent catalytic performance for Suzuki-Miyaura cross-coupling reaction with high isolated yields of about 96-98%.[16] (3) Temporary masking of functional groups: B. Chen et al. obtained HOF-16 that involved carboxyl groups masked by methanol, which can be removed *in vacuo* to leave the carboxylic acid exposed in the pores, allowing high-efficiency separation ability for propylene/propane.[17]

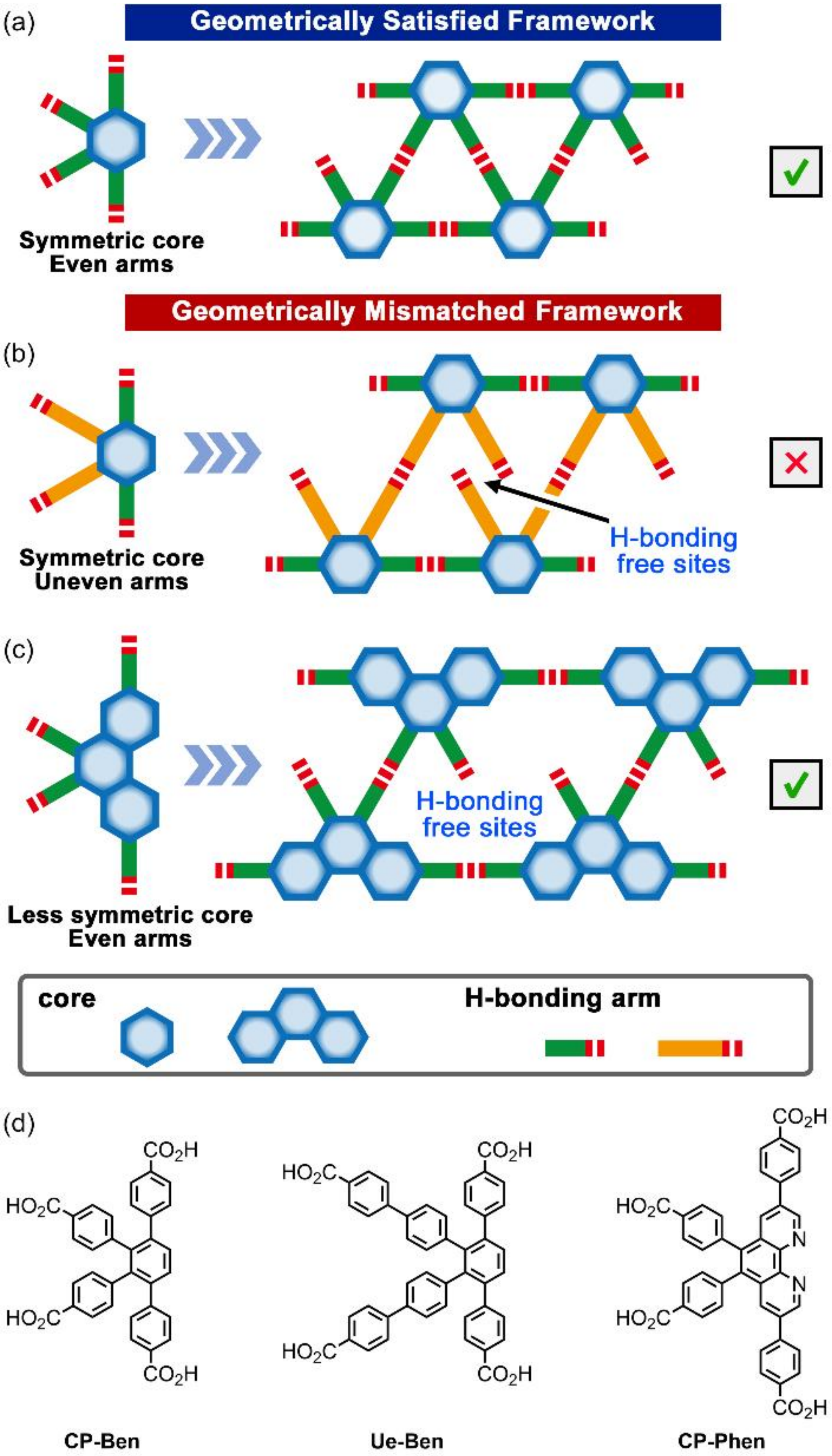
(a)
Geometrically Satisfied Framework
Symmetric core
Even arms
✓
Geometrically Mismatched Framework
(b)
Symmetric core
Uneven arms
H-bonding
free sites
✗
(c)
Less symmetric core
Even arms
H-bonding
free sites
✓
core
H-bonding arm
(d)
CO_2H
HO_2C
HO_2C
CO_2H
CP-Ben
HO_2C
CO_2H
HO_2C
CO_2H
Ue-Ben
CO_2H
HO_2C
N
N
HO_2C
CO_2H
CP-Phen

Figure 4-1. Geometrically mismatched strategy to construct a porous framework with free carboxy groups. (a) Geometrically satisfied framework composed of a molecule possessing a symmetric core and even arms. Geometrically mismatched framework composed of a molecule possessing (b) a symmetric core and arms with different length or (c) less symmetric core and even arms. In the cases of (b) and (c), the resulting frameworks are expected to have free carboxy groups. (d) Specific molecules corresponding to the cases of (a), (b), and (c).

Among them, the third approach is useful because of its easy process and potential for generalized application, while the design strategy is still unestablished. Herein, as a proof-of-concept, I demonstrate that geometrically mismatched H-bonded networks could provide free carboxy groups in the pore of HOFs. As shown in Figure 4-1a, a symmetric building block molecule such as 1,2,3,4-tetrakis(carboxyphenyl)benzene derivative **CP-Ben** forms a symmetrically matched framework with fully satisfied H-bonding.[18] On the other hand, less symmetric building block molecules possessing uneven peripheral arms or core such as tetrasubstituted benzene and phenanthroline derivatives **Ue-Ben** and **CP-Phen**, respectively, are expected to form a geometrically mismatched framework with carboxy groups free from the framework construction (Figures 4-1b and 4-1c, respectively).

Consequently, in this chapter, I revealed that **Ue-Ben** gave no precise framework crystals, while that **CP-Phen** (in Figure 4-1d) formed such a H-bonded framework in which the free carboxy groups work as a binding cites for polar solvent molecules such as N,N-dimethylacetamide (DMA) or N-methyl-2-pyrrolidone (NMP). We also revealed that the solvent included framework underwent two-step structural changes presumably brought by rearrangements of hydrogen bonds upon stepwise loss of two kinds of different included molecules.

4-3. Results and Discussion

Synthesis and Crytallization

Selective arylation at 1,4-positions of 1,2,3,4-tetrabromobenzene under Suzuki-Miyaura cross-coupling reaction condition gave dimethyl 2',3'-dibromo-[1,1':4',1''-terphenyl]-4,4''-dicarboxylate (**1**),[19] which was subsequently coupled with butyl 4'-(4,4,5,5-tetramethyl-1,3,2-dioxaborolan-2-yl)-[1,1'-biphenyl]-4-carboxylate (**2**), giving 1,4-diphenyl-2,3-bis(biphenyl)benzene derivative **3** in 41% yield. Hydrolysis of **3** gave tetrasubstituted benzene derivative possessing uneven aryl arms **Ue-Ben** in 97% yield (Scheme 4-1a). 3,5,6,8-Tetrabromo-1,10-phenanthroline (**4**), which was synthesized through bromination of anhydrous 1,10-phenanthroline as reported in the literature,[20] was similarly cross-coupled with butyl 4-(4,4,5,5-tetramethyl-1,3,2-dioxaborolan-2-yl)benzoate (**5**) to give tetraester derivative **6** in 37% yield, which was subsequently hydrolyzed to give tetrakis(carboxyphenyl)phenanthroline derivative **CP-Phen** in 81% yield (Scheme 4-1b). The products were characterized by ^{1}H and ^{13}C NMR spectroscopy and high-resolution mass spectrometry (for details, see Figure S4-1 to S4-10 in appendix).

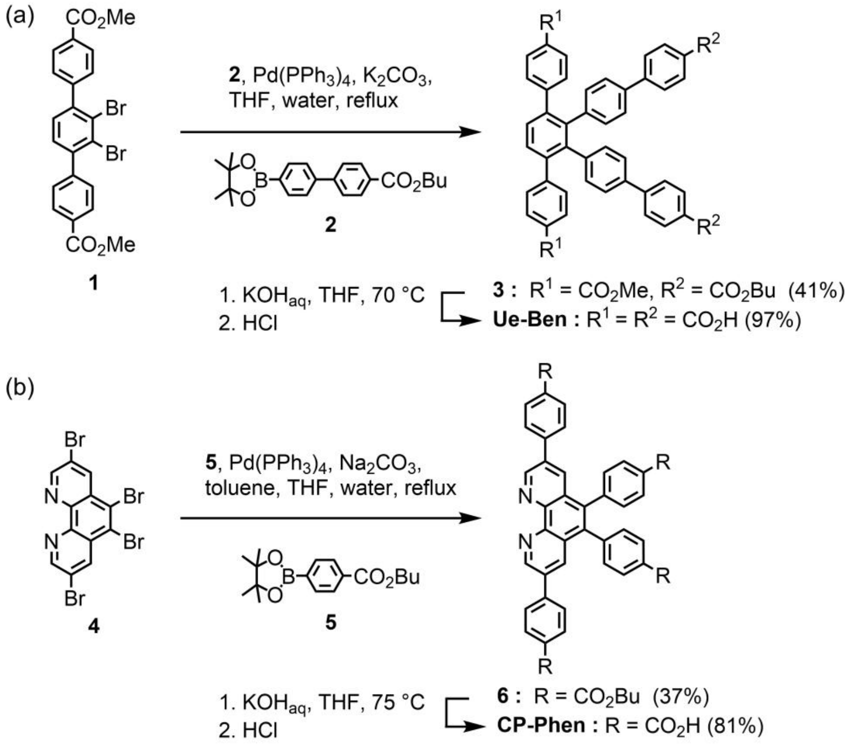

Scheme 4-1. Synthesis of **Ue-Ben** and **CP-Phen**.

Ue-Ben was recrystallized under various conditions. However, it was a regrettable thing that no single crystals suitable for single crystalline X-ray diffraction (SCXRD) analysis were obtained presumably due to unpreferable elongation of arm moieties that often results in formation of crystals with low quality (Figure 4-2).[21] **CP-Phen**, on the other hand, was recrystallized by slow evaporation at 50 °C for one week using a mixed solvent system of N,N-dimethylacetamide (DMA) and 1,2,4-trichlorobenzene (TCB) to yield the corresponding framework **CP-Phen-1(DMA-TCB)** as colorless block crystals (Figure 4-3). Crystallization at 70 °C in 5 days with N-methyl-2-pyrrolidone (NMP) instead of DMA allows to yield crystals of framework **CP-Phen-1(NMP-TCB)** with similar morphology (Figure 4-4).

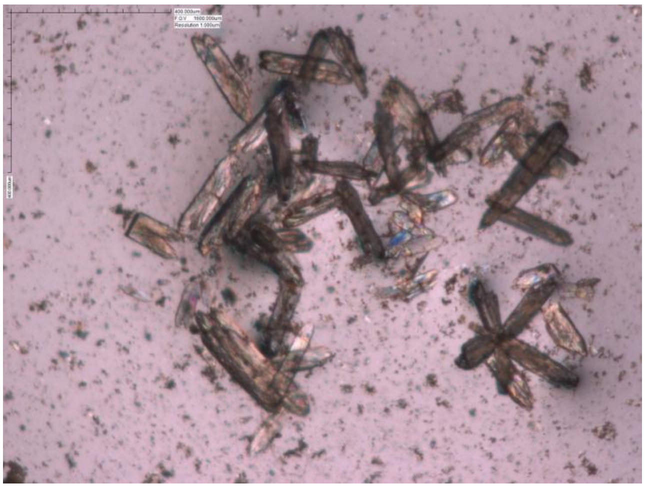

Figure 4-2. Morphology of crystalline precipitate of **Ue-Ben**.

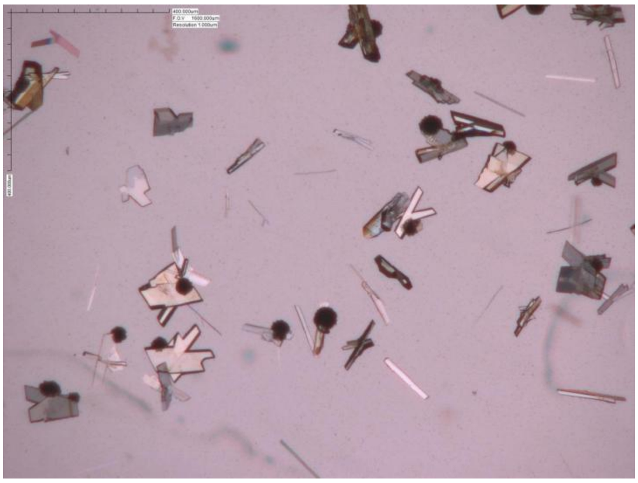

Figure 4-3. Morphology of crystalline precipitate of **CP-Phen-1(DMA-TCB)**.

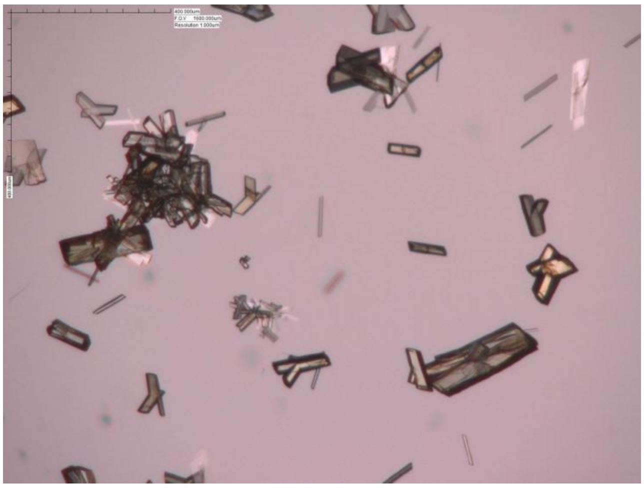

Figure 4-4. Morphology of crystalline precipitate of **CP-Phen-1(NMP-TCB)**.

Crystallography

CP-Phen-1(DMA-TCB) crystallized in space group *P*-1 (Table 1). As expected, three of four carboxy groups in **CP-Phen** form self-complementary H-bonded dimer, where O···O distance range in 2.60 Å to 2.65 Å, to form a ladder-shaped framework (Figure 4-5a). Interestingly, one carboxy group, on the other hand, does not participate in framework formation due to geometrical mismatch, while makes a weak H-bond with a molecule of DMA with O···O distance of 2.89 Å. The remaining void accommodates TCB molecules, which form Cl···O contacts of 3.13 Å and 3.08 Å, respectively, although TCB molecules are disordered in two ways (Figure 4-7). The ladder-motifs are aligned in parallel manner and slip-stacked to give a layered structure (Figure 4-5b). It is not negligible that nitrogen atoms at 1,10-positions of phenanthroline form no significant interactions except for a weak C–H···N interaction with the peripheral phenylene ring of the adjacent molecule (Figure 4-5c). Because of widely overlapped molecular stacking with a distance of 3.46 Å, phenylene rings bound to 3,8-positions are almost co-planar against the central phenanthroline moiety: dihedral angles between phenylene rings (A and B) and phenanthroline. [ω(A-Phen) and ω(B-Phen)] are 10.5° and 11.1°, respectively. The corresponding dihedral angles of phenylene rings C and D

[ω(A-Phen) and ω(B-Phen)], on the other hand, exhibit larger values: 74.1° and 67.3°, respectively.

Table 1. Crystal data of the obtained crystals

	CP-Phen-1 (DMA-TCB)	**CP-Phen-1 (NMP-TCB)**	**CP-Phen(Py)**
Formula	$C_{40}H_{24}N_2O_8\cdot C_4H_9NO\cdot C_6H_3Cl_3$	$C_{40}H_{24}N_2O_8\cdot C_5H_9NO\cdot C_6H_3Cl_3$	$2(C_{40}H_{23}N_2O_8)\cdot C_{40}H_{22.59}N_2O_8\cdot 3.41(C_5H_6N)\cdot 5.59(C_5H_5N)$
Fw	929.17	941.18	2693.73
Crystal system	triclinic	triclinic	triclinic
Space group	*P*-1	*P*-1	*P*-1
a / Å	8.4082(8)	8.3043(6)	15.0819(3)
b / Å	15.0054(13)	15.1728(8)	20.1673(5)
c / Å	17.5547(15)	17.5240(12)	24.5298(6)
α / °	103.380(7)	102.980(5)	68.859(2)
β / °	90.871(7)	90.792(5)	87.858(2)
γ / °	92.855(7)	92.113(5)	76.950(2)
V / Å^3	2151.2(3)	2149.6(2)	6771.2(3)
Z	2	2	2
T/K	113	113	113
GOF	1.234	1.323	1.028
No of reflns. Obs./uniq.	38663, 12564	10517, 4911	166916, 35255,
$R1$ [$I > 2\sigma(I)$], $wR2$ (all data)	0.1222, 0.3967	0.1401, 0.4502	0.0712, 0.2019
CCDC No.	2173793	2173794	2173795

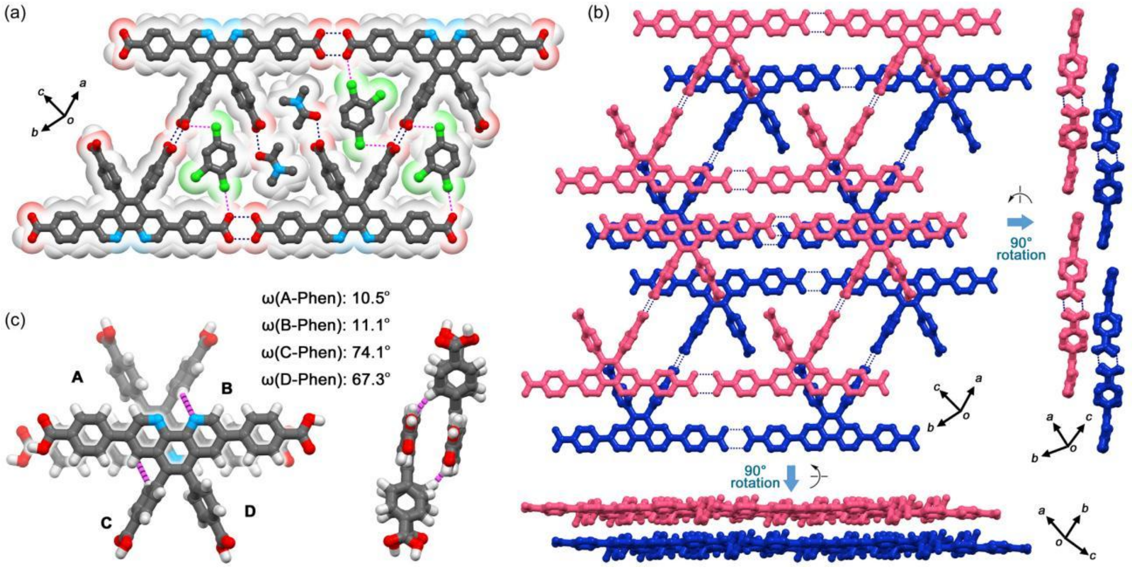

Figure 4-5. Crystal structure of HOF **CP-Phen-1(DMA-TCB)**. (a) Ladder-shaped motif of H-bonded network, in which dotted lines with dark blue and red show the O–H···O hydrogen bond and O···Cl interaction, respectively. (b) Assembly manner of the lanner motifs. (c) π-Stacked dimer of the molecule, in which weak C–H···N hydrogen bonds (pink dash line) are also observed, in addition to π/π stacking.

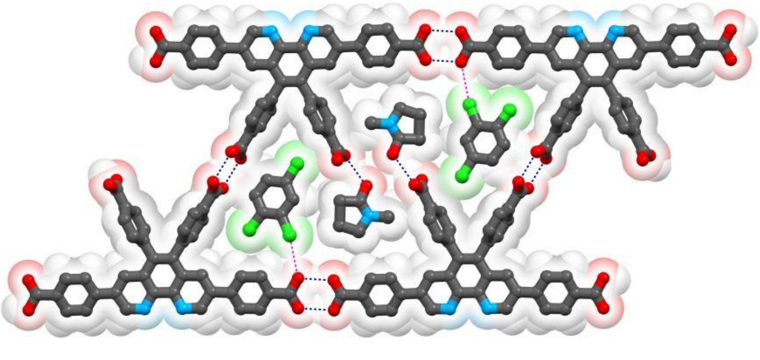

Figure 4-6. Selected crystal structure of HOF **CP-Phen-1(NMP-TCB)**.

Figure 4-6 shows a ladder-shaped framework of **CP-Phen-1(NMP-TCB)**. Similarly, the framework was formed through the self-complementary H-bonded dimers with O· · · O distance ranging in 2.60 Å to 2.64 Å. The carboxy group at the 5-position dose not participate in framework formation and traps a molecule of NMP through H-bond with O···O distance of 2.84 Å. These results indicate that the free carboxy group at the 5-position in the framework of **CP-Phen-1** can work as a trap site of small molecule through a weaker H-bond.

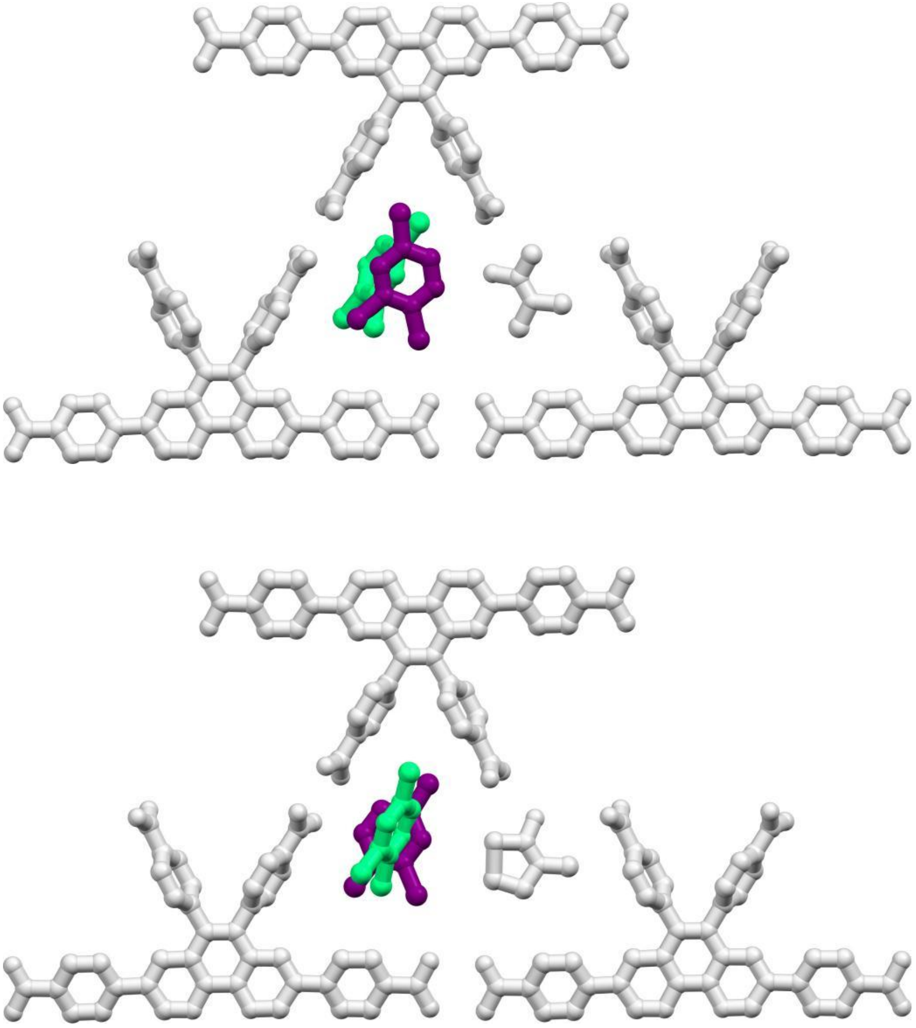

Figure 4-7. A molecule of TCB disordered in two positions (green and purple) in the crystal of (top) **CP-Phen-1(DMA-TCB)** and **CP-Phen-1(NMP-TCB)**.

Contrary to these two frameworks, when **CP-Phen** was crystallized in the presence of molecules exhibiting more basicity such as pyridine, the resulting crystal **CP-Phen(Py)** was composed of non-networked **CP-Phen** molecules (Figure 4-8). The carboxy phenyl groups at 3,8-positions barely retain a 1D structural motif through non-self-complementary H-bonded dimerization interfered by pyridine, while those at 5,6-positions are completely trapped by molecules of pyridine through H-bonds and salt formation with distances ranging from 2.62 Å to 2.66 Å.

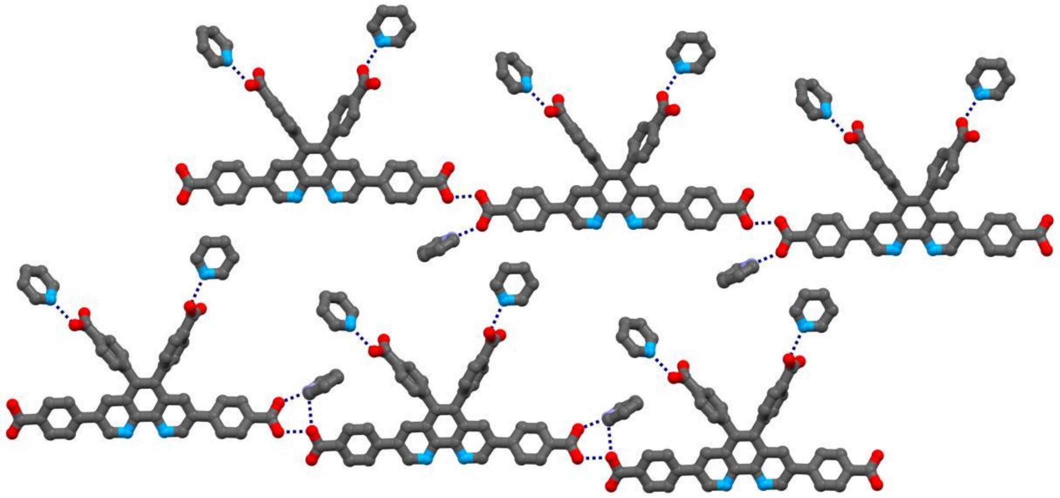

Figure 4-8. Selected H-bonded motif of **CP-Phen(Py)**.

Thermal analysis

Thermogravimetric (TG) analysis of as-formed crystalline bulk of **CP-Phen-1(DMA-TCB)** underwent complete removal of included solvent *via* the two-step releasing of the solvent molecules (Figure 4-9). In the first step, 12% of weight loss was observed up to 140 °C, which corresponds to release of the DMA molecules. The second step up to 230 °C resulted in an additional 18% of weight loss, which corresponds to losing of the TCB molecules. The stepwise loss of the corresponding solvent molecules was confirmed by ^{1}H NMR spectroscopy (Figure S4-11 and Figure

S4-12 in appendix). Further heating over 370 °C leads to the thermal decomposition of the compound.

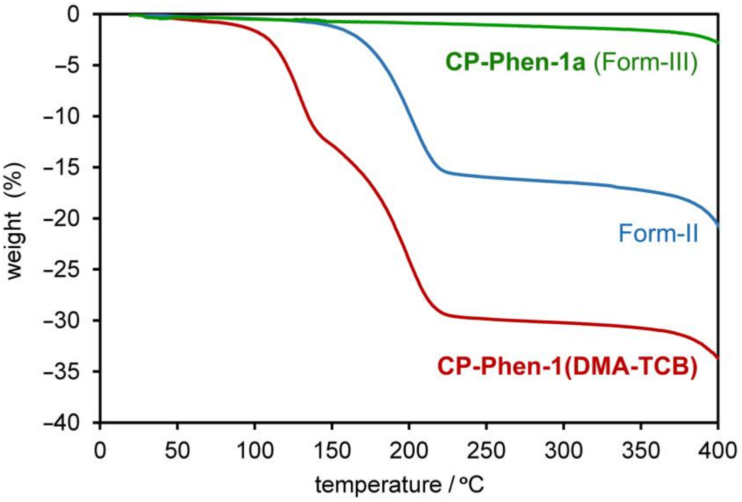

Figure 4-9. Thermogravimetric (TG) curves of **CP-Phen-1(DMA-TCB)** in red, Form-II (in cyan), and **CP-Phen-1a** (Form-III) (in green).

To obtain detailed information of structural variation of the framework upon the guest solvent releasing, the as-formed crystalline bulk of **CP-Phen-1(DMA-TCB)** was subjected to variable temperature powder X-ray diffraction (VT-PXRD) experiment from room temperature to 360 °C (Figure 4-10). The pattern of the initial phase is consistent with that of the original framework. The pattern starts to change from the initial phase to the second phase (Form-II) at around at around 101 °C, at which characteristic diffraction such as that at $2\theta = 5.4^\circ$ gradually appeared accompanied by the loss of the original peaks at 6.0° and 6.9° corresponding to the (0 1 0) and (0 1 −1) planes, respectively. The TG curve of Form-II show a single step weight loss (cyan curve in Figure 4-9), indicating that Form-II contains only TCB molecules. It is also confirmed by ^{1}H NMR (Figure S4-11 in appendix). The further increase of temperature triggered the loss of the third phase (Form-III): When temperatures were higher than 183 °C, a new peak at 4.09° was observed. It is also confirmed by TG analysis that Form-III contains no lattice solvents (green curve in Figure 4-9). Form-III is stable up to 360 °C. It should be noted that Form-III is equal to the activated sample **CP-Phen-1a**. The typical PXRD patterns of the initial form, Form-II, and Form-III are presented in Figure 4-11, together with the simulated pattern for **CP-Phen-1(DMA-TCB)**.

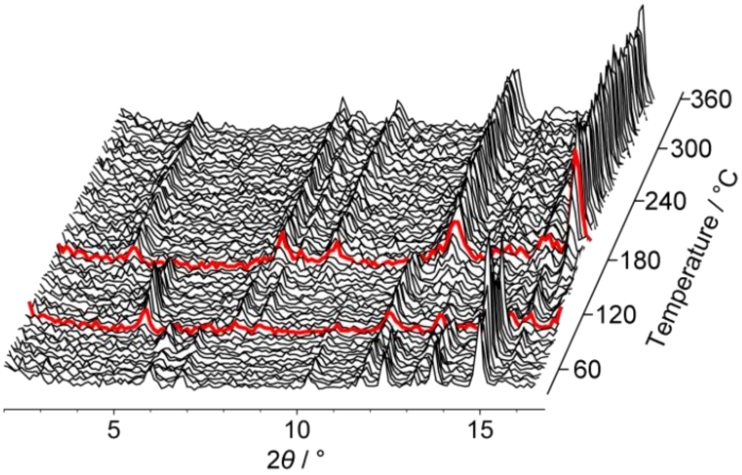

Figure 4-10. Variable temperature (VT-) PXRD patterns of **CP-Phen-1(DMA-TCB)** heated from room temperature to 360 °C.

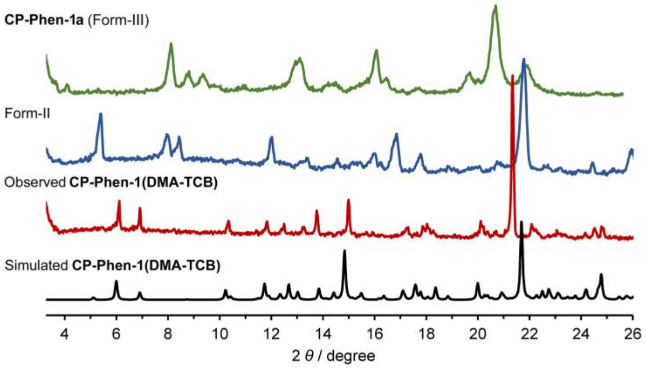

Figure 4-11. Typical PXRD patterns of **CP-Phen-1(DMA-TCB)**, Form-II, and **CP-Phen-1a** (Form-III).

Crystal structure estimation

Although VT-PXRD experiments show two-step structural transformation into the second and third phases via selective solvent release, their crystal structures were not revealed due to loss of single crystallinity and broad PXRD patterns. To deduce crystal structures of the second and third phases, therefore, crystal structure prediction technique was applied.

The molecular structure of **CP-Phen** was optimized by the GGA/PBE function with the DNP-3.5 basis set, except for dihedral angles of the peripheral phenylene rings: their values are based on those in the crystal structure of **CP-Phen-1(DMA-TCB)**. Charge distribution on each of atoms was also calculated for the optimized structure. Using the optimized conformation, crystal structures with frequently observed space groups (*P*-1, *P*21/c, *P*21, $P2_12_12_1$, and *C*2/c) were generated by Monte Carlo calculation, clustered, and optimized by the force field (Dreiding) to give 6884 crystal structures (Figure 4-12a). In this prediction, I did not consider inclusion of solvent molecules in the lattice, although the experimental Form-II includes TCB molecules in the lattice. Based on the obtained structures, I carefully made the comparison between PXRD patterns of the predicted structures and the experimental patterns of Forms-II and -III. Although I were

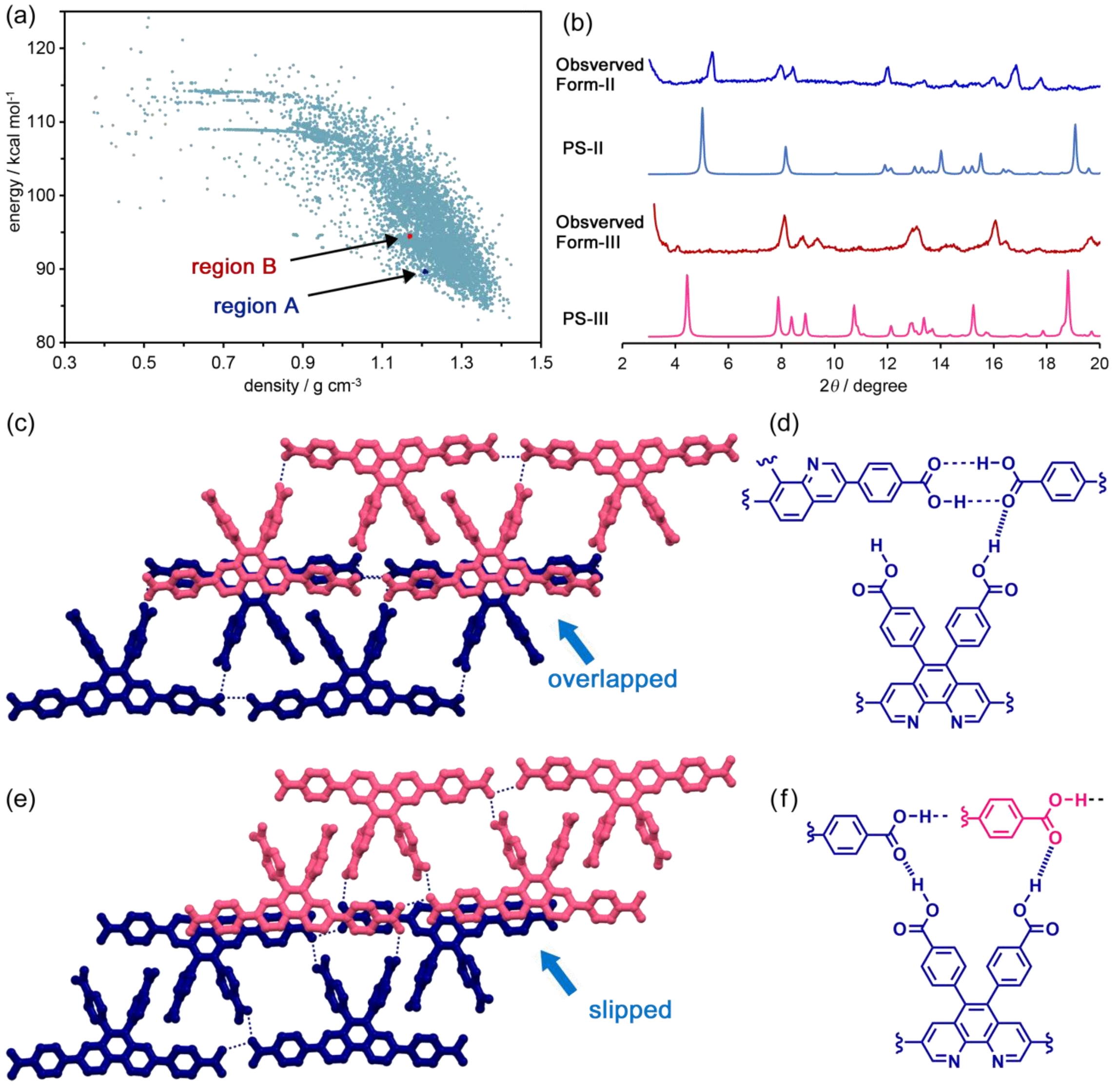

Figure 4-12. Proposed structures of Forms-II and -III based on a crystal structure prediction method. (a) Density-energy plots. Regions A and B involved PS-II and PS-III, respectively. (b) PXRD patterns of observed Forms-II and -III and their candidate structures PS-II and PS-III, respectively. Selected molecular packing diagram of (c) PS-II and (d) PS-III. Illustration of H-bonding patterns in (d) PS-II and (f) PS-III.

not able to found exactly appropriate structures, and I selected two predicted structures (PS-II and PS-III, respectively) as the candidates, which showed the most similar PXRD pattern with the corresponding experimental one as shown in Figure 4-12b (For other candidate structures with less similarity, see Tables 2 and 3, Figure 4-13 to Figure 4-16). A molecular packing manner of PS-II is shown in Figure 4-12c. A molecule of **CP-Phen** forms a π-stacked dimer similar with that in **CP-Phen-1(DMA-TCB)** and the dimers are connected by H-bonds between carboxyphenyl groups at the 3,8-position to give a 1D motif. On the other hand, carboxyphenyl groups at the 5- or 6-position form no H-bonded dimer, while form branched H-bond via cleavage of the dimer followed by rearrangement (Figure 4-12d). In PS-III, the molecule forms a slip-stacked dimer with less molecular overlap compared with PS-II and **CP-Phen-1(DMA-TCB)** and the dimers are connected by H-bonds to give the 1D motif (Figure 4-12e). The carboxyphenyl groups at both 5- and 6-positions form branched H-bonds (Figure 4-12f).

Table 2. Cell parameters of predicted crystal structures in region-A.

	P-1(650) (PS-II)	*P*-1(634)	*P*-1(551)	*P*-1(671)	*P*-1(719)
a [Å]	15.3038	19.7260	18.5807	19.2327	15.8206
b [Å]	20.3639	7.0365	13.1572	7.1084	7.1346
c [Å]	7.5678	14.1706	8.4235	17.9448	17.5136
α [°]	120.2588	72.8553	95.6831	70.3068	73.7826
B [°]	117.4022	89.2347	113.0502	123.7873	96.9698
γ [°]	77.2073	75.7415	102.6143	117.3351	107.5120
V [Å^3]	1808.4	1817.87	1809.68	1800.18	1808.69
D [gcm^{-3}]	1.213	1.207	1.214	1.219	1.207
E [kcal mol^{-1}]	89.564	89.505	89.149	89.651	89.806

Table 3. Cell parameters of predicted crystal structures in region-B.

	P-1(2620) (PS-III)	*P*-1(2586)	*P*-1(2646)	*P*-1(2684)	*P*-1(2594)
a [Å]	8.3032	16.3018	21.6975	12.5292	12.5922
b [Å]	24.1234	12.3223	12.4931	9.2345	15.4892
c [Å]	13.8033	16.5540	9.1750	30.8788	9.9550
α [°]	90.6659	112.2381	111.5709	121.6958	77.0556
Β [°]	55.4468	114.7258	116.2544	117.4197	88.3036
γ [°]	62.5159	117.7254	101.0510	107.5030	82.9098
V [Å^3]	1873.38	1875.42	1877.79	1876.57	1877.84
D [gcm^{-3}]	1.170	1.170	1.168	1.169	1.168
E [kcal mol^{-1}]	94.387	94.286	94.449	94.555	94.295

These results imply that the geometrically mismatched H-bonded framework **CP-Phen-1(DMA-TCB)** undergoes shrinkage of the framework through H-bond rearrangements.

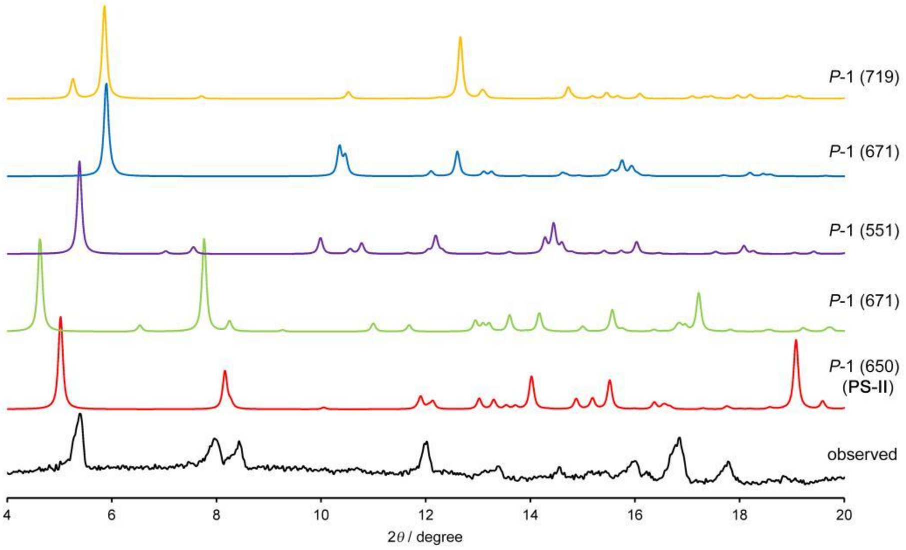

Figure 4-13. PXRD patterns of predicted structures in region A.

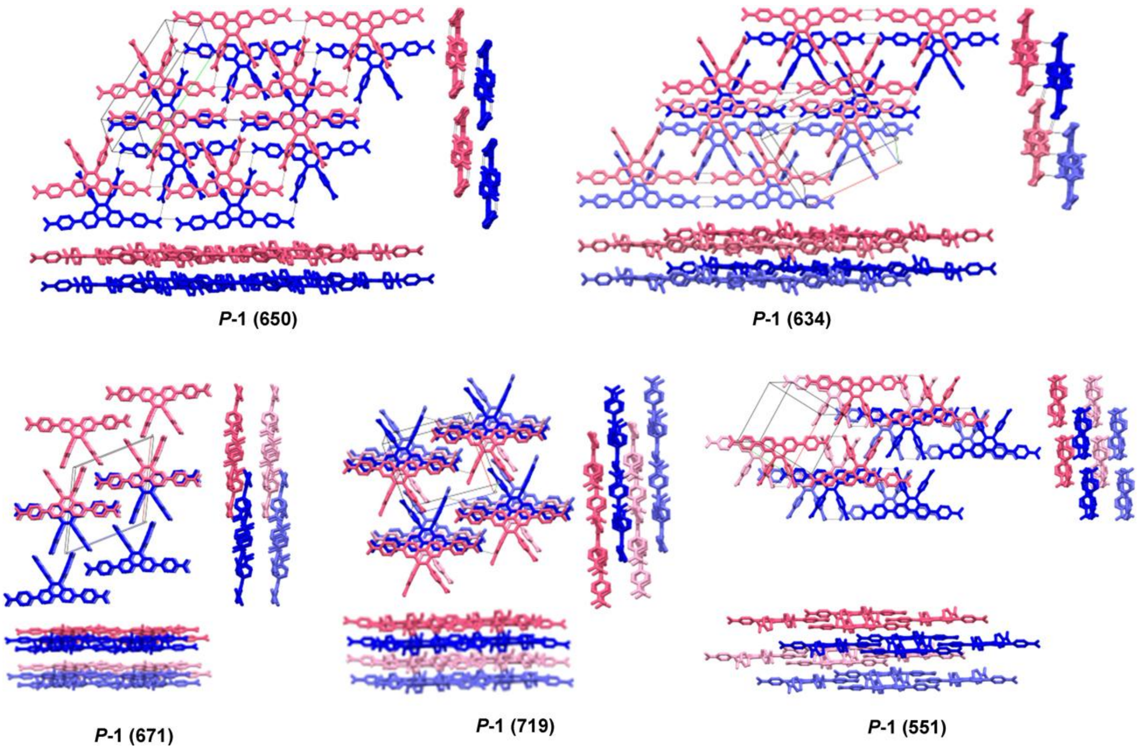

Figure 4-14. Candidate structures of Form-II observed in region-A.

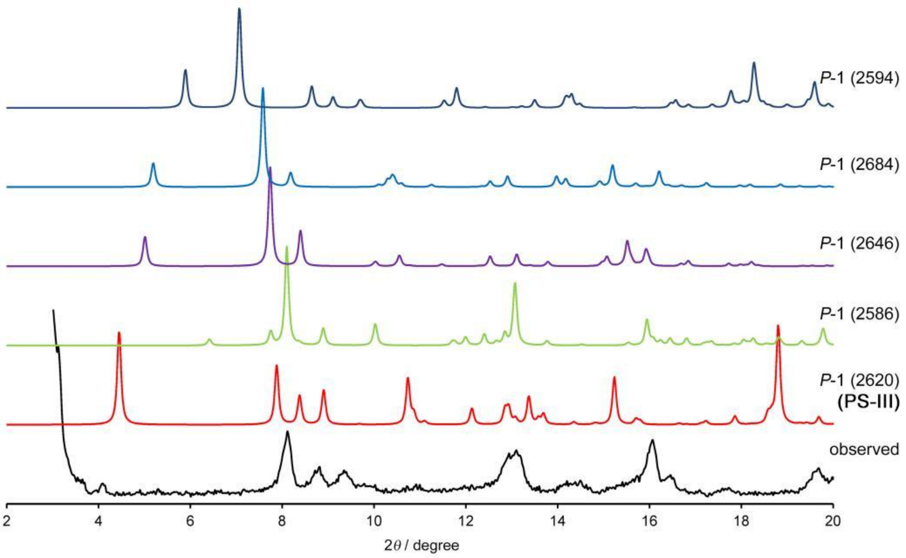

Figure 4-15. PXRD patterns of predicted structures in region B.

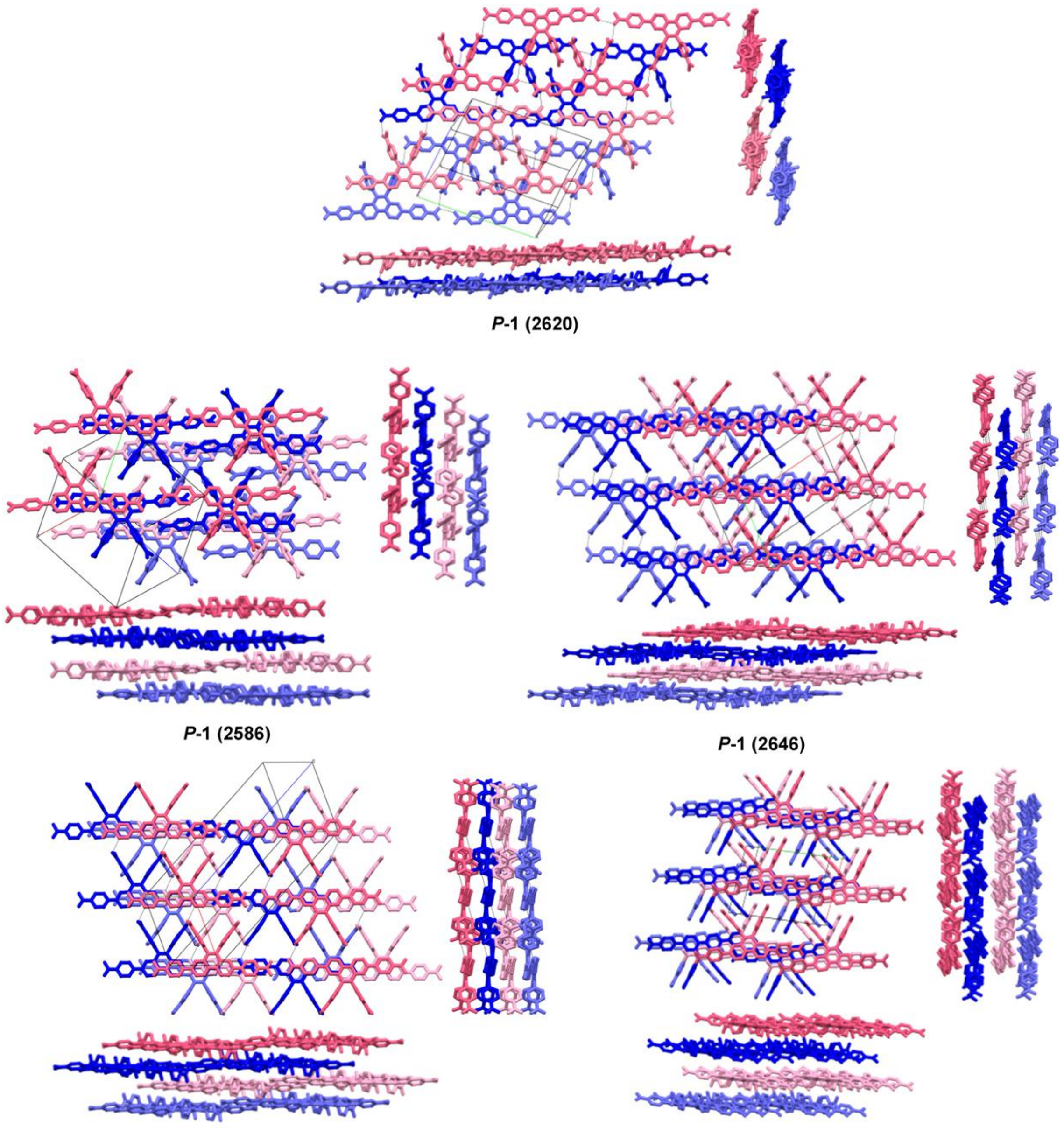

***P*-1 (2620)**

***P*-1 (2586)**

***P*-1 (2646)**

***P*-1 (2684)**

***P*-1 (2594)**

Figure 4-16. Candidate structures of Form-II observed in region-B.

Permanent porosity evaluation

Activation of **CP-Phen-1(DMA-TCB)** was conducted by heating at 200 °C under a vacuum condition for 5 days to give activated crystalline material **CP-Phen-1a** that has the same PXRD pattern with Form-III, the structure and complete removal of the solvent were confirmed by PXRD pattern and ^{1}H NMR spectrum (Figure S4-12 in appendix) measured in DMSO-*d6* solution. **CP-Phen-1a** was subject to N_2 and CO_2

sorption experiments to evaluate its permanent porosity. The HOF showed almost no adsorption of N_2 at 77 K in the low-pressure region, while showed type-I CO_2 adsorption isotherms with uptake of 58.9 cm^3 (STP) g^{-1} at $P/P_0 = 0.99$ at 195 K, indicating existence of micropore in **CP-Phen-1a**.(Figure 4-17) The BET surface area was calculated to be 196 $m^2\ g^{-1}$ based on the CO_2 sorption (Figure 4-18). The observed CO_2 selective absorption probably caused by smaller kinetic diameter of CO_2 than N_2, as well as attractive electrostatic interactions between quadrupolar CO_2 molecules and pore surface of the HOF.

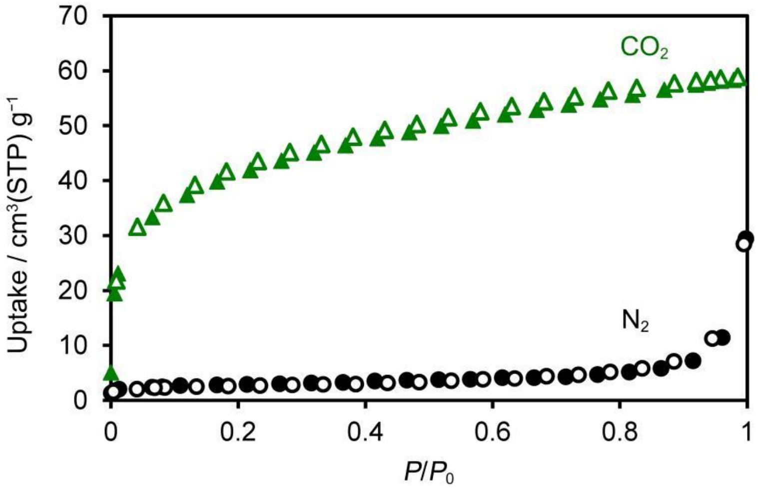

Figure 4-17. N_2 and CO_2 sorption isotherms of activated HOF **CP-Phen-1a** recorded at 77 K and 195 K, respectively. Solid and open symbols indicate adsorption and desorption processes, respectively.

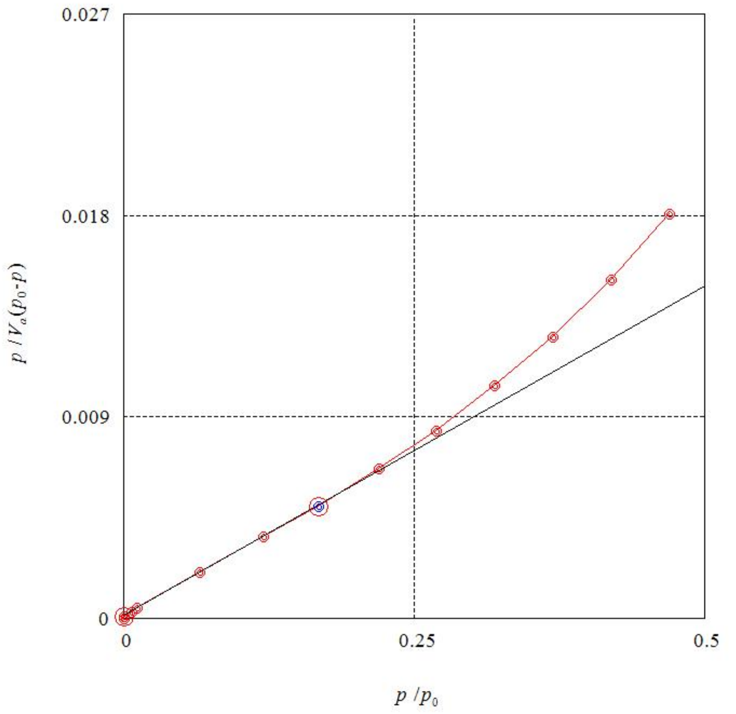

Slope	2.94E-02	
Intercept	1.27E-04	
Correlation coefficient	0.9998	
BET range limit (p/p0=0.1669)	6th point	
Va(p0-p)$_{\mathrm{max}}$	3362.7	
Vm	33.822	[cm^3 (STP) g^{-1}]
SA(BET)	1.96E+02	[m^2 g^{-1}]
C	233.72	
Total volum (p/p0=0.990)	0.1615	[cm^3 g^{-1}]

Figure 4-18. BET analysis of **CP-Phen-1a** based on CO_2 sorption isotherm at 195 K.

4-4. Conclusion

In this chapter, it was demonstrated that tetratopic carboxy acid derivative possessing a phenanthroline core and four peripheral carboxyphenyl groups (**CP-Phen**) gave a geometrically mismatched ladder-phased framework. In the framework, three of the four carboxy groups form H-bonded dimer to keep a ladder-shaped skeleton, while the remained one does not participate in framework formation, instead plays as a trapping site of solvent molecules through weak H-bonding. Although **CP-Phen-1** undergoes 2-step structural transformation accompanied with H-bond cleavage and rearrangements, the resultant activated framework shows good thermal stability up to 360 °C and selective adsorption behavior toward carbon dioxide. These results imply that our proposed strategy, that is geometrically mismatched assembly, is effective to provide free interactive sites in porous organic frameworks.

4-5. Experimental Section

General

All reagents and solvents were used as received from commercial suppliers. ^{1}H NMR spectra were measured by a Bruker AV400M spectrometer. Residual protons and carbons of deuterated solvents were used as internal standards for the measurements: δ = 7.26 ppm ($CDCl_3$), δ = 5.32 ppm (CD_2Cl_2) and 2.50 ppm (DMSO-d_6) for ^{1}H NMR and δ = 77.0 ppm ($CDCl_3$) and 29.76 ppm (DMSO-d_6) for ^{13}C NMR. Thermogravimetric (TG) analysis was performed on Rigaku TG8120 under an N_2 purge (300 mL min^{-1}) at a heating rate of 10 K min^{-1}. HR-MS analysis was performed on a JEOL JMS-700 spectrometer. Powder X-ray diffraction (PXRD) data were collected on a Rigaku Ultima-IV (40 kV, 44 mA) or PANalytical XPert PRO X'Celerator using graphite-monochromatized Cu-Kα radiation at room temperature. A scan rate is 2.0° min^{-1}. N_2 and CO_2 sorption experiments were conducted at 77 K and 195 K, respectively, on BELSORP-max (BEL, Japan)

Single crystal X-ray measurement and analysis

Diffraction data of **CP-Phen-1(DMA-TCB)**, **CP-Phen-1(NMP-TCB)**, and **CP-Phen-Py** were collected with a two-dimensional X-ray detector (PILATUS 200K/R) equipped on a Rigaku XtaLAB P200 diffractometer by using Mo-Kα radiation monochromated with multilayer mirror (λ = 0.71073 Å). Diffraction Data collection, cell refinement, and data reduction were carried out with CrysAlis PRO.[22] SHELXT[23] was used for the structure solution of the crystals. These calculations were performed with the observed reflections [$I > 2\sigma(I)$] with the program OLEX-2 crystallographic software.[24] Structural refinement was performed by SHELXL.[25] All non-hydrogen atoms were refined with anisotropic displacement parameters, and hydrogen atoms were placed in idealized positions and refined as rigid atoms with the relative isotropic displacement parameters. SQUEEZE function equipped in the PLATON program was used to treat severely disordered solvent molecules in voids.[26]

Crystal structure prediction

Inputted molecular model of **CP-Phen** was optimized by the DFT calculation at the GGA-PBE level by the DMol^3 program, except for dihedral angles of the peripheral phenylene rings: their values are based on those in the crystal structure of **CP-Phen-1(DMA-TCB)**. A polymorph calculation was conducted on the optimized model with a Dreiding force field by using the Polymorph program equipped in Material Studio ver 6.1.[S6] Space groups of *P*-1, *P*2$_1$/c, *P*21, *P*2$_1$2$_1$2$_1$, and *C*2/*c*, were applied for the calculation. Totally 6884 structures were obtained as a result of sequential Monte Carlo calculation, clustering, and optimization.

Synthesis of Compounds

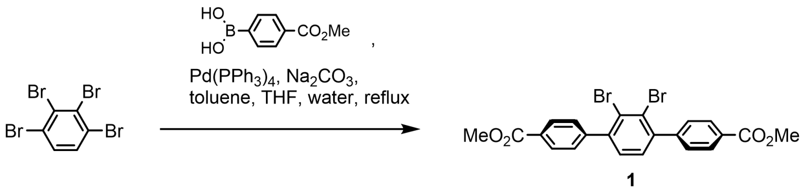

dimethyl 2',3'-dibromo-[1,1':4',1''-terphenyl]-4,4''-dicarboxylate (1). A deoxygenated mixture of 1,2,3,4-tetrabromobenzene (1.59 g, 4.04 mmol), 4-methoxycarbonylphenyl bronic acid (1.60 g, 8.89 mmol), NaOH (0.286 g, 7.15 mmol), Pd(PPh$_3$)$_4$ (0.478 g, 0.414 mmol) in a mixed solvent of methanol (40 mL), toluene (40 mL), and 1,4-dioxane (40 mL) was refluxed for 48 h under N$_2$ atmosphere. The reaction mixture was evaporated to remove the solvent, and the resulting solid was well washed with water to remove NaOH. The product was purified by sonicating ethanol suspension of the solid, followed by filtration of the precipitate to give **1** (1.13 g, 55%) as a white solid. M.p. 173 °C; ^{1}H NMR (400 MHz, $CDCl_3$) δ 8.13 (d, J = 8.4 Hz, 4H), 7.48 (d, J = 8.4 Hz, 4H), 7.30 (s, 2H), 3.96 (s, 6H). ^{13}C NMR (100 MHz, $CDCl_3$) δ 166.89, 146.24, 143.85, 129.85, 129.61, 129.47, 129.35, 126.63, 52.41 ppm. HR-MS (FAB) calcd. For $C_{22}H_{16}Br_2O_4$ [M]: 501.9415; found: 501.9411.

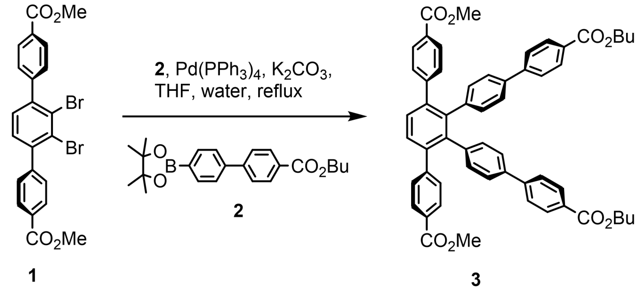

Dibutyl 3'',6''-bis(4-(methoxycarbonyl)phenyl)-[1,1':4',1'':2'',1''':4''',1''''-quinquephenyl]-4,4''''-dicarboxylate (3) A three-necked flask was charged with terphenyl derivative **1** (50.4 mg, 0.100 mmol), boronate **2** (83.7 mg, 0.220 mmol), $Pd(PPh_3)_4$ (21.2 mg, 18.3 μmol), and K_2CO_3 (69.1 mg, 0.500 mmol) in degassed THF (10 mL) and H_2O (5 mL). The reaction mixture was refluxed at 70 °C for 20 h under the protection of N_2 atmosphere. After cooling to the room temperature, the organic solvent was removed by an evaporator. The residual was extracted with $CHCl_3$, washed with water and brine, and dried over anhydrous $MgSO_4$. The product was purified by column chromatography (silica gel, 8% ethyl acetate / Hexane) to give **3** (34.5 mg, 41%) as a pale yellow solid. M.p. 247 °C; ^{1}H NMR (400 MHz, CD_2Cl_2) 7.99 (d, J = 8.4 Hz, 4H), 7.84 (d, J = 8.4 Hz, 4H), 7.57 (s, 2H), 7.54 (d, J = 8.4 Hz, 4H), 7.27 (dd, J = 12.4, 8.4 Hz, 8H) 6.97 (d, J = 8 Hz, 4H), 4.29 (t, J = 6.6 Hz, 4H), 3.84 (s, 6H), 1.77-1.71 (m, 6H), 1.52-1.43 (m, 6H), 0.97 (t, J = 7.4 Hz, 6H)). ^{13}C (100 Hz, $CDCl_3$) δ 166.95, 166.53, 146.39, 144.67, 140.70, 139.91, 139.19, 137.45, 132.01, 129.93, 129.88, 129.61, 129.15, 129.08. 128.23, 126.64, 126.01, 64.84, 52.06, 30.79, 19.27, 13.76 ppm. HR-MS (FAB) calcd. For $C_{56}H_{50}O_8$ [M]: 850.3506; found: 850.3510.

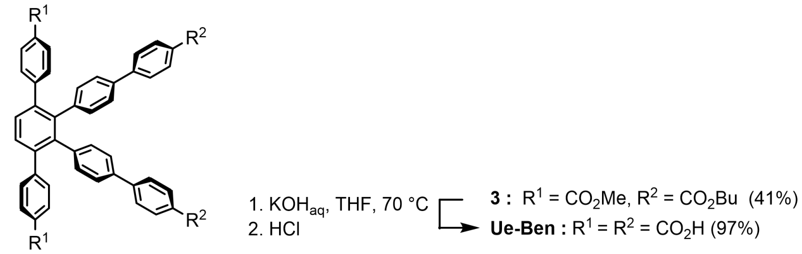

3'',6''-bis(4-carboxyphenyl)-[1,1':4',1'':2'',1''':4''',1''''-quinquephenyl]-4,4''''-dicarboxylic acid (UeBen) To a reaction mixture of **3** (229 mg, 0.269 mmol) in THF (15 mL) was added 3M KOH_{aq} (15 mL). The mixture was stirred at 70 °C for about 2 days. After cooling to the room temperature, THF was stripped off in vacuo, following the addition of 6M HCl_{aq} into the mixture until no more precipitate was formed. After separated by centrifugation, the solid was washed with water, and dried under vacuum to obtain **Ue-Ben** (185 mg, 97%) as a brown solid. M.p. > 300 °C; ^{1}H NMR (400 MHz, DMSO-*d*$_6$) 12.85 (s, 4H), 7.90 (d, *J* = 8.4 Hz, 4H), 7.75 (d, *J* = 8.4 Hz, 4H), 7.66 (d, *J* = 8.8 Hz, 4H), 7.60 (s, 2H), 7.42 (d, *J* = 8.4 Hz, 4H), 7.28 (d, *J* = 8.4Hz, 4H), 7.02 (d, *J* = 8.0 Hz, 4H). ^{13}C (100 Hz, DMSO-*d*$_6$) δ 167.01, 167.00, 145.68, 143.13, 140.18, 139.55, 139.17, 136.10, 131.91, 129.92, 129.86, 129.76, 129.45, 128.80, 128.70, 126.28, 125.38 ppm. HR-MS (FAB) calcd. For $C_{46}H_{30}O_8$ [M]: 710.1941; found: 710.1942.

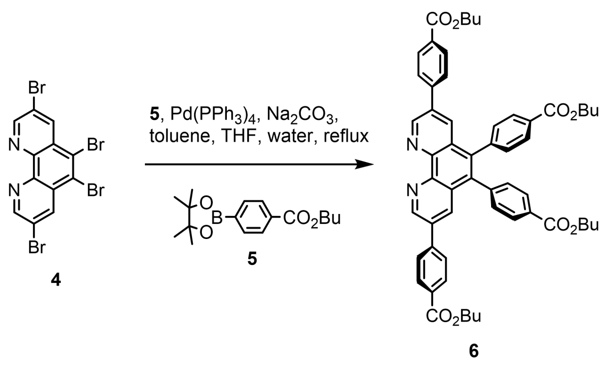

Tetrabutyl 4,4',4'',4'''-(1,10-phenanthroline-3,5,6,8-tetrayl)tetrabenzoate (6). 3,5,6,8-Tetrabromo-1,10-phenanthtoline (**1**) (180 mg, 363 μmol), boronic acid pinacol ester **2** (552 mg, 1.81mmol), $Pd(PPh_3)_4$ (42.8 mg, 37.1 μmol) was dissolved in a deoxygenated toluene (20 mL), THF (20 mL) and 1M Na_2CO_3 aqueous solution (10 mL). The mixture was stirred for 40 h at 110 °C. After being cooled to the room temperature, the organic solvent was removed by a rotary evaporator and the product was extracted with chloroform, washed with water and brine, and dried over anhydrous Na_2SO_4. The product was purified with column chromatography (silica gel, MeOH: $CHCl_3$=1 : 20) to give **3** (118 mg ,37%) as light yellow solid. **3.** M.p. 185 °C; ^{1}H NMR (400 MHz, $CDCl_3$) δ 9.48 (s, 2H), 8.13 (d, J = 8.0 Hz, 4H), 8.01 (d, J = 8.0 Hz, 6H), 7.64 (d, J = 8.0 Hz, 4H), 7.31 (d, J = 8.0 Hz, 4H), 4.33 (t, J = 6.6 Hz, 8H), 1.80–1.69 (m, 8H), 1.54–1.42 (m, 8H), 1.02–0.94 (m, 12H). ^{13}C NMR (100 MHz, $CDCl_3$) δ 166.32, 166.25, 149.42, 144.64, 141.74, 141.57, 137.16, 135.39, 133.07, 130.99, 130.72, 130.60, 130.16, 129.69, 128.28, 127.59, 65.29, 65.20, 30.91(2C), 19.43, 19.42, 13.89, 13.87 ppm. HR-MS (FAB) calcd. For $C_{56}H_{57}N_2O_8$ $[M+H]^+$: 885.4037; found: 885.4106.

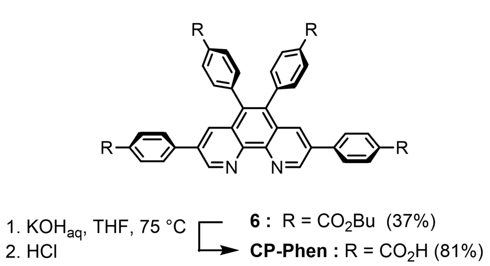

4,4',4'',4'''-(1,10-phenanthroline-3,5,6,8-tetrayl)tetrabenzoic acid (CP-Phen). To a suspension of butyl ester derivative **3** (39.8 mg, 44.9 μmol) in THF (15 mL), 10% KOH aqueous solution (15 mL) was added and stirred for 72 h at 70 °C. After removing THF by a rotary evaporator, 3M HCl aqueous solution was added dropwise until the precipitate was sufficiently formed. The precipitate was separated by centrifugation and washed at least three times with water to give **CP-Phen** (24.1 mg, 81%) as a white solid.

CP-Phen. M.p. > 300 °C; ^{1}H NMR (400 MHz, DMSO-*d*$_6$) *δ* 13.04 (s, 4H), 9.53 (s, 2H), 8.04 (d, *J* = 8.4 Hz, 4H), 7.99 (s, 2H), 7.92 (d, *J* = 8.0 Hz, 4H), 7.79 (d, *J* = 8.4 Hz, 4H), 7.47 (d, *J* = 8.0 Hz, 4H). ^{13}C NMR (101 MHz, DMSO-*d*$_6$) *δ* 166.93, 166.80, 148.57, 143.31, 141.11, 140.43, 136.77, 134.25, 132.33, 131.11, 130.71, 130.21, 129.94, 129.02, 127.67, 127.43 ppm. HR-MS (FAB) calcd. For $C_{40}H_{25}N_2O_8$ [M+H]+: 661.1533; found: 661.1614.

Reference

1. J. Jiao, W. Gong, X. Wu, S. Yang, Y. Cui, *Coord. Chem. Rev.* **2019**, *385*,174-190.
2. a) A. Kirchon, L. Feng, H. F. Drake, E. A. Joseph, H. -C. Zhou, *Chem. Soc. Rev.* **2018**, *47*, 8611-8638; b) S. A. A. Razavi, A. Morsali, *Coord. Chem. Rev.* **2019**, *399*, 213023.
3. B. N. Bhadra, I. Ahmed, H. J. Lee, S. H. Jhung, *Coord. chem. Rev.* **2022**, *450*, 214237.
4. D. K. Yoo, I. Ahmed, M. Sarker,H. J. Lee, A. Vinu, S. H. Jhung, *Mater. Today* **2021**, *51*, 566-585.
5. S. Mukherjee, Y. He, D. Franz, S. -Q. Wang, W. -R. Xian, A. A.Bezrukov, B. Space, Z. Xu, J. He, M. Zaworotko, *Chem. Eur. J.* **2020**, *26*, 4923-4929.
6. J. Jiang, O. M. Yaghi, *Chem. Rev.* **2015**, *115*, 6966-6997.
7. H. Ghasempour, K. -Y. Wang, J. A. Powell, F. ZareKarizi, X. -L. Lv, A. Morsali, H. -C. Zhou, *Coord. chem. Rev.* **2021***, 426,* 213542.
8. Y. Tian, G. Liang, T. Fan, J. Shang, S. Shang, Y. Ma, R. Matsuda, M. Liu, M. Wang, L. Li, S. Kitagawa, *Chem. Mater.* **2019**, *31*, 8494-8503.
9. C. Marsh, X. Han, J. Li, Z.Lu, S. P. Argent, I. d. Silva, Y. Cheng, L. L. Daement, A. J. R. Cuesta, S. P. Thompson, A. J. Blake, S. Yang, M. Schroder, *J. Am. Chem. Soc.* **2021**, *143*, 6586-6595.
10. a) I. Hisaki, X. Chen, K. Takahashi, T. Nakamura, *Angew. Chem. Int. Ed.* **2019**, *58*, 11160-11170; b) R. -B. Lin, Y. He, P. Li, H. Wang, W. Zhou, B. Chen, *Chem. Soc. Rev.* **2019**, *48*, 1362-1389; c) J. Tian, L. Chen, D. -W. Zhang, Y. Liu, Z. -T. Li, Chem. Commun. **2016**, 52, 6351-6362; d) J. Lv, C. P. Krap, M. Suyetin, N. H. Alsmail, Y. Yan, S. Yang, W. Lewis, E. Bichoutskaia, C. C. Tang, A. J. Blake, R. Cao, M. Schroder, *J. Am. Chem. Soc.* **2014**, *136*, 12828-12831; e) A. Yamamoto, T. Hamada, I. Hisaki, M. Miyata, N. Tohnai, *Angew. Chem. Int. Ed.* **2013**, *52*, 1709-1712. f) H. -C. Zhou, J. R. Long, O. M. Yaghi, *Chem. Rev.* **2012**, *112*, 673-674; g) X. Feng, X. S.

Ding, D. L. Jiang, *Chem. Soc. Rev.* **2012**, *1*, 6010-6022; h) J. Q. Dong, X. Han, Y. Liu, H. Y. Li, Y. Cui, *Angew. Chem.* **2020**, *132*, 13826-13837; i) Z .F. Wang, S. N. Zhang, Y. Chen, Z. J. Zhang, S. Q. Ma, *Chem. Soc. Rev.* **2020**, *49*, 708-735; j) M. S. Lohse, T. Bein, Adv. Funct. Mater. 2018, 28, 1705553.

11. a) C. A. Zentner, H. W. H. Lai, J. T. Greenfield, R. A. Wiscons, M. Zeller, C. F. Campana, O. Talu, S. A. FitzGerald, J. L. C. Rowsell, *Chem. Commun.* **2015**, *51*, 11642-11645; b) I. Hisaki, N. Ikenaka, E. Gomez, B. Cohen, N. Tohnai, A. Douhal, *Chem. Eur. J.* **2017**, *23*, 11611-11619; c) F. Hu, C. Liu, M. Wu, J. Pang, F. Jiang, D. Yuan, M. Hong, *Angew, Chem. Int. Ed.* **2017**, *56*, 2101-2104; d) Q. Yin, P. Zhao, R. -J. Sa, G. -C. Chen, J. Lv, R. Cao, *Angew. Chem. Int. Ed.* **2018**, *57*, 7691-7696; e) p. Li, P. Li, M. R. Ryder, Z. C. Liu, C. L. Stern, O. K. Farha, J. F. Stoddart, *Angew. Chem. Int. Ed.* **2019**, *58*, 10345-10352; f) T. Takeda, M. Ozawa, M. Akutagawa, *Angew. Chem. Int. Ed.* **2019**, *58*, 10345-10352; g) Q. Yin, P. Zhao, R. J. Sa, G. C. Chen, J. Lv, T. -F. Liu, R. Cao, *Angew. Chem. Int. Ed.* **2018**, *57*, 7691-7696.
12. a) Y. He, S. Xiang, B. Chen, *J. Am. Chem. Soc.* **2011**, *133*, 14570-14573; b) P. Li, Y. He, J. Guang, L. Weng, J. C. -G. Zhao, S. Xiang, B. Chen, *J. Am. Chem. Soc.* **2014**, *136*, 547-549. c) J. D. Wuest, *Chem. Commun.* **2005**, *47*, 5830-5837; d) Y. C. Tang, C. Y. Zhang, L. L. Fan, Y. X. Shang, Y. Feng, J. Pang, X. L. Cui, G. D. Kong, R. M. Wang, Z. X. Kang, D. F. Sun, *Cryst. Growth Des.* **2021**, *21*, 5292-5299; e) L. S. Gong, Y. X. Ye, Y. Liu, Y. B. Li, Z. B. Bao, S. C. Xiang, Z. J. Zhang, B. L. Chen, *ACS Appl. Mater. Interfaces* **2022**, *14*, 19623-19628; f) T. Khadivjam, H. C. Quang, T. Maris, Z. Ajoyan, A. Howaeth, J. D. Wuest, *Chem. Eur. J.* **2020**, *26*, 7026-7040; g) Y. N. Han, T. Zhang, X. Y. Chen, J. J. Hao, W. C. Song, Y. F. Zeng, P. C. Xue, *ACS Appl. Mater. Interfaces* **2021**, *13*, 32270-32277. h) S. Feng, Y. Shang, Z. Wang, Z. Kang, R. Wang, J. Jiang, L. Fan, W. Fan, Z. Liu, G. Kong, Y. Feng, S. Hu, H. Guo, D. Sun, *Angew. Chem. Int. Ed.* **2020**, *59*, 3840-3845.
13. a) T.-H. Chen, I. Popov, W. Kaveevivitchai, Y.-C. Chuang, Y.-S. Chen, O. Daugulis, A. J. Jacobson, O. S. Miljanic, *Nat. Commun.* **2014**, *5*, 5131-5138; b) M. I. Hashim,

H. T. M. Le, T.-H. Chen, Y.-S.Chen, O. Daugulis, C. -W. Hsu, A. J. Jacobson, W. Kaveevivitchai, X. Liang, T. Makarenko, O. S. Miljanic, I. Popovs, H. V. Tran, X. Wang, C.-H. Wu, J. I. Wu, *J. Am. Chem. Soc.* **2018**, *140*, 6014–6026; c) X. -Z. Luo. X. -J. Jia, J. -H. Deng, J. -L. Zhong, H. -J. Liu, K. -J. Wang, D. -C. Zhong, *J. Am. Chem. Soc.* **2013**, *135*, 11684-11687; d) W. Q. Yan, X. P. Yu, T. Yan, D. F. Wu, E. L. Wu, Y. Qi, Y. F. Han, Q. W. Li, *Chem. Commun.* **2017**, *53*, 3677-3680; e) H. Yamagishi, H. Sato, A. Hori, Y. Sato, R. Matsuda, K. Kato, T. Aida, *Science*, **2018**, *361*, 1242-1246.

14. a) M. Mastalerz, I. M. Oppel, *Angew. Chem. Int. Ed.* **2012**, *51*, 5252-5255; b) A. Pulido, L. Chen, T. Kaczorowski, D. Holden, M. A. Little, S. Y. Chong, B. J. Slater, D. P. McMahon, B. Bonillo, C. J. Stackhouse, A. Stephenson, C. M. Kane, R. Clowes, T. Hasell, A. I. Cooper, G. M. Day, *Nature* **2017**, 543, 657-664.
15. I. Hisaki, Y. Suzuki, E. Gomez, Q. Ji, N. Tohnai, T. Nakamura, A. Douhal, *J. Am. Chem. Soc.* **2019**, 141, 2111-2121.
16. B. Han, H. Wang, C. Wang, H. Wu, W. Zhou, B. Chen, J. Jiang, *J. Am. Chem. Soc.* **2019**, *141*, 8737-8740.
17. J. Gao, Y. Cai, X. Qian, P. Liu, H. Wu, W. Zhou, D. -X. Liu, L. Li, R. -B. Lin, B. Chen, *Angew. Chem. Int. Ed.* **2021**, *60*, 20400-20406.
18. I. Hisaki, S. Nakagawa, N. Tohnai, M. Miyata, *Angew. Chem. Int. Ed.* **2015**, *54*, 3008-3012.
19. C. Eickmeier, H. Junga, A. J. Matzger, F. Scherhag, M. Shim, K. P. C. Vollhardt, *Angew. Chem. Int. Ed.* 1997, **36**, 2103-2108.
20. G. Manolikakes, A. Gavryushin, P. Knochel, *J. Org. Chem.* **2008**, *73*, 1429-1434.
21. Y. Suzuki, M. Gutierrez, S. Tanaka, E. Gomez, N. Tohnai, N. Yasuda, N. Matubayasi, A. Douhal, I. Hisaki, *Chem. Sci.* **2021**, *12*, 9607-9618.
22. Rigaku Oxford Diffraction (2015), Software CrysAlisPro 1.171.38.41o. Rigaku Corporation, Tokyo, Japan.
23. G. M. Sheldrick, *Acta Crystallogr. Sect. A* **2015**, 71, 3–8.

24. (a) Rigaku (2018). CrystalStructure. Version 4.3. Rigaku Corporation, Tokyo, Japan; (b) O. V. Dolomanov, L. J. Bourhis, R. J. Gildea, J. A. K. Howard, H. Puschmann, H. *J. Appl. Cryst.* **2009**, 42, 339–341; (c) L. J. Bourhis, O. V. Dolomanov, R. J. Gildea, J. A. K. Howard, H. Puschmann, *Acta Crystallogr. Sect. A* **2015**, 71, 59–75.
25. G. M. Sheldrick, *Acta Crystallogr. C* **2015**, 71, 3–8.
26. (a) P. v. d. Sluis, A. L. Spek, *Acta Crystallogr. Sect. A* **1990**, 46, 194; (b) A. L. Spek, *Acta Crystallogr. Sect. D* **2009**, 65, 148–155.

Chapter 5

Conclusions and Perspectives

5-1. Conclusions

In the thesis, several HOFs based on tetratopic carboxylic acid derivatives have been constructed successfully, including **BTIA**, **BTTA**, **CP-Phen(DMA-TCB)**, **CP-Phen(NMP-TCB)** and **CP-Phen-Py**. The crystal structures were precisely determined, and the properties were also investigated comprehensively. In particular, electrostatic and geometric effects of tectons were verified to have important influence on the construction of hydrogen-bonded organic frameworks.

In **chapters 2** and **3**, the isostructural 2D HOFs **BTIA** and **BTTA** based on BT moieties and tetracarboxylic acids were obtained. It can been observed that unidirectional aligned slip-stacking of BT moieties and directional hydrogen bond between carboxy groups in the networks, which indeed make sense for construction of stable HOFs. For **BTIA**, a dipole-dipole interaction between the BT moieties, in addition to directional H-bond formation and a rigid molecular skeleton, play a role to form structurally-predictable 2D HOF. Its activated form **BTIA-1a** through traditional activation method with BET surface area of 237 m^2 g^{-1} showed selective adsorption of CO_2 and retained the original structure at least up to 270 °C. Making the comparison to the activated form through solvent exchange method, **BTIA-1a** showed a higher BET surface area of 720 m^2 g^{-1}, which proved solvent exchange as a reliable method for activating materials. In terms of **BTTA**, orthogonally-working two kinds of interactions, which composed directional hydrogen bond between carboxy groups and slip-stacking of BT groups with unidirectional alignment, play important roles to give the well-defined porous layered HOF. The **BTTA** shows thermal stability up to 275 °C, permanent porosity with BET surface area of 1145 m^2 g^{-1}, and photoconductivity.

In **chapter 4**, the Phen based HOF was constructed as expected, which formed self-complementary H-bonded dimer through three of four carboxy groups in tectons. It’s worth noting that the rest one carboxy group does not participate in network formation duo to the geometrical mismatch while makes a weak H-bond with a molecule of DMA. In the activation process, **CP-Phen-1** underwent 2-step structural transformation accompanied by H-bond cleavage and rearrangements, the resultant activated framework showed good thermal stability up to 360 °C and selective adsorption behavior toward CO_2. These results indeed implied geometrically mismatched assembly as a effective strategy for direct supply of active sites inside of frameworks.

5-2. Perspectives

(1) In **chapters 2** and **3**, I demonstrated that BT-HOFs are stable platform for multifunctional application. Cooperating dicarboxy-m-terphenyl (DmT) moieties with the BT derivative cores, a series of tectons were predesigned as in Figure 5-1. I conceive that all of these tectons could assembly in 2D HOFs, and evaluate their optical properties for whole spectrum-tunable light materials.[1,2]

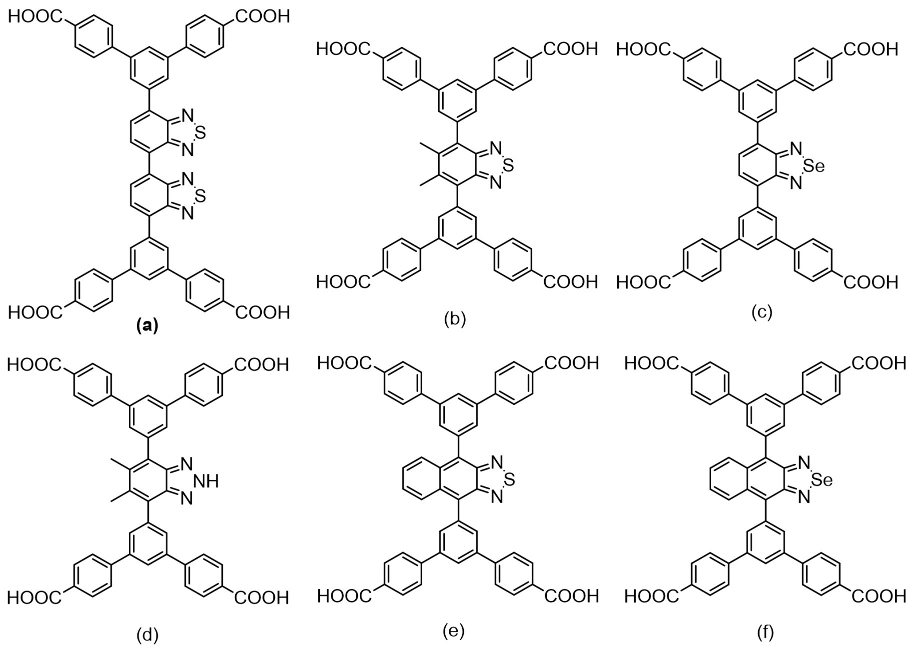

Figure 5-1. The tectons containing BT derivatives and Dicarboxy-m-terphenyl (DmT) moieties.

(2) Based on the strategy and results in **chapter 4**, the following two tactons (Figure 5-2) have been design. I expect that there will be active sites remaining in the networks of obtained HOFs, such as N atoms and free carboxyl groups, which could be modified in the future steps.

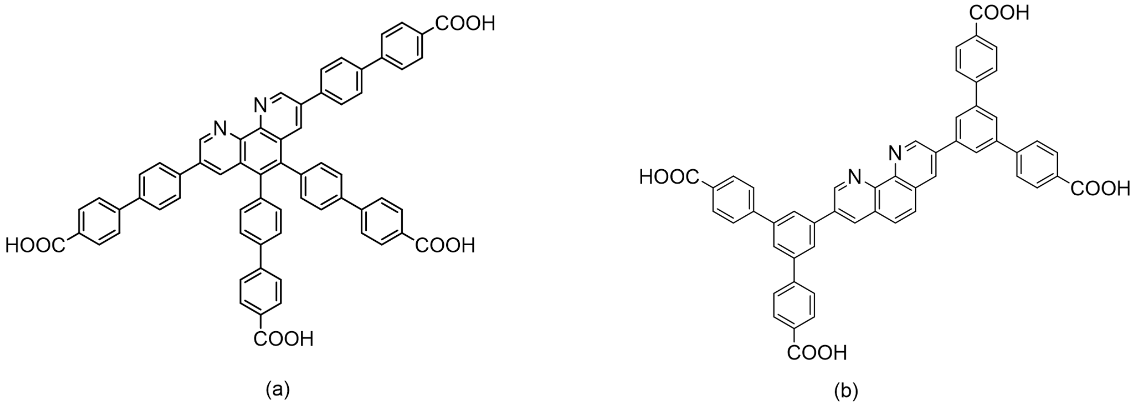

Figure 5-2. The tectons based on Phen derivatives.

Reference

1. S. Wu, D, Ren, K. Zhou, H. -L. Xia, X. -Y. Liu, X. Wang, J. Li, *J. Am. Chem. Soc.* **2021**, *143*, 10547-10552.

2. D. Ren, H. -L. Xia, K. Zhou, S. Wu, X. -Y. Liu. X. Wang, J. Li, *Angew. Chem. Int. Ed.* **2021** , *60*, 25048-25054.

List of publication

Chapter 2

Two-dimensional Porous Framework Assembled through Hydrogen-bonds and Dipole-dipole Interactions. *Chem. Lett.* **2021**, *50*, 1909-1912.

Zhuxi Yang, Ayana Moriyama, Ryusei Oketani, Takayoshi Nakamura,* Ichiro Hisaki*

Chapter 3

Slip-Stacking of Benzothiadiazole Can Provide a Robust Structural Motif for Porous Hydrogen-bonded Organic Frameworks. *Cryst. Growth Des.* **2022**, *22*, 4472‑4479.

Zhuxi Yang, Akinori Saeki, Asato Inoue, Ryusei Oketani, Kazuhide Kamiya, Shuji Nakanishi, Takayoshi Nakamura,* and Ichiro Hisaki*

Chapter 4

Geometrically Mismatched Hydrogen-bonded Framework Composed of Tetratopic Carboxylic Acid. *Chem. Eur. J.* **2022**, e202201571.

Zhuxi Yang, Taito Hashimoto, Ryusei Oketani, Takayoshi Nakamura,* Ichiro Hisaki*

Appendix

Appendix I: Chapter 2

The necessary ^{1}H and ^{13}C NMR spectra in **chapter 2**.

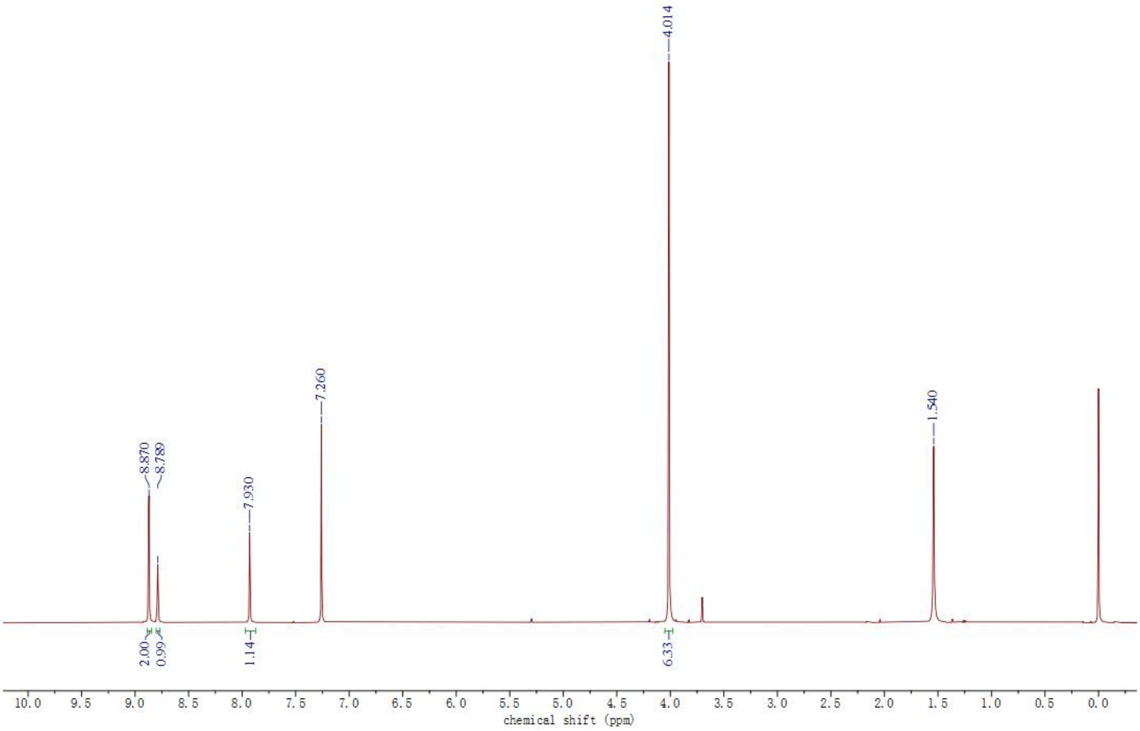

Figure S2-1. ^{1}H NMR (400 MHz, $CDCl_3$) spectrum of **BTIA-ester**.

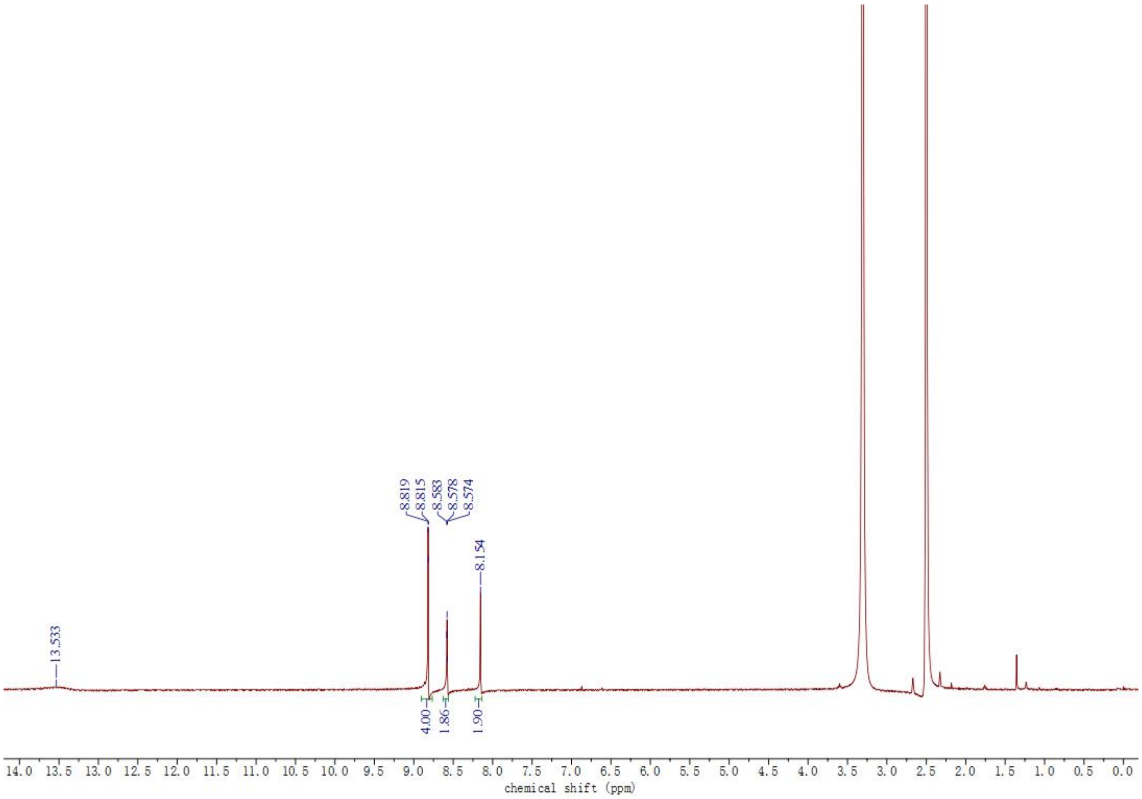

Figure S2-2. ^{1}H NMR (400 MHz, DMSO-d_6) spectrum of **BTIA**.

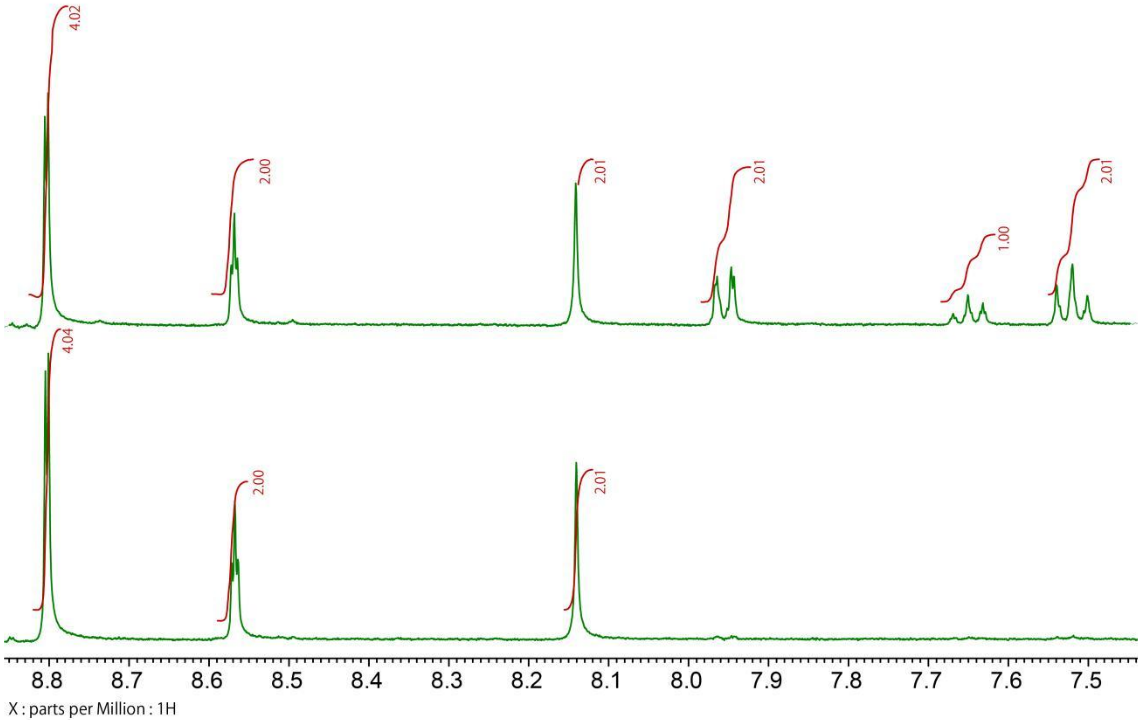

Figure S2-3. ^{1}H NMR spectra of crystalline bulk of HOF **BTIA-1** heated up to 150 °C (top) and up to 270 °C (bottom) dissolved in DMSO-d_6.

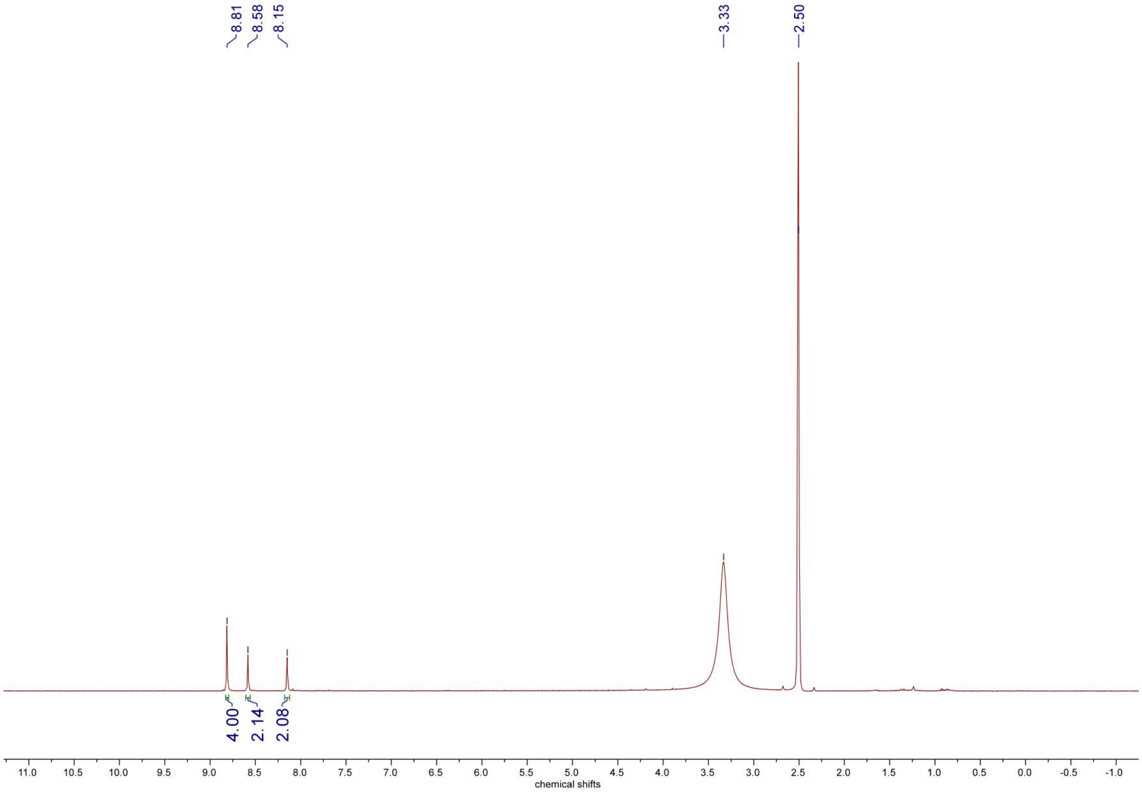

Figure S2-4. ^{1}H NMR spectrum of crystalline bulk of activated HOF **BTIA-1a** dissolved in DMSO-d_6.

Appendix II: Chapter 3

The necessary ^{1}H and ^{13}C NMR spectra in chapter 3

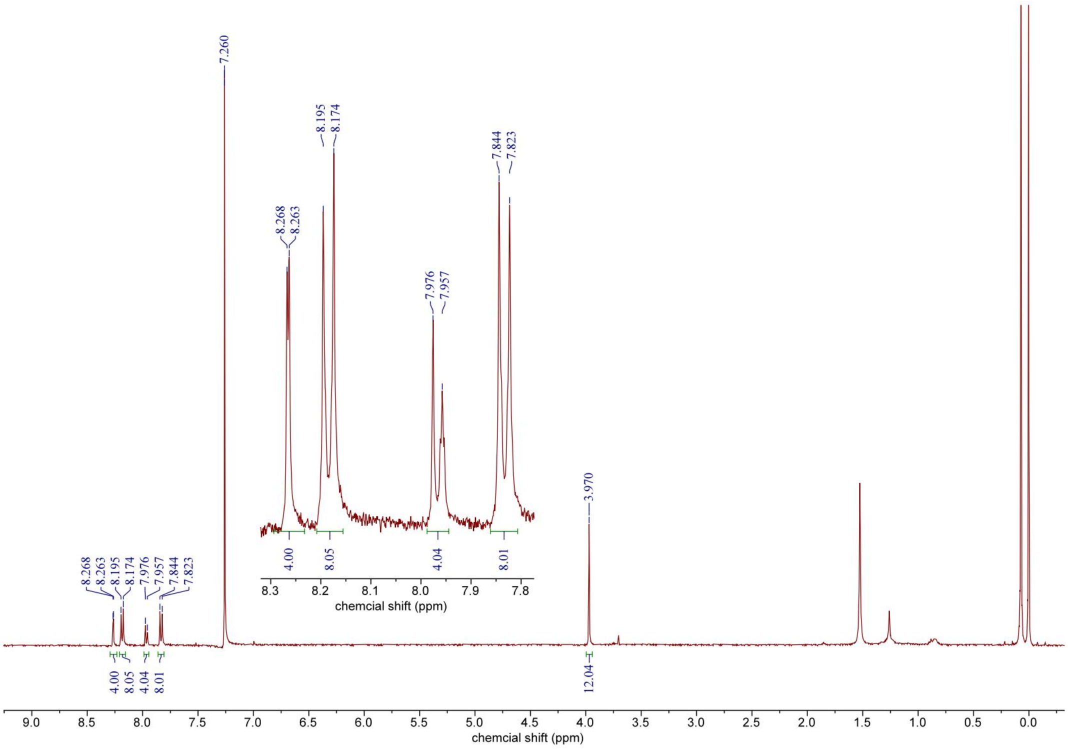

Figure S3-1. ^{1}H NMR (400 MHz, CDCl$_3$) spectrum of **3**.

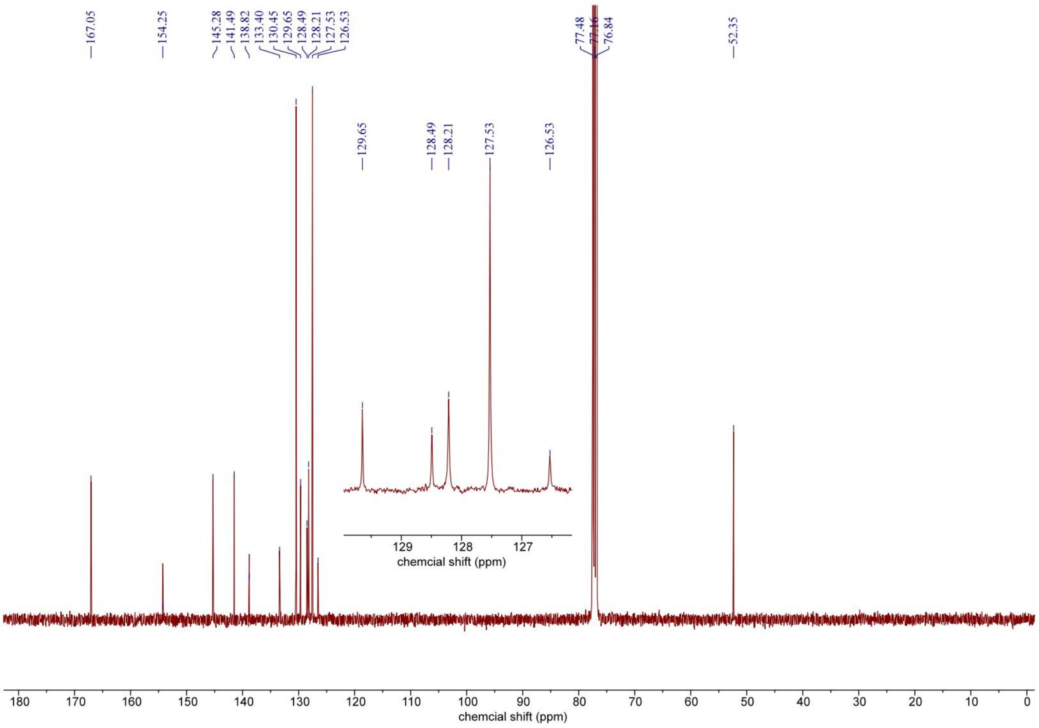

Figure S3-2. ^{13}C NMR (100 MHz, CDCl$_3$) spectrum of **3**.

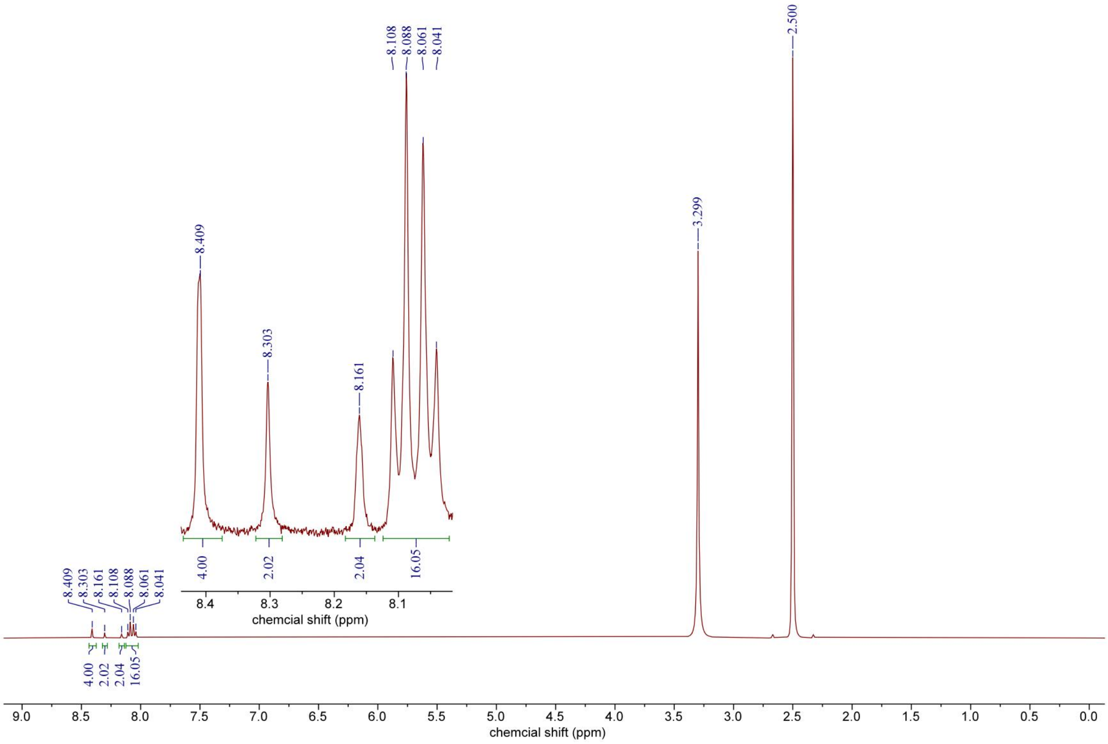

Figure S3-3. ^{1}H NMR (400 MHz, DMSO-*d6*) spectrum of **BTTA**.

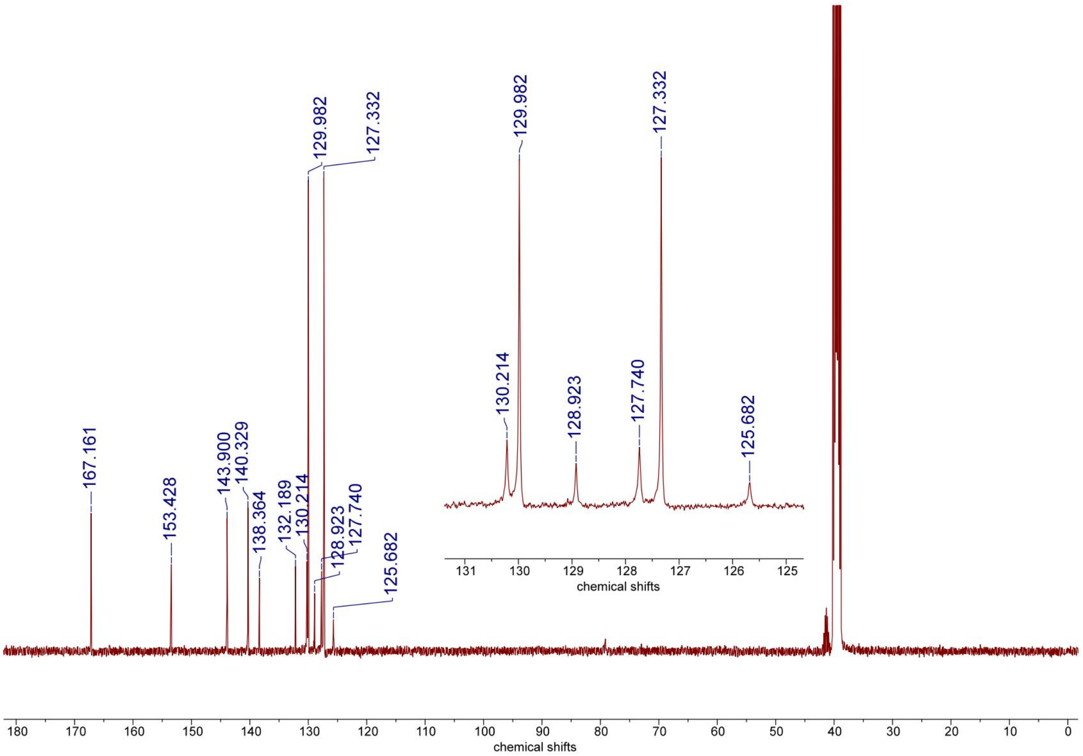

Figure S3-4. ^{13}C NMR (100 MHz, DMSO-d_6) spectrum of **BTTA**.

Stoichiometry

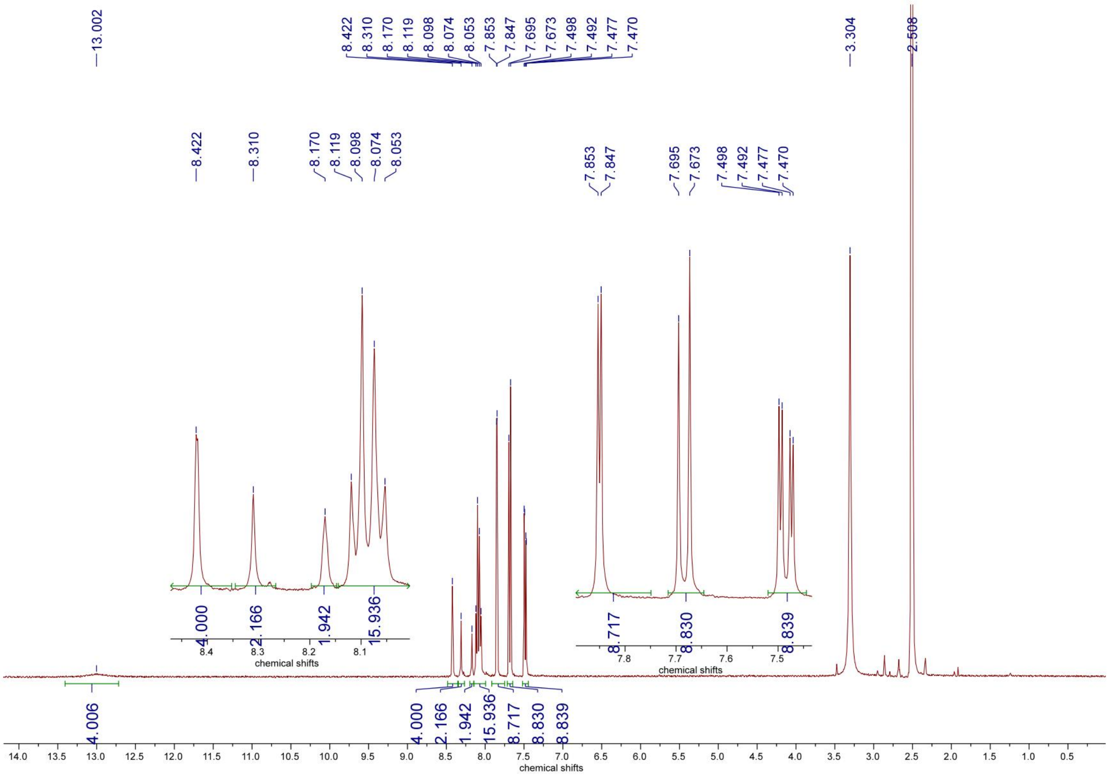

Figure S3-5. ^{1}H NMR spectrum of crystalline bulk of **BTTA-1(TCB)** dissolved in DMSO-d_6.

Evaluation of Permanent Porosity

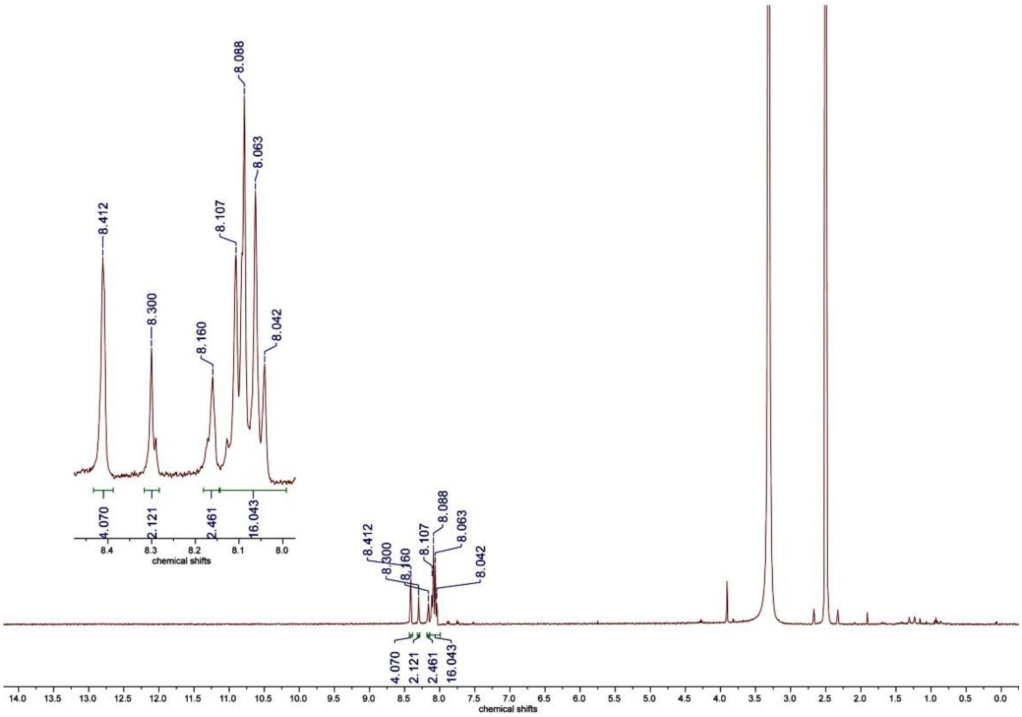

Figure S3-6. ^{1}H NMR spectrum of bulk of **BTTA-1a** dissolved in DMSO-d_6.

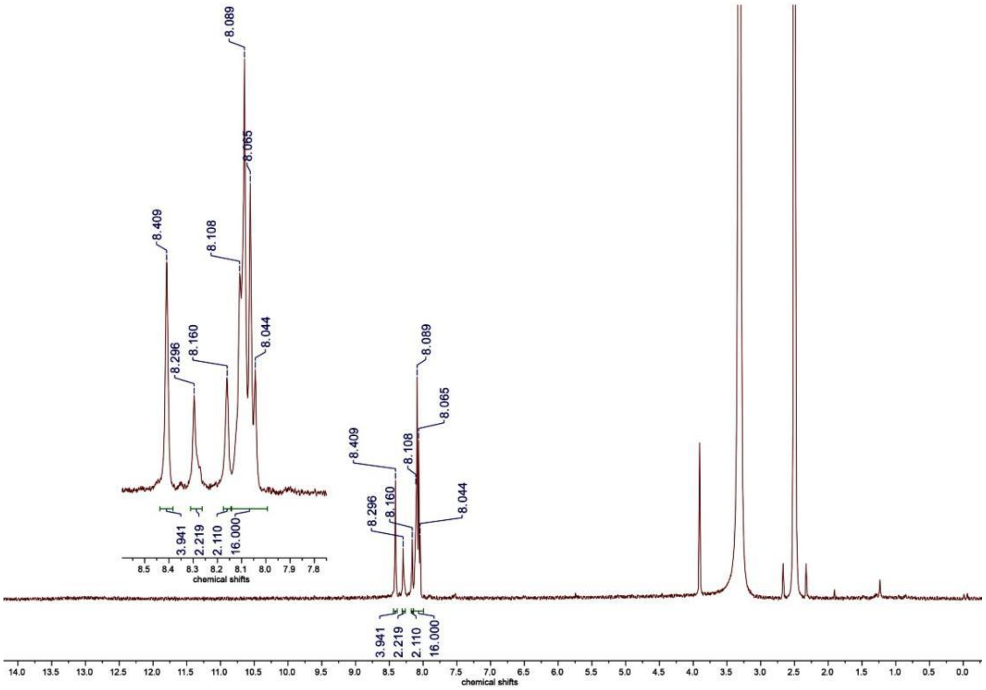

Figure S3-7. ^{1}H NMR spectrum of bulk of **BTTA-1a** after heating at 275 °C for 24 h

Appendix III: Chapter 4

The necessary ^{1}H and ^{13}C NMR spectra in **chapter 4**

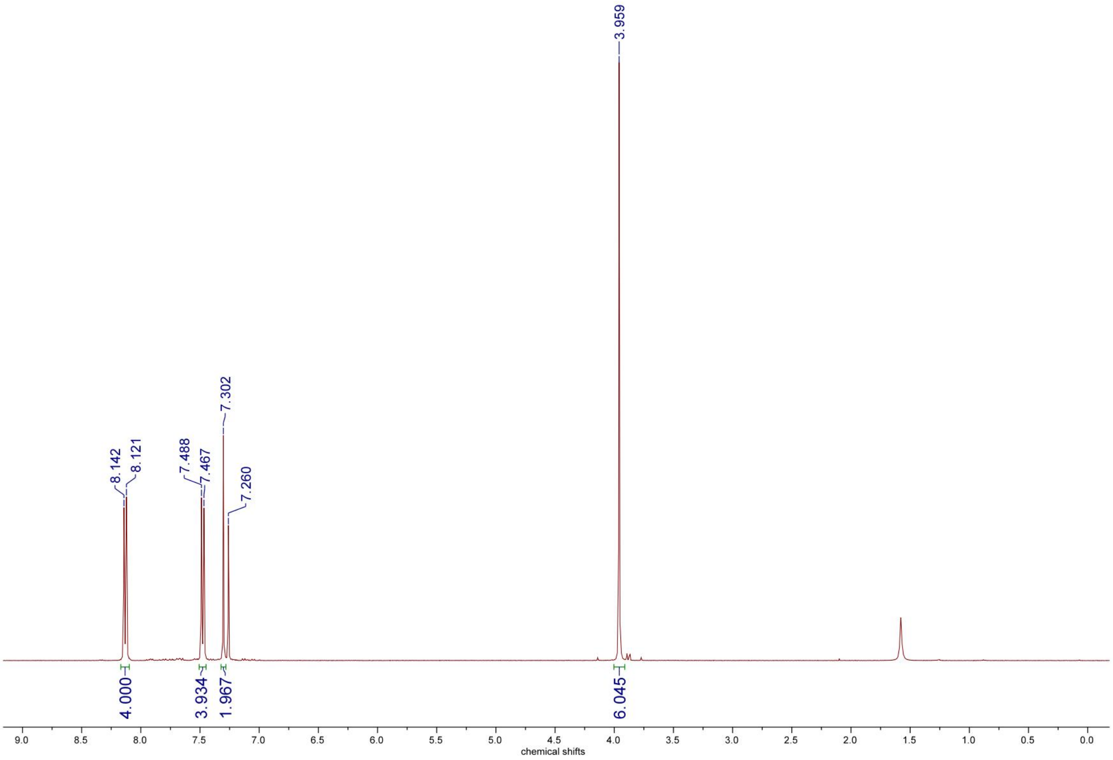

Figure S4-1. ^{1}H NMR (400 MHz, $CDCl_3$) spectrum of **1**.

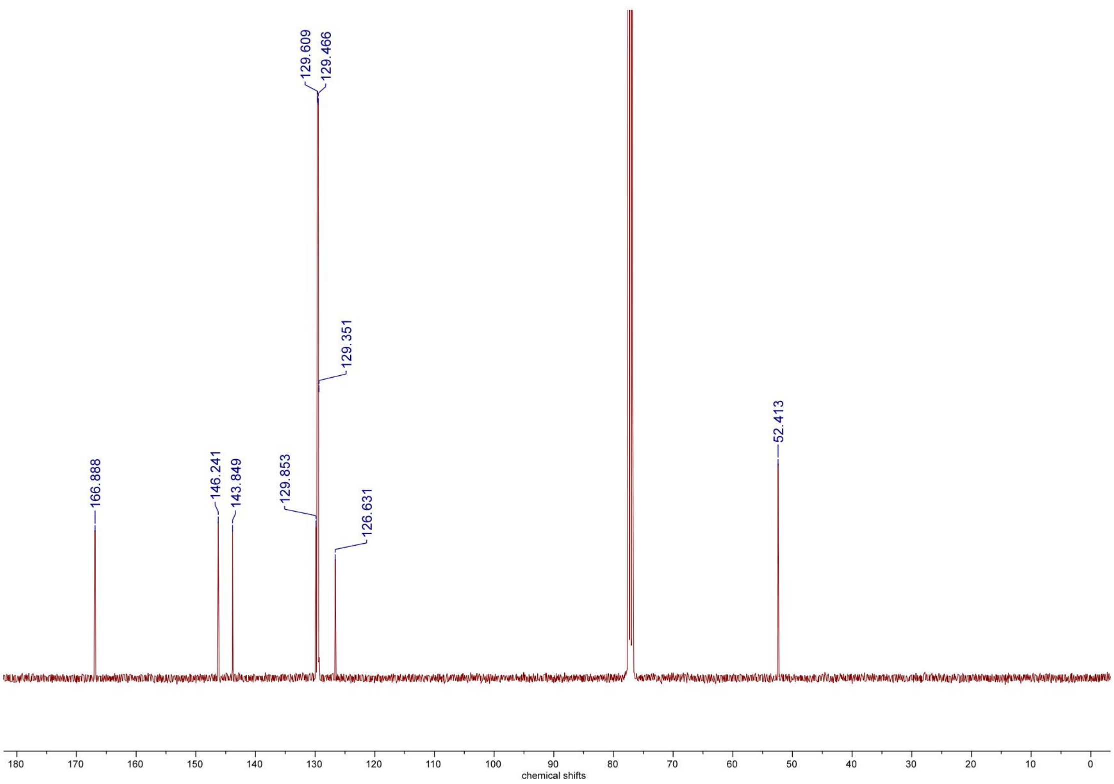

Figure S4-2. ^{13}C NMR (400 MHz, $CDCl_3$) spectrum of **1**.

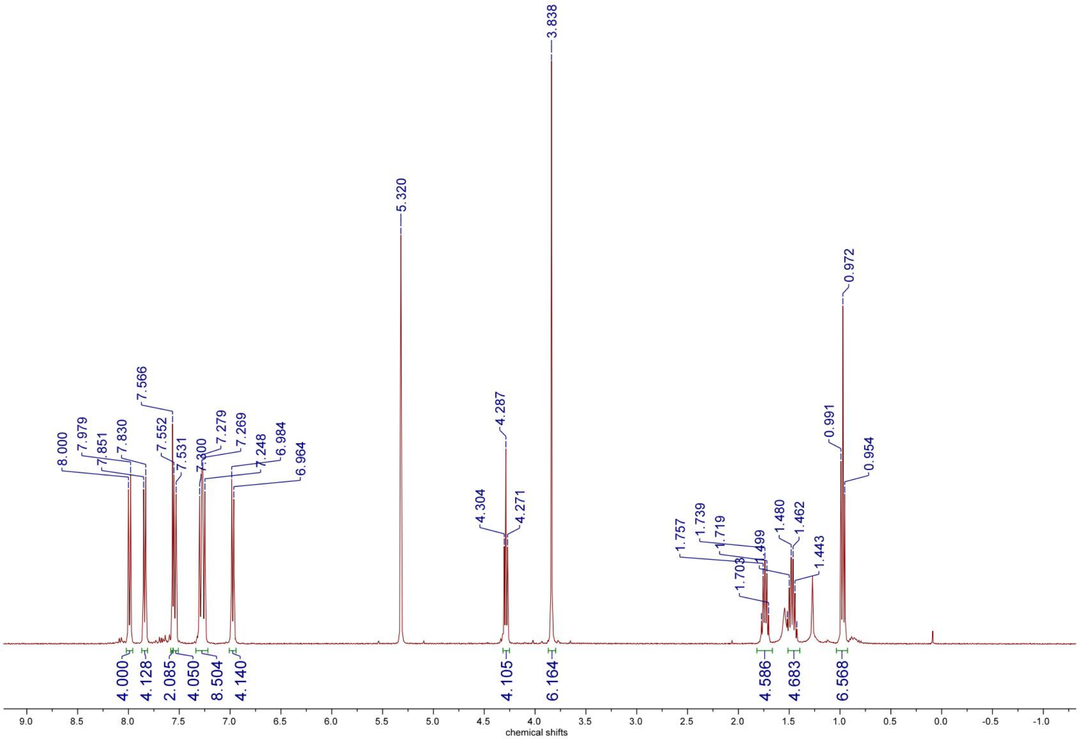

Figure S4-3. ^{1}H NMR (400 MHz, CD_2Cl_2) spectrum of **3**.

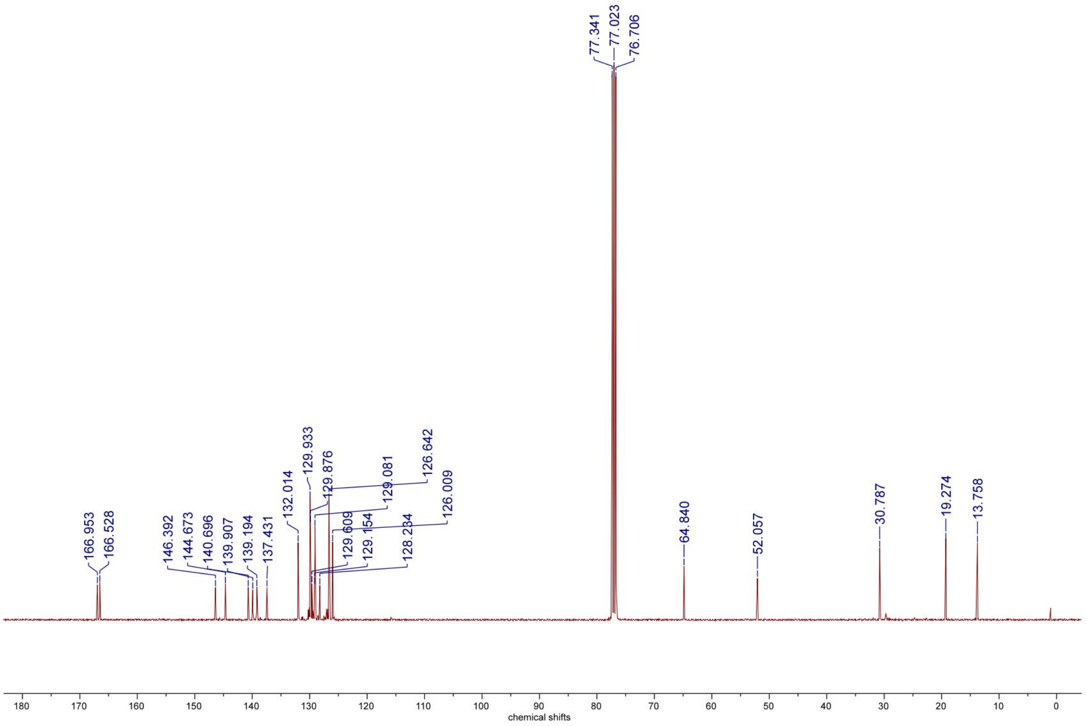

Figure S4-4. ^{13}C NMR (100 MHz, $CDCl_3$) spectrum of **3**.

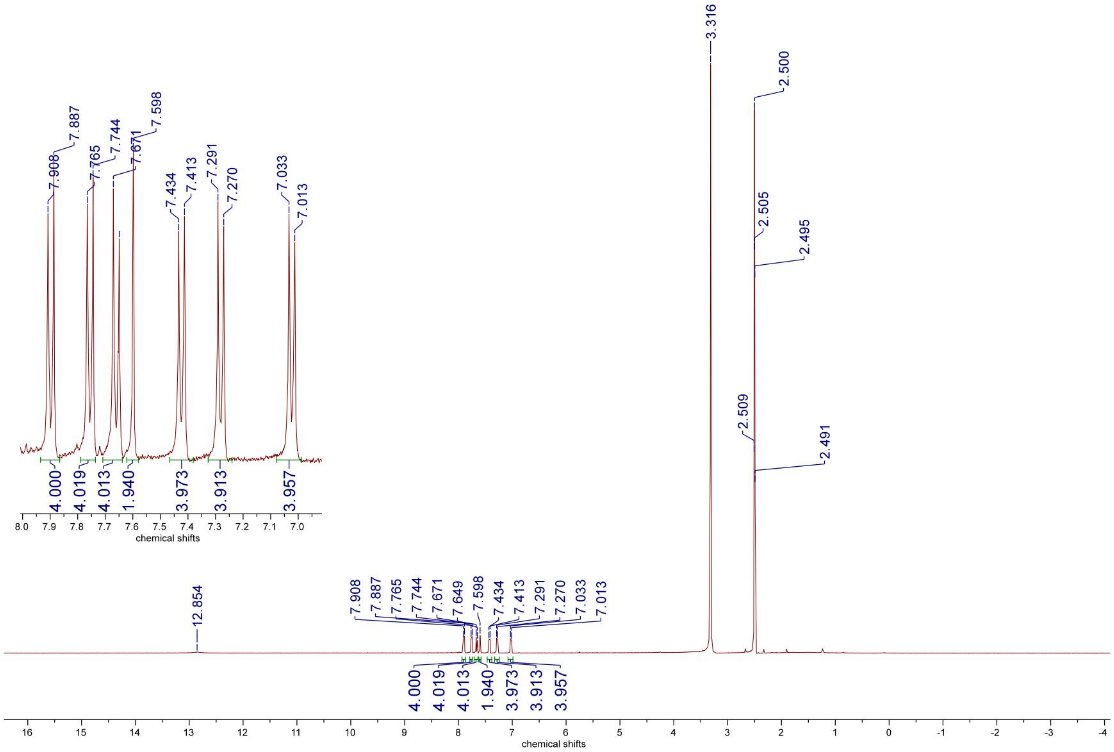

Figure S4-5. ^{1}H NMR (400 MHz, DMSO-d_6) spectrum of **Ue-Ben**.

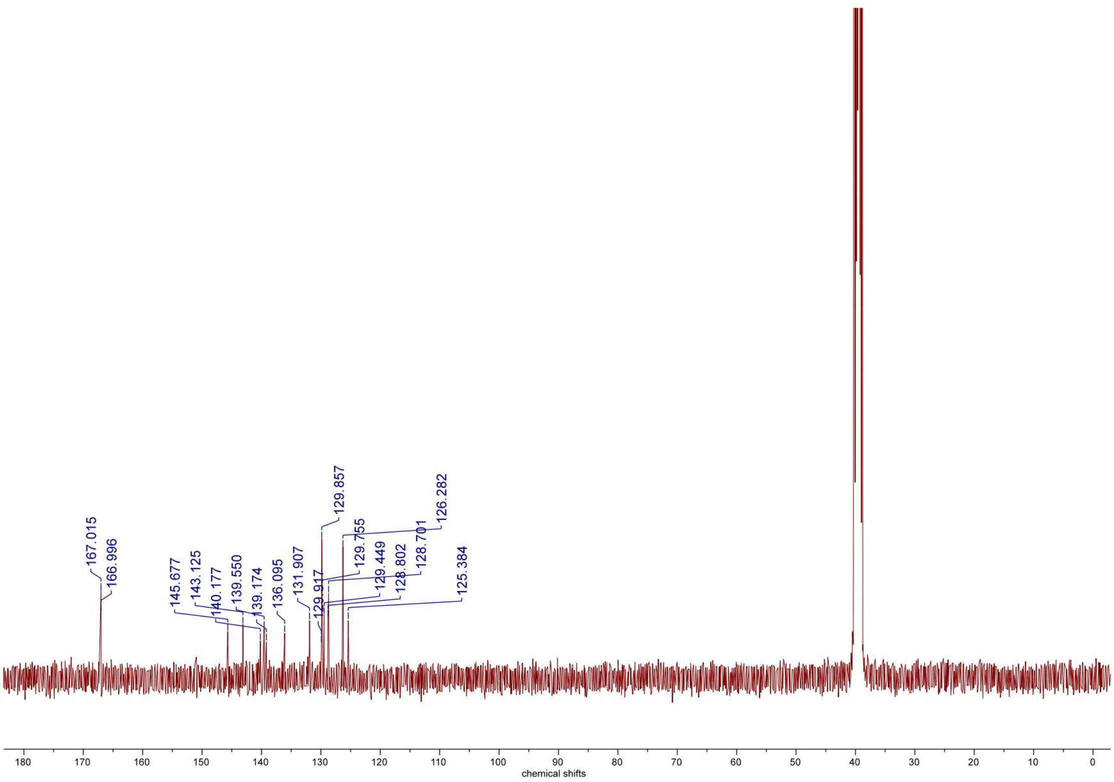

Figure S4-6. ^{13}C NMR (100 MHz, DMSO-d_6) spectrum of **Ue-Ben**.

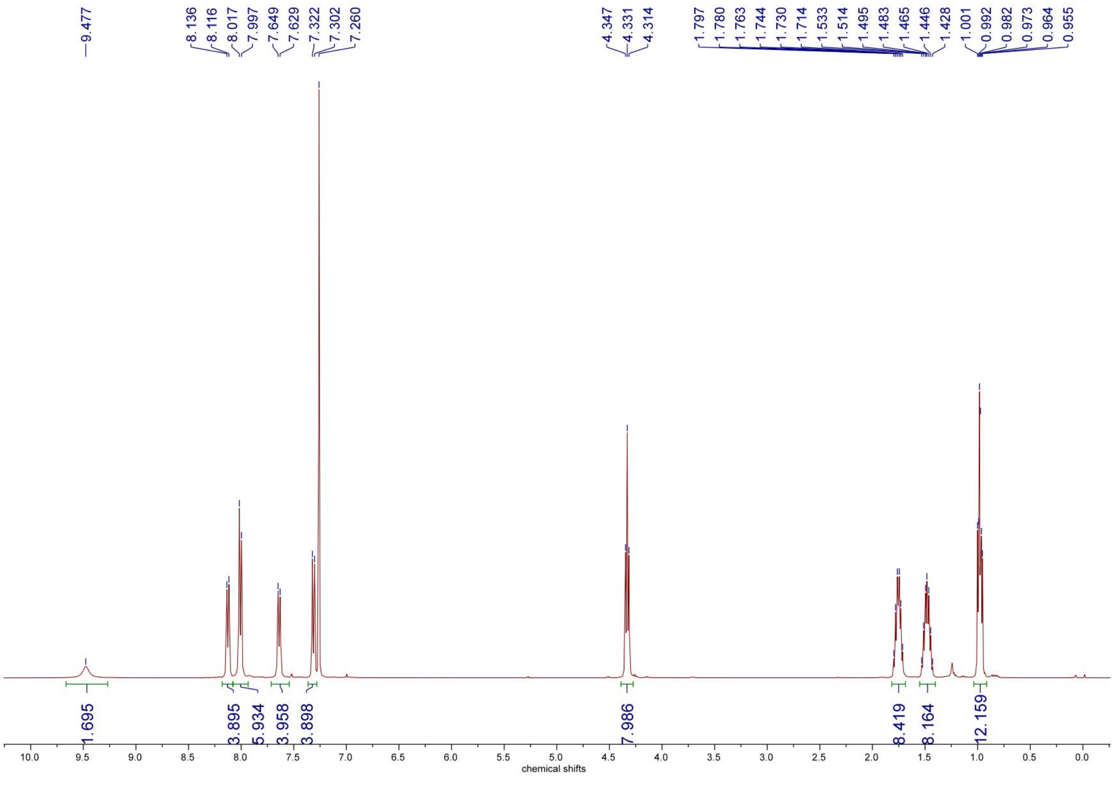

Figure S4-7. ^{1}H NMR (400 MHz, CDCl$_3$) spectrum of **6**.

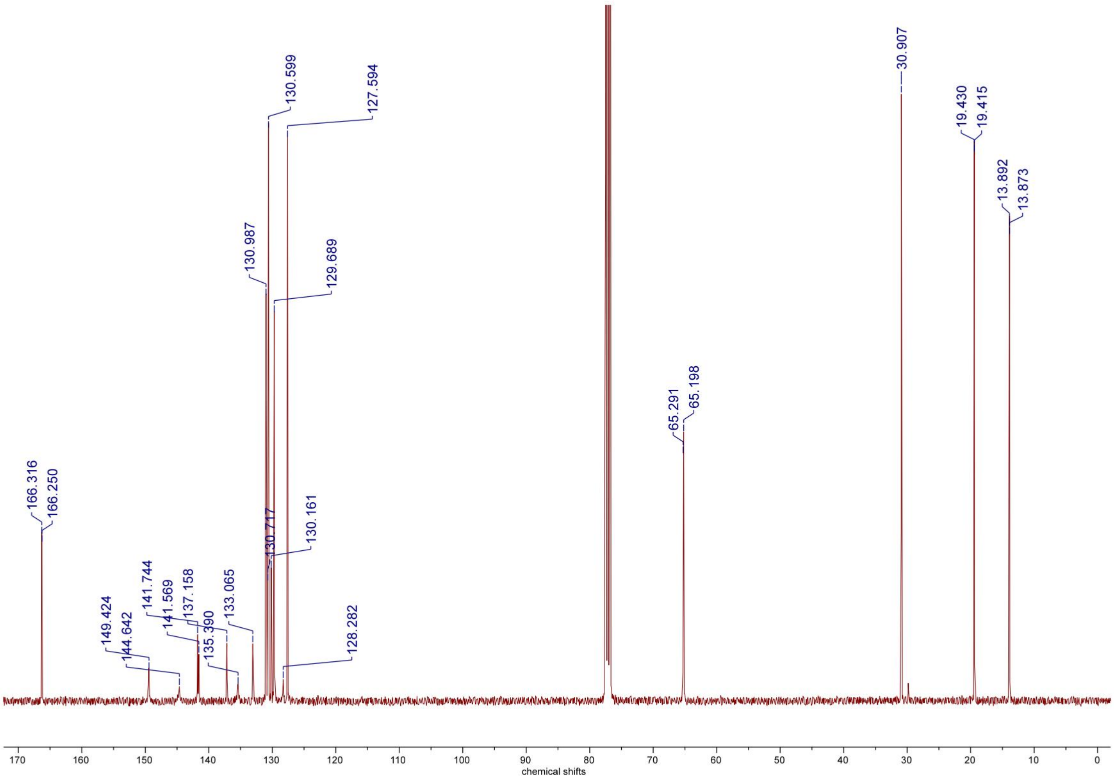

Figure S4-8. ^{13}C NMR (100 MHz, CDCl$_3$) spectrum of **6**.

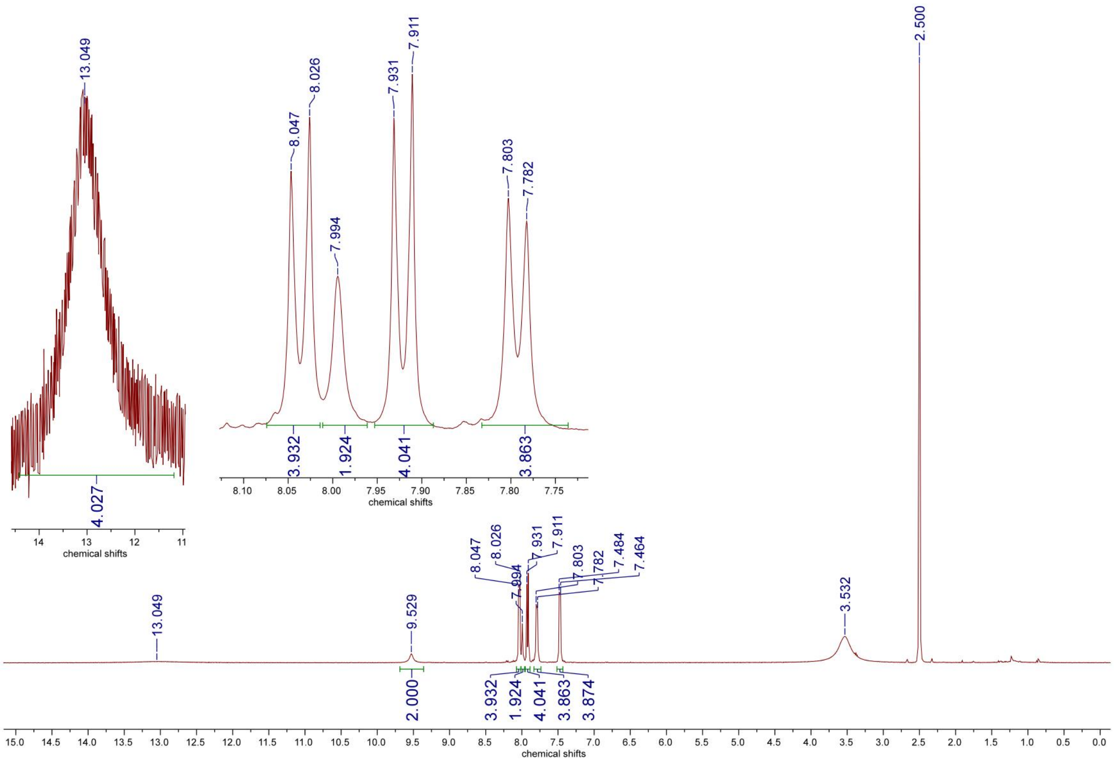

Figure S4-9. ^{1}H NMR (400 MHz, DMSO-d_6) spectrum of **CP-Phen**.

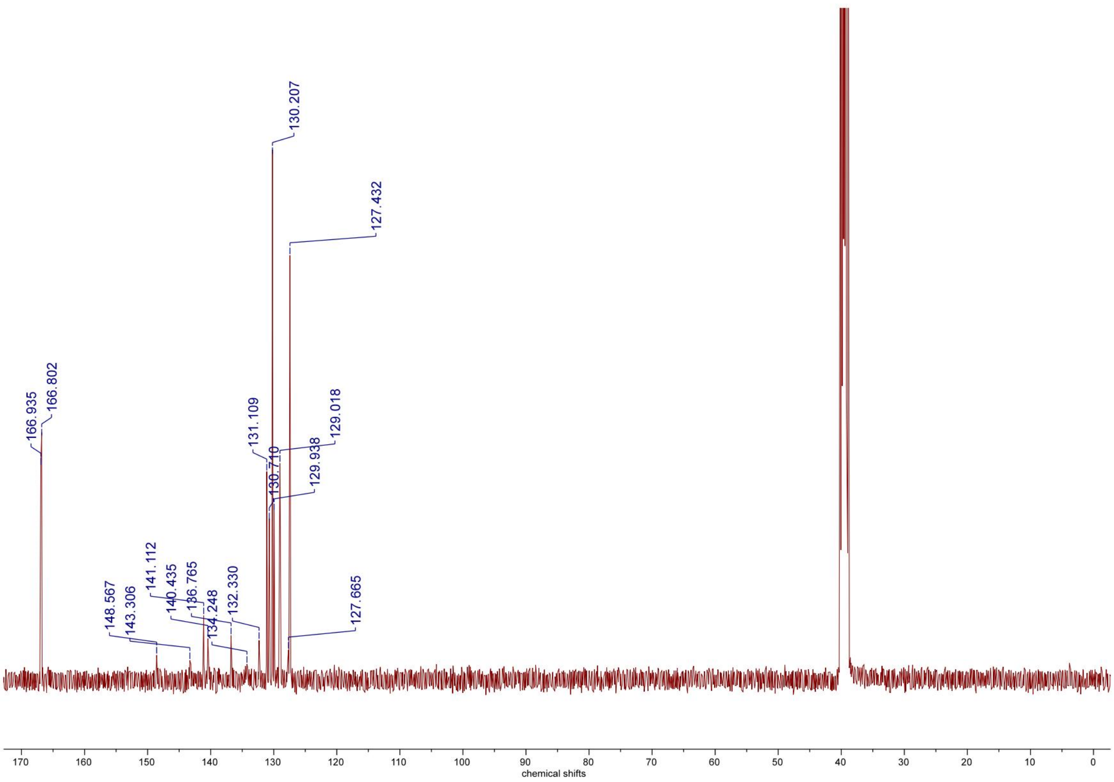

Figure S4-10. ^{13}C NMR (100 MHz, DMSO-d_6) spectrum of **CP-Phen**.

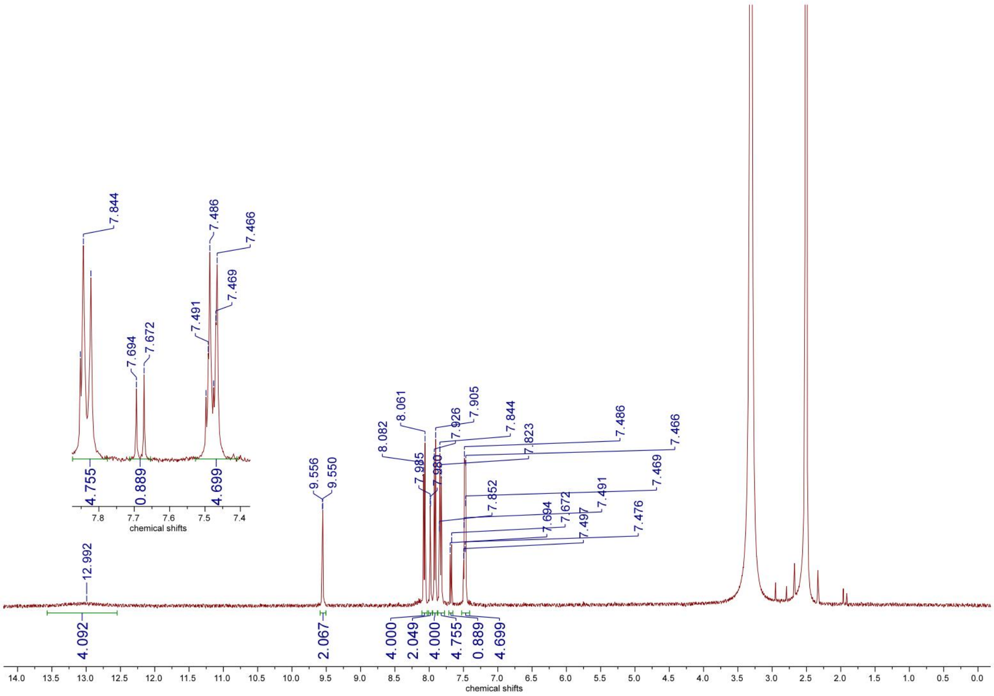

Figure S4-11. ^{1}H NMR (400 MHz, DMSO-d_6) spectrum of **CP-Phen-1(DMA-TCB)** after heated up to 128 °C.

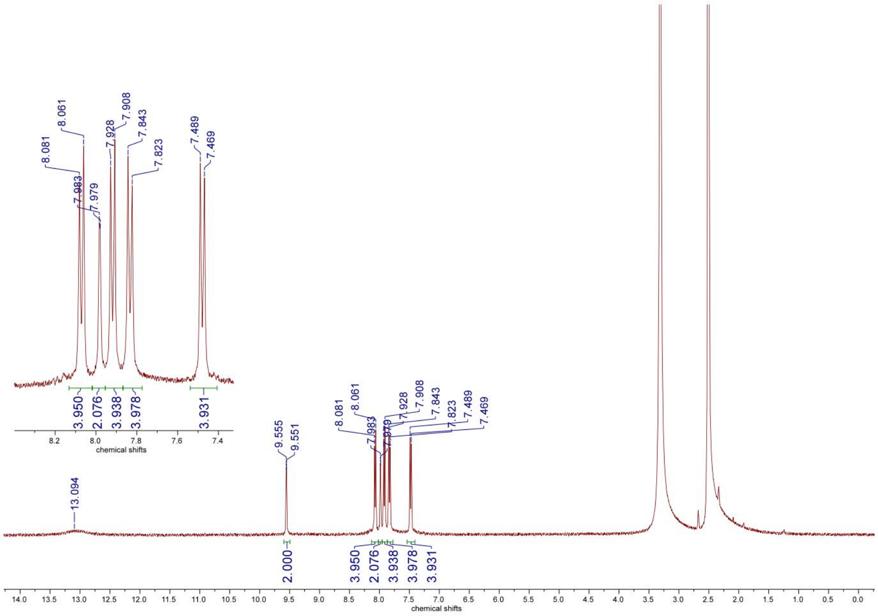

Figure S4-12. ^{1}H NMR (400 MHz, DMSO-d_6) spectrum of **CP-Phen-1(DMA-TCB)** after heated up to 200 °C.